BRNO UNIVERSITY OF TECHNOLOGY
VYSOKÉ UČENÍ TECHNICKÉ V BRNĚ

FACULTY OF ELECTRICAL ENGINEERING AND COMMUNICATION
FAKULTA ELEKTROTECHNIKY A KOMUNIKAČNÍCH TECHNOLOGIÍ

DEPARTMENT OF RADIO ELECTRONICS
ÚSTAV RADIOELEKTRONIKY

HALF MODE SUBSTRATE INTEGRATED WAVEGUIDE SLOT ANTENNAS

ŠTĚRBINOVÉ ANTÉNY NA BÁZI VLNOVODU INTEGROVANÉHO DO SUBSTRÁTU PRACUJÍCÍHO V POLOVIČNÍM MÓDU

DOCTORAL THESIS
DIZERTAČNÍ PRÁCE

AUTHOR — Ing. Patrik Hubka
AUTOR PRÁCE

SUPERVISOR — doc. Ing. Jaroslav Láčík, Ph.D.
ŠKOLITEL

BRNO 2021

Abstract

This dissertation deals with the research of slot antennas based on a half-mode substrate-integrated waveguide (HMSIW). By using HMSIW, the physical size of the antenna is reduced by approximately half while maintaining excellent antenna performance.

The thesis is consists of two factual parts. The first one (Chapter 4) proposes and describes linearly and circularly polarized HMSIW polarized U-slot antenna. The combination of these two antennas resulted in a polarization reconfigurable HMSIW slot antenna. The functionality of all these antennas are experimentally verified. These antennas achieve better performance compared to current developments of the similar HMSIW antennas. The functionality of the linearly and circularly polarized antenna are further investigated in deep by characteristic modal analysis and parametric procedure. Based on those investigations, design guides of those antennas are proposed. The second one (Chapter 5) deals with design and description of the simple circularly polarized HMSIW U-slot antenna array with linear organization of 1 × 4 basic radiators. The experimental verification proved that the antenna array with a simple feeding network achieved the competitive performance in comparison to the similar antenna array described in the literature.

Keywords

slot antenna, polarization, antenna reconfiguration, substrate half mode integrated waveguide operating (HMSIW), antenna array

Abstrakt

Disertační práce je zaměřena na výzkumem štěrbinových antén na bázi vlnovodu integrovaný do substrátu pracující v polovičním módu (HMSIW). Díky použití HMSIW je fyzická velikost antény redukována přibližně o polovinu při zachování výborných anténních parametrů. Práce je rozdělena do dvou částí. První z nich (kapitola 4) se zabývá návrhem lineárně a kruhově polarizované HMSIW štěrbinové antény ve tvaru písmene U. Kombinací těchto dvou antén vznikla polarizačně rekonfigurovatelná HMSIW štěrbinová anténa. Funkčnost všech antén je experimentálně ověřena. Tyto antény často dosahují lepších výsledků ve srovnání se současným vývojem podobných HMSIW antén. Funkčnost lineárně a kruhově polarizované antény je podrobně popsána pomocí parametrické studie a charakteristickou modální analýzou. Jsou vytvořeny metodiky návrhu těchto antén. Druhá kapitola (kapitola 5) se zabývá návrhem a popisem jednoduché kruhově polarizované HMSIW anténní řady s lineárním řazením s 1 × 4 základními zářiči. Experimentální ověření prokázalo, že anténní pole s jednoduchou napájecí sítí dosahuje konkurenceschopných vlastností ve srovnání s podobnými anténními poli popsanými v literatuře.

Klíčová slova

štěrbinová anténa, polarizace, rekonfigurace antény, vlnovod integrovaný do substrátu pracující v polovičním módu (HMSIW), anténní řada

Declaration

I declare that I have written my doctoral thesis on the theme of "Half mode substrate integrated waveguide slot antennas" independently, under the guidance of the doctoral thesis supervisor and using the technical literature and other sources of information which are all quoted in the thesis and detailed in the list of literature at the end of the thesis.

As the author of the doctoral thesis I furthermore declare that, as regards the creation of this doctoral thesis, I have not infringed any copyright. In particular, I have not unlawfully encroached on anyone's personal and/or ownership rights and I am fully aware of the consequences in the case of breaking RegulationS11 and the following of the Copyright Act No. 121/2000 Coll., and of the rights related to intellectual property right and changes in some Acts (Intellectual Property Act) and formulated in later regulations, inclusive of the possible consequences resulting from the provisions of Criminal Act No. 40/2009 Coll., Section 2, Head VI, Part 4.

Brno …… ……..

(author's signature)

Bibliographic citation

HUBKA, P. *Half mode substrate integrated waveguide slot antennas*. Doctoral thesis. Brno: FEKT v Brně, 2021. pp. 96.

Acknowledgement

I would like to express my gratitude to my supervisor Ing. Jaroslav Lačík, Ph.D., for his advice and invaluable guidance throughout my research. This thesis would have been impossible without his precious ideas and support.

Brno …… ……..

(author's signature)

Contents

1. Introduction 1
2. State of the Art of HMSIW Antennas 3
   2.1 Linearly and circularly polarized antennas 3
   2.2 Reconfigurable antennas 10
   2.3 Other antennas based on the HMSIW 12
   2.4 Antenna array based on the HMSIW 13
3. Objectives of the Thesis 15
4. HMSIW U-Shape Slot Antenna 16
   4.1 Linearly Polarized HMSIW U-Shape Slot Antenna 16
      4.1.1 Antenna structure 16
      4.1.2 Simulated Results 17
      4.1.3 Experimental Verification 19
      4.1.4 Characteristic Modal Analysis 21
      4.1.5 Parametric Study 23
      4.1.6 Design Guide 27
      4.1.7 Experimental Verification 31
      4.1.8 Summary 35
   4.2 Circularly Polarized HMSIW U-Shape Slot Antenna 35
      4.2.1 Antenna structure 36
      4.2.2 Simulated Results 36
      4.2.3 Experimental Verification 39
      4.2.4 Characteristic Modal Analysis 41
      4.2.5 Parametric Study 43
      4.2.6 Design Guide 51
      4.2.7 Summary 51
   4.3 Reconfigurable HMSIW U-Shape Slot Antenna 52
      4.3.1 Antenna Structure - Concept 52
      4.3.2 Simulated Results – Concept 53
      4.3.3 Experimental Verification – Concept 57
      4.3.4 Antenna structure – Electronic Control 59
      4.3.5 Simulated Results – Electronic Control 60
      4.3.6 Experimental Results – Electronic Control 64
      4.3.7 Summary 67
5. Circularly polarized HMSIW Antenna Array 68
      5.1.1 Antenna array structure 68
      5.1.2 Simulated Results 69
      5.1.3 Experimental Verification 73
      5.1.4 Summary 75
6. Conclusion 77

7. References 78
List of Abbreviations 83
List of Figures 84
List of Tables 88
A Curriculum Vitae 89

1. Introduction

In past decades, a rapid development of microwave components has been reported, such as antennas, filters, directional couplers, etc. With increasing complexity of microwave applications, new feeding structures with low losses, low profile and fabrication complexity are desirable. In 1998, a microwave structure called Substrate Integrated Waveguide (SIW) was introduced. The SIW is based on a conventional rectangular waveguide and preserves its advantages, such as low losses, high quality factor and self-consistent electrical shielding [1]. Moreover, it has many more advantages compared to a conventional waveguide, such as low manufacturing cost, a low profile, and easy integration with planar circuits. The SIW is comprised by two rows of vias within the single layered dielectric substrate and the two metal parallel plates at the top and at the bottom of dielectric substrate [2]. In order to reduce computing time, the vias can be substituted by a solid wall made of the perfect electrical conductor. The distribution of the electric and magnetic field in the SIW is similar to a conventional rectangular waveguide. For TE_{m0} modes, slots on bilateral narrow walls of the rectangular waveguide do not cut the surface current on the narrow walls. However, TM_{0n} or TE_{mn} (with n not being equal zero) modes produce a longitudinal surface current which is cut by the transverse slots on the vertical walls could bring about a large amount of unwanted radiation. Thus, only TE_{m0} modes can propagate in the SIW.

For some applications, especially at lower frequencies, SIW can be too wide. Thus, the reduction of the SIW size is very desirable task. To reduce the width of SIW, the ridge SIW (RSIW) [3], C-type folded SIW (CFSIW) [4] or T-type folded SIW (TFSIW) [5] technologies can be used. Unfortunately, all these technologies are based on a multilayer concept which increases demands of the design and fabrication process. Other option is to exploit a half-mode SIW (HMSIW) technology [6] since it preserves all advantages of the SIW technology and its size is reduced nearly by half with lower design and fabrication complexity than RSIW, CFSIW and TFSIW.

The HMSIW is depicted in Fig. 1. One side of the waveguide is created within the substrate by a row of vias and the other one is open. Due to the large ratio of the waveguide width to the height, the open side can be equivalent to a magnetic wall. Thus, only $TE_{m-0.5;0}$ modes can propagate in HMSIW.

The HMSIW can be manufactured by a Printed Circuit Process (PCB) and at mm-wave by a Low-Temperature Co-fired Ceramic (LTCC) technology. The low cost PCB fabrication process makes HMSIW components more mass producible with small sizes and low weight. In additional, HMSIW components can be integrated with other active or passive components on one board.

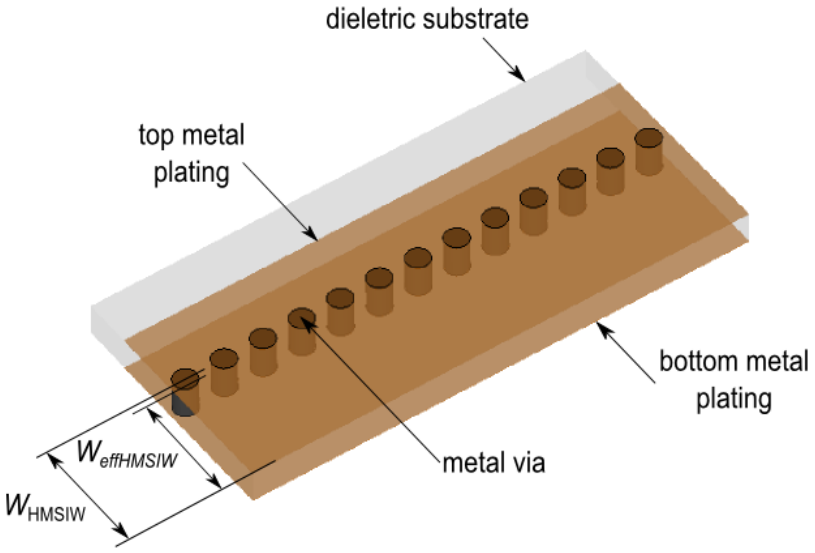

Fig. 1. Structure of HMSIW.

2. State of the Art of HMSIW Antennas

2.1 Linearly and circularly polarized antennas

In past years, with the rapid development of microwave wireless communications systems, demands for the miniaturization of low profile, low loss and low-cost slot antennas with suitable radiation performance and compatibility with other planar circuits have been greatly increased. One of most feasible solution for miniaturization of slot antennas is to exploit the HMSIW technology.

The first antenna based on the HMSIW technology is a longitudinal narrow rectangular slot [7] etched at the top wall of the HMSIW (Fig. 2). It is a simple radiator with a linear polarization (LP). However, the impedance bandwidth of the antenna is only 1.1 % for the reflection coefficient less (s_{11}) than -10 dB.

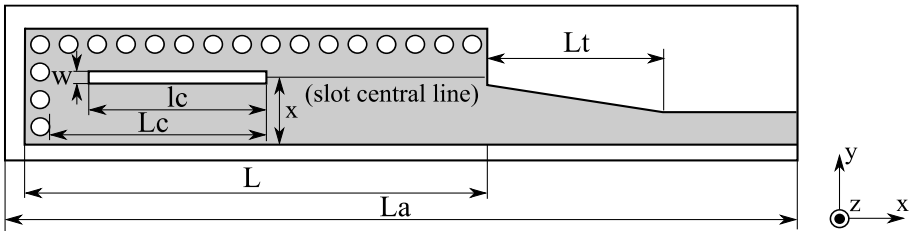

Fig. 2. Geometry of the first HMSIW slot antenna (the bottom side of the antenna is fully coated by metal).

A very simple HMSIW slot antenna was published in [8]. The antenna consists of a slot located at the top side and it is fed by a coaxial probe (Fig. 3). The antenna seems to be suitable for MIMO configuration because of its very low mutual coupling lower than -22 dB. The antenna has a compact size.

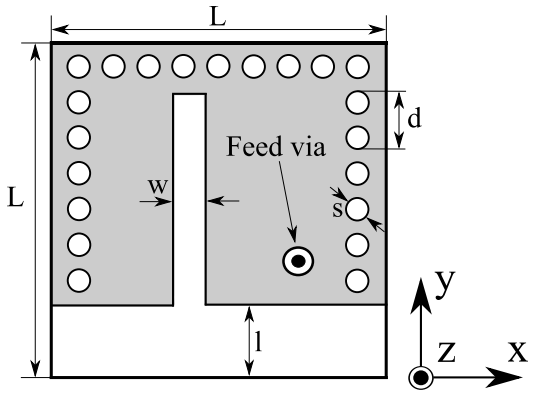

Fig. 3. Geometry of the simple HMSIW slot antenna (the bottom side of the antenna is fully coated by metal).

In [9], a linearly polarized cavity-backed antenna based on HMSIW was introduced (Fig. 4a). The antenna is a single layer, has a triangular shape and a dielectric aperture. The open edge (magnetic wall) of the antenna acts as a radiator and it radiates a linearly polarized wave. To excite a circularly polarized (CP) wave, an orthogonal slot is etched at the top wall of the HMSIW [10] (Fig. 4b). The maximum radiation for both types of antennas is perpendicular to the antenna plane. For the right-handed circular polarization (RHCP) antenna, the slot is etched at the top surface of the cavity (Fig. 4b). The left-handed circular polarization antenna (LHCP), the slot is etched at the ground plane of the

structure (Fig. 4c and d). The properties of all the antennas depicted in Fig. 4 are summarized in Table 1.

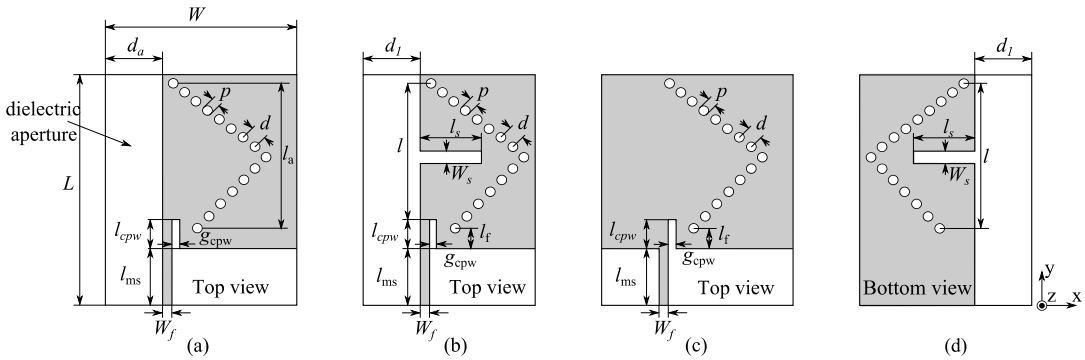

Fig. 4. Geometry of the HMSIW cavity-backed (a) linearly polarized antenna (the bottom side of the antenna is fully coated by metal.), (b) RHCP antenna (the bottom side of the antenna is fully coated by metal.) and (c) LHCP antenna and its (d) bottom view.

Table 1. Measured results of the HMSIW cavity-backed antennas.

Polarization of antenna	Impedance bandwidth for s_{11}<-10 dB [%]	Peak gain [dBi]	Axial ratio bandwidth for AR<3 dB [%]
LP	4.9	6.7	—
RHCP	6	4.48	1.74
LHCP	6	4.2	0.66

A simple HMSIW cavity-backed antenna reported in [11] is depicted in Fig. 5. The ground plane is fully coated by a metal. The open edge acts like a radiator and the antenna radiates linearly polarized wave. The version of the cavity operates in the fundamental dominant mode of $TE_{0.5;0}$. The antenna resonates at 6.78 GHz, and its impedance bandwidth is 125 MHz for the reflection coefficient less (s_{11}) than -10 dB. The peak gain is 5 dBi. The operating frequency of the antenna can be tuned by adding a slot [12]. The slot is an addition radiator of the antenna which could be etched either in the top or the ground plane (Fig. 6). The length and position of the slot controls the operating frequency.

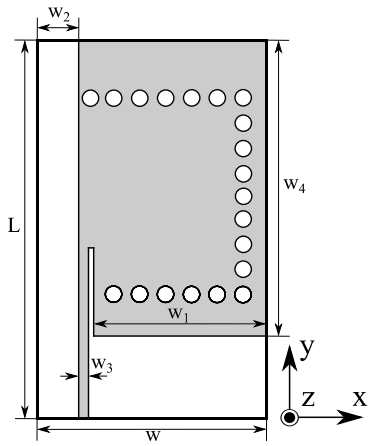

Fig. 5. Geometry of the HMSIW cavity-backed antenna (the bottom side of the antenna is fully coated by metal).

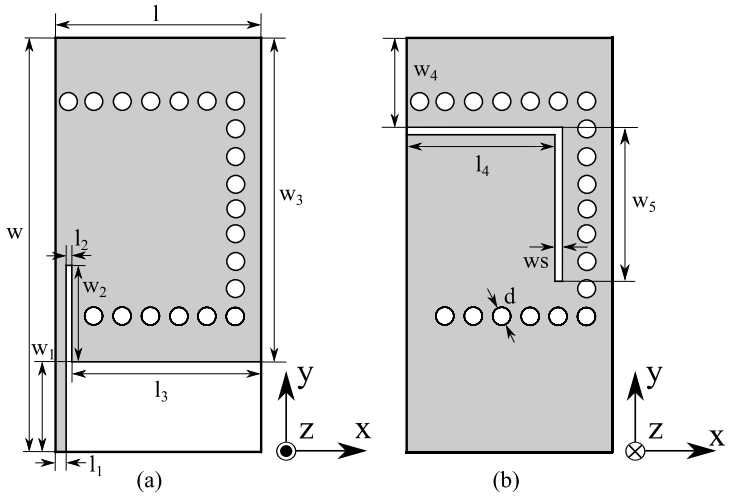

Fig. 6. Geometry of the HMSIW cavity-backed antenna with the slot: (a) top view and (b) bottom view.

The conjunction of a HMSIW cavity and a microstrip patch leads to impedance bandwidth improvement. Based on this idea, patch HMSIW cavity hybrid antennas radiating linearly (LP) and circularly polarized (CP) wave were introduced in [13] (Fig. 7). The linearly polarized wave is radiated by a rectangular patch placed at the distance *g* from the HMSIW semi-circular cavity. To generate a circularly polarized wave, the rectangular patch is substituted by a square patch with a narrow slot. As a result, two orthogonal modes with 90° phase difference are excited. The cavity is fed by a microstrip line. The feeding structure is printed on the backside of the substrate to eliminate the spurious radiation. For both types of those antennas, the measured impedance bandwidth is about 10.0%. The maximum radiation of antennas is in a broadside direction. The measured peak gain for the linearly and circularly polarized antenna are 7.5 dBi and 6.8 dBi, respectively. The measured axial ratio (AR) bandwidth for the AR<3 dB of the CP antenna is 1.0 %.

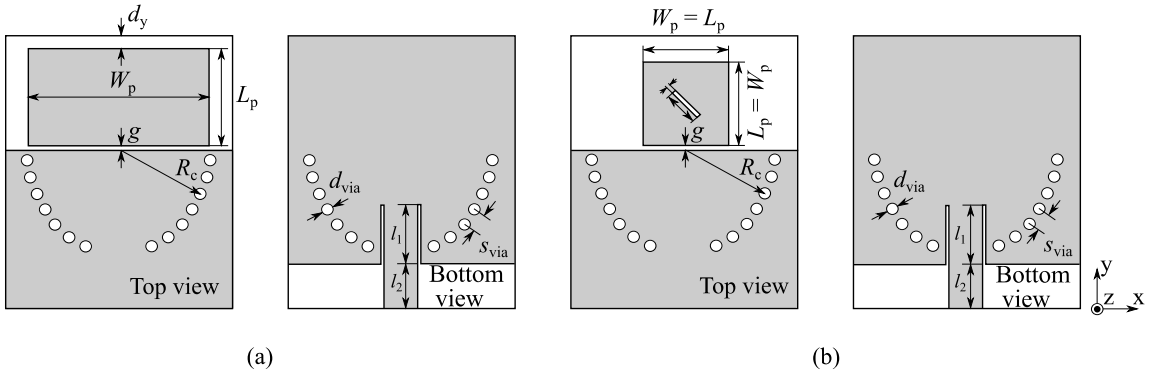

Fig. 7. Geometry of patch HMSIW cavity hybrid antennas: (a) linearly polarize version and (b) circularly polarized version.

An equilateral triangular and semi-circular antenna based on the HMSIW (Fig. 8(a) and (b)) were published in [14]. Two HMSIW semi-hexagonal antennas (Fig. 8(c) and (d)) were published in [15]. All four antennas were designed for IEEE 802.11a WLAN U-NII band applications. The properties of these antenna are summarized in Table 2. All four antennas radiate linearly polarized wave and they are compact.

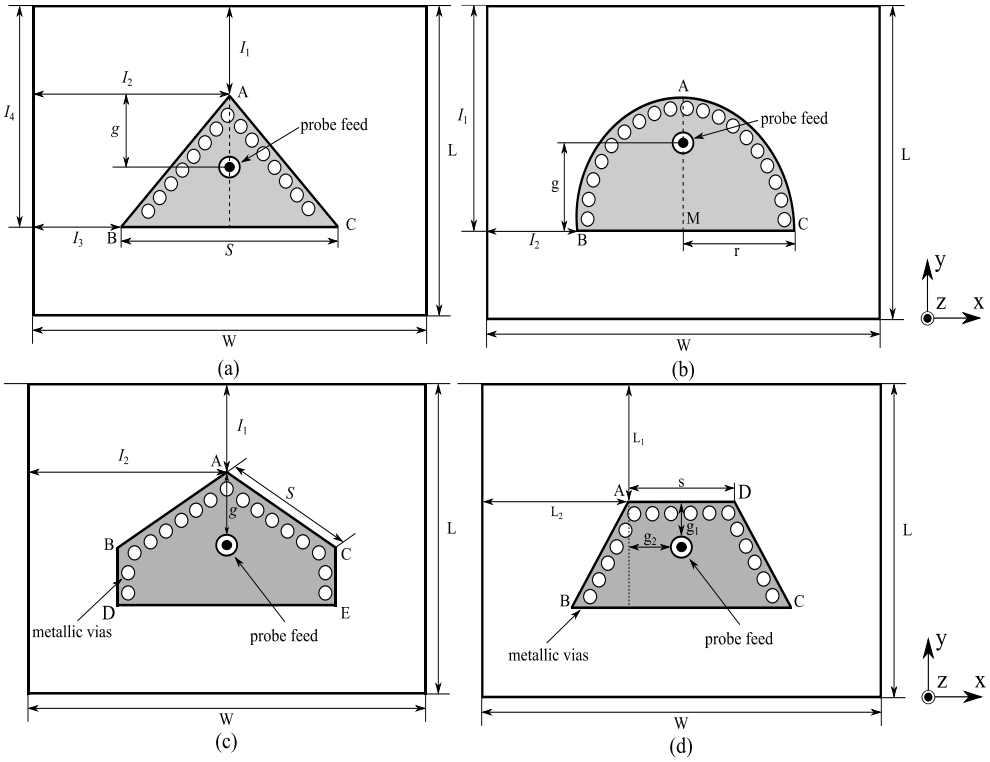

Fig. 8. Geometry of the HMSIW (a) equilateral triangular, (b) semi-circular antennas, (c) semi-hexagonal #1 and (d) semi-hexagonal #2. The bottom sides of all antenna are fully coated by metal.

Table 2. Measured results of the HMSIW triangular, semi-circular and two semi-hexagonal antennas.

Type of the antenna	Minimum of reflection coefficient [dB]	Impedance bandwidth for s_{11}<-10dB [%]	Peak gain [dBi]
triangular	-29@5.28 GHz	1	5.6
semi-circular	-25.5@5.22 GHz (sim)	0.8 (sim)	6.5 (sim)
semi-hexagonal #1	-38@5.55 GHz	0.5	5.3
semi-hexagonal #2	-33@5.8 GHz	0.9	5.5

To tune the antennas without changing their physical dimensions, a narrow slot is added into the antennas' configurations (Fig. 9(a) – 9(f)) [15 – 18]. The semi-circular antenna exploits one or two slots placed along the magnetic wall as revealed in Fig 5(c) and (d). Of course, the physical dimensions of the slot have to be determined to achieve a desirable operating frequency of the antenna. Table 3 shows the shift of the minimum of the reflection coefficient due to placing the slot for the antenna configuration depicted in Fig. 9.

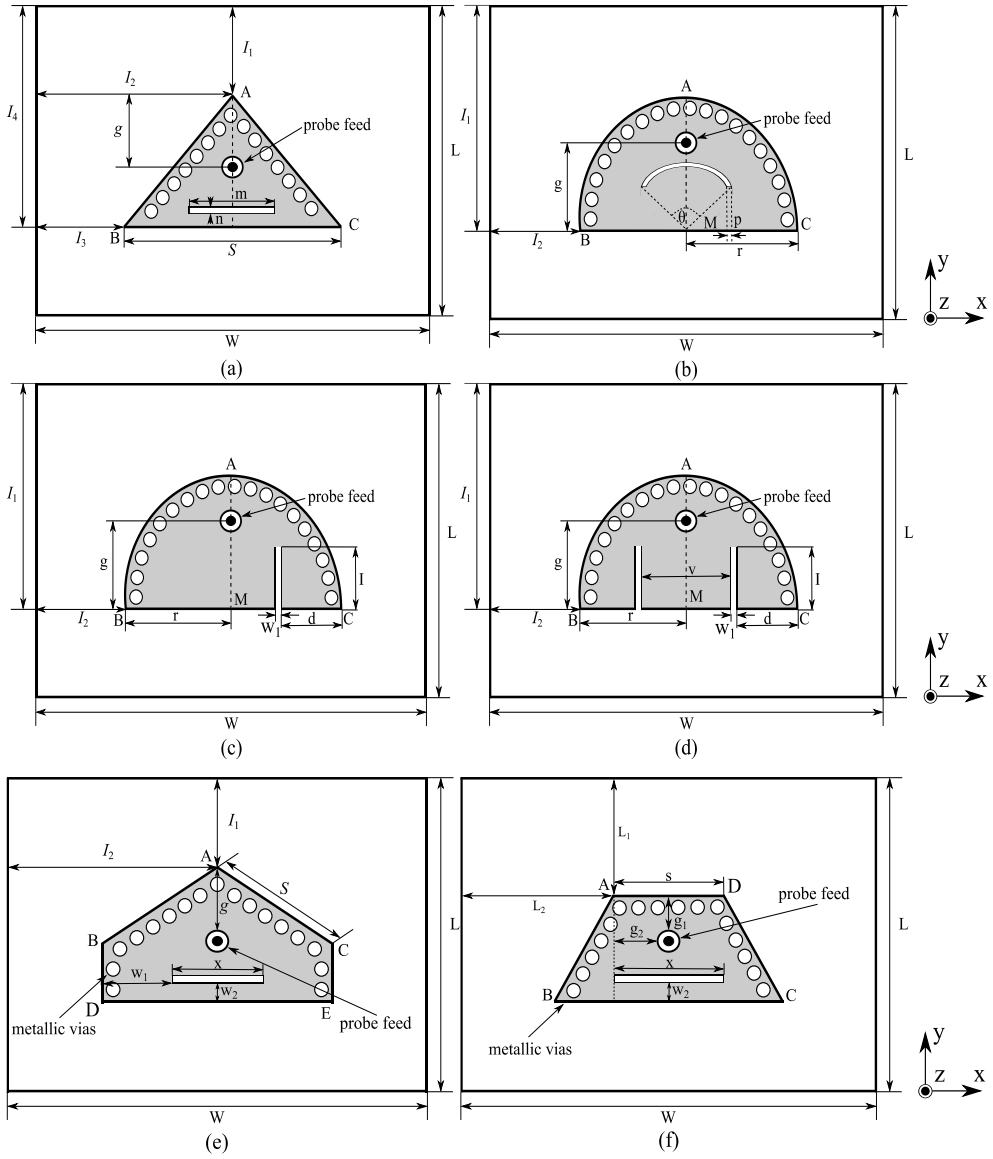

Fig. 9. Geometry of the HMSIW (a) equilateral triangular with the slot, (b) semi-circular antennas with the arc shaped slot, (c) semi-circular antennas with the slot, (d) semi-circular antennas with the two slot, (e) semi-hexagonal #1 with the slot and (f) semi-hexagonal #2 with the slot. The bottom sides of all antennas are fully coated by metal.

Table 3. Measured shift of reflection coefficient minimum.

Type of the antenna	Minimum of the reflection coefficient before placing the slot [GHz]	Minimum of the reflection coefficient after placing the slot [GHz]	Shift [MHz]
Triangular (Fig. 9a)	5.28	4.41	-870
semi-circular – arc shaped slot ($\theta = 90°$) (Fig. 9b)	5.22	4.61	-610
semi-circular – one slot (Fig. 9c)	5.22	4.65	-570
semi-circular – two slots (Fig. 9d)	5.22	3.9	-1320
semi-hexagonal #1 (Fig. 9e)	5.55	4.79	-760
semi-hexagonal #2 (Fig. 9f)	5.8	4.77	1030

An E-shaped HMSIW semi-circular antenna was published in [19] (Fig. 10). The concept of the antenna is the same as the antenna depicted in Fig. 9(d), however, instead of a coaxial probe a microstrip line is used to feed the antenna. The antenna in Fig. 9(d) can also be equipped with a microstrip line. This version of the antenna consists of a resonator and a two slots. The two symmetrical slots disturb the current path of the resonant mode, resulting in the resonant mode shifting toward lower frequency. Therefore, the open edge (magnetic wall) acts as a radiator. The measured operating frequency of the antenna is 7.55 GHz. The antenna achieves a maximum gain of 4.6 dBi and the cross-polarization level of -15 dB at the broadside direction.

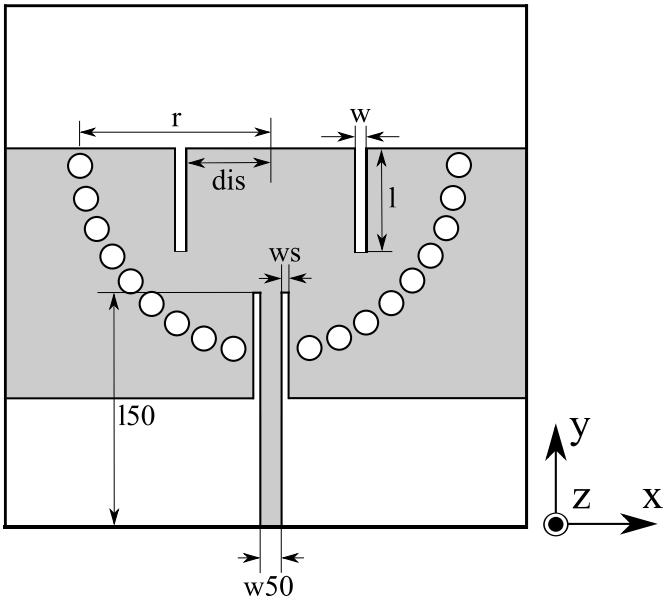

Fig. 10. Geometry of the E-shaped HMSIW semi-circular antenna (the bottom side of the antenna is fully coated by metal).

A circularly polarized HMSIW semi-circle slot antenna (Fig.11) was presented in [20]. The right-handed circular polarization is obtained with the help of two orthogonal E-fields, which are separately generated by the semi-circle slot and the longitudinal edge with a 90° phase difference. In order to achieve a wider impedance bandwidth, a matching row of vias is placed between the feeding point and the semi-circular slot. The antenna was tuned for the operating frequency of 28 GHz and achieved the measured impedance bandwidth and the axial ratio bandwidth of 12.8 % and 2.3 %, respectively. The measured peak gain was 5.54 dBi.

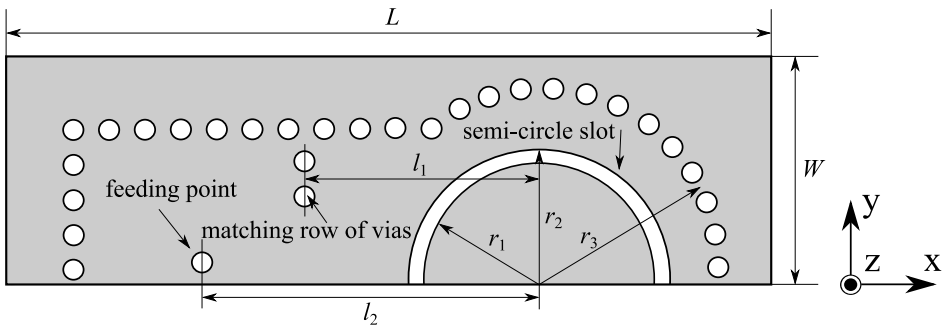

Fig. 11. Geometry of the HMSIW semi-circular slot antenna (the bottom side of the antenna is fully coated by metal).

In [21], a HMSIW slot antenna was proposed. The geometry of the antenna is depicted in Fig. 12. The antenna radiates a linearly polarized wave with the maximum radiation in the broadside direction. The impedance bandwidth of the antenna is 3.5 %. The measured peak gain is 5.6 dBi. The antenna archives very low cross-polarization level.

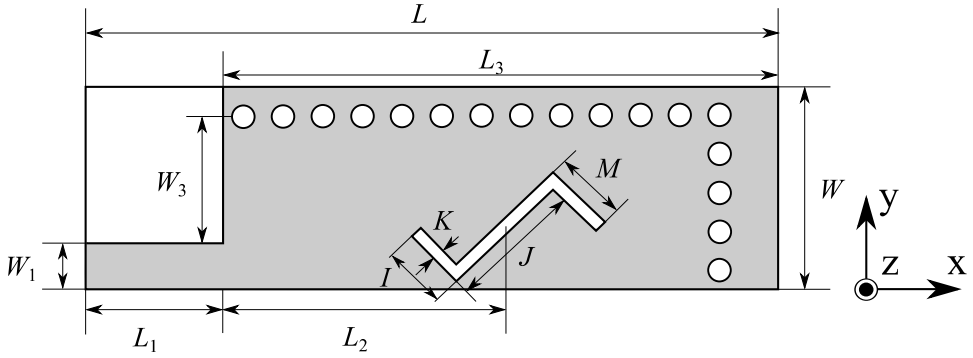

Fig. 12. Geometry of the HMSIW compact slot antenna (the bottom side of the antenna is fully coated by metal).

By using a cross slot with unequal length (Fig. 13), a two-band antenna radiating CP wave at a lower frequency band and LP wave at a higher frequency band can be obtained [22]. The simulated impedance bandwidth is 2.1 % at the lower frequency (8.25 GHz) band and 1.2 % at the higher frequency band (9.5 GHz). The antenna radiates a left-handed polarized wave with the maximum radiation in the broadside direction. The axial ratio bandwidth is 1.7 % and the gain of 5 dBi.

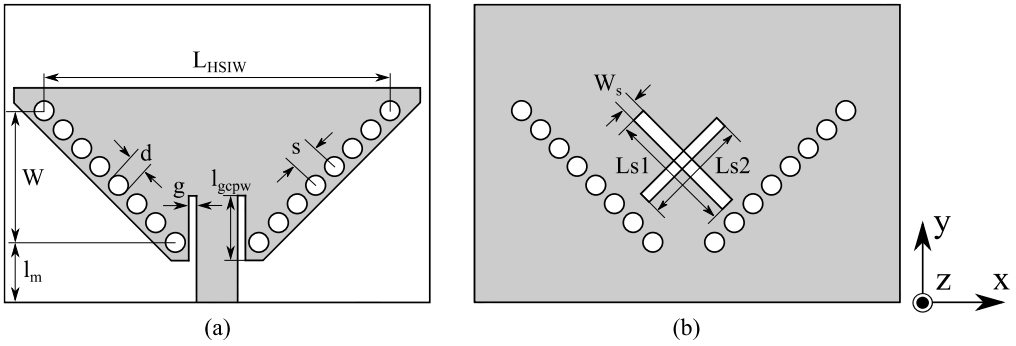

Fig. 13. Geometry of the HMSIW dual band cavity-backed antenna: (a) top view and (b) bottom view.

A very interesting solution for obtaining wider impedance bandwidth is to load a slot by a dielectric resonator. Thus, a dielectric resonator antenna (DRA) based on HMSIW is obtained [23]. The antenna was designed for the frequency band of 60 GHz and its linearly polarized version is depicted in Fig. 14(a). The antenna consists of a transverse slot used for the feeding of a dielectric resonator. This antenna configuration achieves the impedance bandwidth of 24.0 % and the gain is more than 5.5 dBi in the entire operating frequency band.

It is well known that a pair of crossed slots cut into the board wall of a rectangular waveguide can radiate circularly polarized wave if the slots are located at a position where the transverse and longitudinal magnetic field components of the dominant TE_{10} mode are equal in the amplitude. The dominant mode $TE_{0.5,0}$ in HMSIW is approximately half of the dominant mode TE_{10} in the rectangular waveguide. Based on this fact, two crossed slots for circular polarization can be centered at the spot where two orthogonal magnetic field components of the dominant $TE_{0.5,0}$ mode have an identical amplitude. The dielectric resonator is also glued on the crossed slots and the geometry of the DRA is shown in Fig.

14(b). The measured impedance bandwidth is 4.5%, the axial ratio bandwidth is 4.0% and the gain is 5.5 dBi.

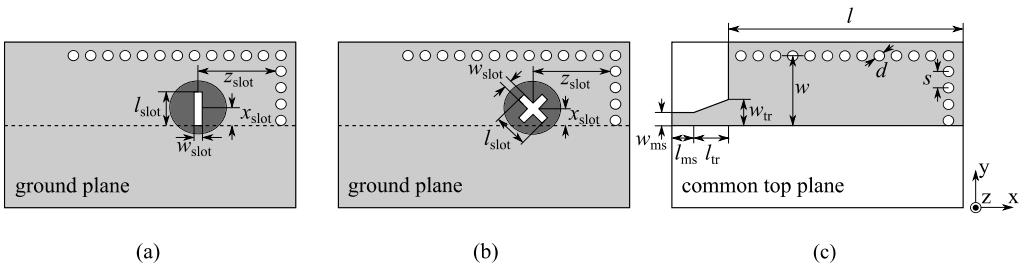

Fig. 14. Geometry of the HMSIW slot antenna loaded by the dielectric resonator with: (a) LP and (b) CP and (c) common top plane.

A dual band HMSIW cavity-backed L-shaped slot antenna was presented in [24]. The antenna consists of a two U-shaped slot (Fig. 15). In order to prevent the undesired higher orthogonal mode, a special metal via is placed between the slots. The smaller slot affects the operating frequency at the higher frequency band while the longer slot affects the operating frequency at the lower frequency band. The antenna is designed for the operating frequency of 5.8 and 7.0 GHz and it has the impedance bandwidth of 2.2 % and 2.4 %, respectively. The peak gains are 5.9 dBi and 5.1 dBi, respectively. Since the radiation efficiency of the antenna is about 75 %, this antenna concept seems perspective for practical applications.

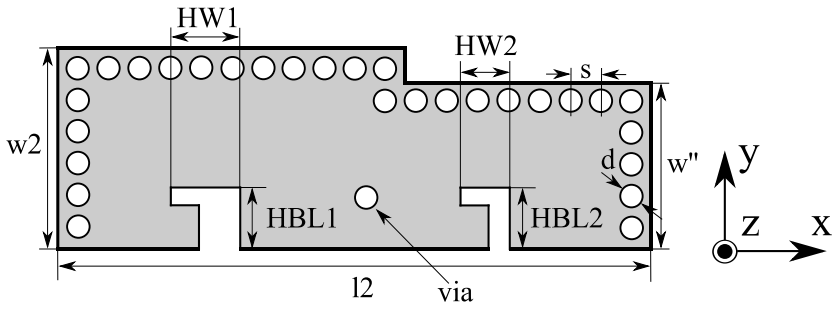

Fig. 15. Geometry of the duel band HMSIW cavity-backed U-slot antenna (the bottom side of the antenna is fully coated by metal).

2.2 Reconfigurable antennas

The rapid development of microwave wireless applications urges miniaturization of antennas with polarization diversity. Polarization reconfigurable antennas, which can offer various polarizations at the same operating frequency, has received desirable attention because they can increase performance of wireless communication systems.

In [26], a frequency reconfigurable HMSIW linearly polarized slot antenna was proposed (Fig. 16). The antenna was based on the concept of the short-ended composite right/left-handed resonator [27]. The operating frequency can be controlled by a single varactor diode placed in the interdigital capacitor slot. In order to maximize the tuning range, the varactor is placed where the magnitude of the E-field has its maximum. By changing the bias voltage from 0 to 30 V, the resonant frequency can be electronically controlled between 2.99 and 3.59 GHz. The maximum radiation of antennas is in the broadside direction. The measured gain of the antenna is lower in comparison to the other slot antennas. The peak gain is from -4 to 1.8 dBi.

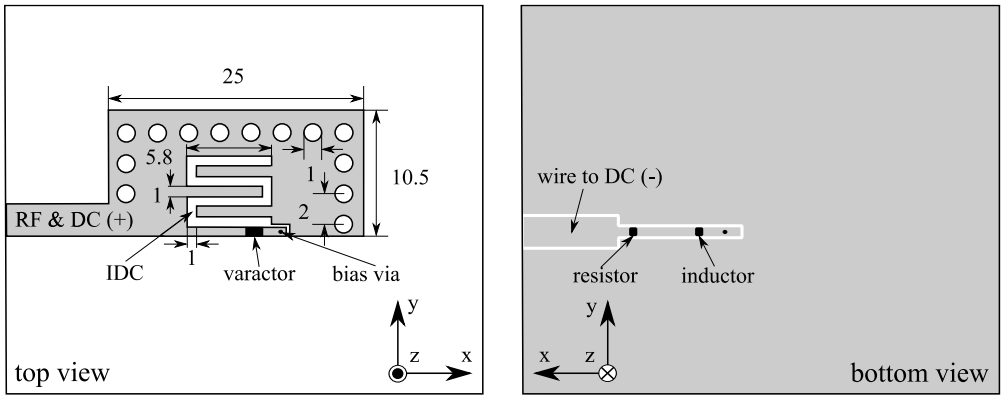

Fig. 16. Geometry of the frequency reconfigurable HMSIW antenna (a) top view and (b) bottom view.

Many various antennas operating at 2.4/5.8 GHz frequency band have been reported in [31]–[47]. These works were mainly concentrated on the design related to the switching between LP and circular polarization (CP), or between LHCP and RHCP. However, only few concepts [32], [33] and [36], which could switch between LHCP, RHCP and two orthogonal LP, were published.

Another approach for tuning a HMSIW antenna lies in changing the effective permeability μ_{eff} of a ferrite inserted into the antenna structure [28]. The yttrium iron garnet ferrite slab of the same height as the antenna substrate was embedded in the substrate (Fig. 17(a) and (b)). In order to improve the antenna radiation performance, two slots were inserted at the ground plane to change the current distribution. During experimental testing of this structure [28], two Nd-Fe-B magnets were placed above and below the ferrite slab to supply the bias magnetic field. For practical applications, the magnetic field strength could be changed by using a micromechanical processing technology such as ultrasonic motor. The frequency tunability of the proposed antenna was from 5.07 to 6.23 GHz. The gain was 1.41 dBi (5.64 GHz) and 0.61 dBi (6.23 GHz).

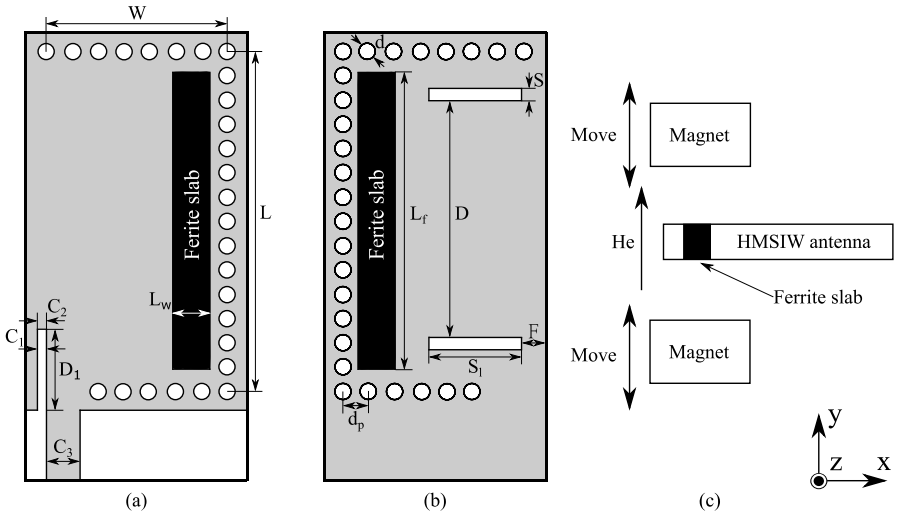

Fig. 17. Geometry of the frequency reconfigurable HMSIW antenna with ferrite slab: (a) topview, (b) bottom view and (c) measurement setup.

In [47], a reconfigurable quadri-polarization diversity aperture-coupled patch antenna was proposed. The antenna operated at 2.4 GHz and had the gain about 5 dBi and could switch among LHCP, RHCP and two orthogonal LP. However, the antenna concept was

multi-layered with dual-fed system and it required eight PIN diodes which made the antenna structure and dc-bias network very complex.

In [48], a single-fed microstrip patch antenna with switchable quadri-polarization was studied. The antenna operated at 2.4 GHz frequency band and had the gain of 6 dBi. A multi-layered patch antenna fed by two slots controlled by a monolithic microwave integrated circuit (MMIC) was reported in [49]. The antenna was designed for the operating frequency of 7.5 GHz and had the gain about of 7 dBi. In [50], a perturbed square-ring slot antenna with reconfigurable polarization was proposed. The operating frequency of the antenna was 10 GHz and had the gain about 5 dBi. The antenna could switch between LHCP/RHCP and it can be used for satellite communication. Many those antennas used PIN diodes for the polarization switching. A piezoelectric transducers (PETs) can be used as an alternative to PIN diodes for polarization switching. In [51], a polarization reconfigurable microstrip antenna using PETs was proposed. Either RHCP or LHCP could be obtained by changing the bias-voltage of two PETs at 5.8 GHz.

2.3 Other antennas based on the HMSIW

A new approach for the feeding of microstrip patch antennas was presented in [25]. The work dealt with a dual band microstrip patch antenna fed by the HMSIW for X-band applications. Two microstrip patches of different size were inserted into the HMSIW at the open edge to couple power from the HMSIW. The position of the two patches are at the distances of odd multiples of quarter wavelength from the shorted end of the HMSIW. The antenna has in the broadside direction is the gains of 8.6 dBi and 9.2 dBi at the frequencies 9.95 GHz and11.35 GHz, respectively.

An interesting concept of the antenna based on HMSIW technology was proposed in [29]. In this case, the open edge of HMSIW cavity plays the role of a radiator. The equivalent magnetic current generates an endfire radiation with a vertical linear polarization. At the two conductor arms printed on either side of dielectric substrate, the electric current generates endfire radiation with a horizontal linear polarization. For a single feed configuration, a Y-shape double side slot couple line along the diagonal of HMSIW is utilized to achieve energy coupling. The parallel strip line guaranteeing the required phase shift between the two complementary diode antennas. The antenna radiates circularly polarized electromagnetic wave with the axial ratio bandwidth of 4.31 %, the impedance matching bandwidth 2.07 % for the reflection coefficient less than -10 dB, and the gain of 4.1 dBi.

Horn antennas can be also implemented by the HMSIW technology. The HMSIW H-plane horn antenna has been introduced in [30]. The antenna is comprised by only one wall of vias and dielectric substrate. The both sides of the dielectric substrate is covered by metal sheet. The size reduction is around 32% compared to the SIW horn antenna. The antenna radiates linearly polarized wave in the H-plane with the measured gain of 5.88 dBi. The measured impedance bandwidth is only 1.18%.

Nowadays, a wearable antennas designed at Industrial, Scientific and Medical (ISM) bands (2.4, 5.8 and 61 GHz) attract a lot of attention. Antennas for on-body communication at 2.45 GHz, 5.8 GHz and 60 GHz were reported in [52] – [56]. By using brass eye-lets and a combination of conducting and non-conductive textile materials, a diamond-shape cavity backed dual-band textile antenna based on HMSIW has been reported in [52]. The antenna works at 2.4 and 5.8 GHz ISM band. The dielectric substrate is substituted by the textile with relative permittivity $\varepsilon_r = 1.495$ and loss tangent $\tan(\delta) =$

0.016. The antenna is comprised by the two slots. The small one is for tuning resonate frequency in the higher frequency band. Enlarging this small slot decreases the resonance frequency of the second-order mode and provides larger bandwidth in the higher frequency band. The measured impedance bandwidth of the antenna are 4.9 % and 5.1 % in the ISM frequency band of 2.4 GHz and 5.8 GHz, respectively. The measured peak gain of the antenna are 4.1 dBi and 5.8 dBi, in those operating frequency bands.

A compact 60-GHz tapered slot antenna printed on LCP substrate for WPAN applications has been introduced in [55]. The antenna is printed on a low-permittivity liquid crystal polymer (LCP) substrate. The antenna has the 25 % impedance bandwidth for reflection coefficient less than – 10 dB. In [56], a textile dual band-band patch antenna was presented. The antenna is comprised by an inner patch, it operates at 5.8 GHz. In [57], the authors focus on the crumbling of the antenna. It was demonstrated that heavy crumbling has negative influences on operating frequency, minimum of the reflection coefficient and radiation patterns

2.4 Antenna array based on the HMSIW

In past years, many antenna arrays based on the HMSIW have been reported [67 – 82]. The main advantage of a HMSIW antenna array is a higher gain and narrower radiation patter in comparison to a single HMSIW antenna. Slot antennas are very often used for the design of HMSIW antenna arrays. In [67], the HMSIW T-shaped slot antenna is reported. The antenna consists of three T-shaped slots arranged in a row in the shorted HMSIW. Unfortunately, the impedance bandwidth is only 2.4 % for the reflection coefficient less than – 10 dB at 8.3 GHz. The peak gain is 8.2 dBi. In [68], a HMSIW transverse slot array for X-band and Ka-band was proposed. The antenna operates in the fundamental mode $TE_{0,5;0}$. The author described equivalent circuit of the single element of the antenna and propagation of the electric filed distribution in the array antenna. The antenna operates in 2.81 % and 2.7 % impedance bandwidth in X-band and Ka-band, respectively. In X-band, the level of cross-polarization reaches higher level in the main lobe of radiation pattern due the leakage from the side open aperture. The measured peak gain is 11.7 dBi. In Ka-band, the measured gain is 10.1 dBi. A slot antenna array with omnidirectional radiation patterns was reported in [69]. The antenna consists of four narrow wall radiating slot antenna elements and a four-way power divider. The slot antenna element realizes energy radiation from the open side of the HMSIW by etching several pairs of transversal slots both on the upper and the lower surfaces of the HMSIW and alternately arranging the slot pairs. A HMSIW four-way power divider is achieved to feed the slot antenna elements by loading four metallic vias to guide the surface currents into the HMSIW branches. The antenna operates at 3 GHz with measured impedance bandwidth of 2.3 % for reflection coefficient less than -10 dB. The measured peak gain is 5.8 dBi.

In [70], another approach of design of the HMSIW antenna array was proposed. The leaking electric filed from the open edge of HMSIW is utilized to feed the narrow rectangular patches located near the edge on the same layer. Due to the coupling gap between open edge and the rectangular patch, the patches act like a radiating element meanwhile the HMSIW serves as a transmission link. The authors designed the HMSIW antenna array with two radiating patches with the same dimensions. The antenna array works in two frequency band of 24 GHz and 60 GHz. The peak gain is 6.44 dBi and 8.1 dBi.

A Leaky Wave Antenna (LWA) is a guided-wave structure that allows leakage of energy along its longitudinal direction. A LWA with beam steering capability is introduced in [71]. The beam steering is carried out by capacitors connected to the open edge of the HMSIW and to the row of vias located along the open edge of the HMSIW. The antenna steers the main beam at different values of capacitances. When the capacitance of the capacitors is 0.1 pF or 3 pF, the direction of the main beam is 57° or 36 °. The antenna operates at 24 GHz. The antenna gain ranges from 11 dBi to 14.5 dBi.

3. Objectives of the Thesis

The HMSIW is very interesting feeding technique to reduce size of antennas with preserving all advantages compared to the SIW. Apart from the antenna technology, it can be also exploited for the design of microwave circuits, like filters, power dividers, couplers, etc. Thanks to the high attention to the HMSIW and slot antennas, several HMSIW antennas have been developed with good impedance and radiating performance.

It is indispensable that every presented antenna has own design procedure. Unfortunately, the published antennas are usually described superficially and the design guide usually missing. A deeper description needs to be focused to propagating of higher modes in the antenna, surface current and electric field in the substrate. In addition, there is high demand about antenna radiators who are able to control its polarization.

Based on the above comments and the state of the art presented in the previous chapter, the objectives of thesis can be formulated as follows:

- Detail description of novel concepts of HMSIW slot linearly and circularly polarized antennas with focus on achieving better HMSIW slot antenna performance.
- Exploitation of obtained knowledge in the previous objective of the thesis for the design of antenna arrays. Detail description of antenna arrays based novel concepts of HMSIW slot antennas should be given.

4. HMSIW U-Shape Slot Antenna

This chapter deals with the first objective of this thesis. The research is focused on the HMSIW U-shaped slot antenna radiating linearly and circularly polarized wave. These antennas were proposed in [58] and [59]. Detail description of the linearly polarized antenna was proposed in [83]. The attention of this chapter is further concentrated on a polarization reconfigurable version of this antenna proposed in [60].

4.1 Linearly Polarized HMSIW U-Shape Slot Antenna

In this chapter, a linearly polarized HMSIW U-shape slot antenna [58] is proposed and described. It is based on the SIW version of the antenna published in [63]. The SIW version of the antenna achieves measured impedance bandwidth of 4.3 % and simulated peak gain of 8.2 dBi, and it is fed by a coaxial probe. In the HMSIW version of the antenna, it seems that feeding via coaxial probe is not suitable due to a high sensitivity of the coaxial probe position to the impedance matching of the antenna. So it was observed that it is better to exploit for the antenna feeding a grounded coplanar waveguide (GCPW) – to HMIW transition.

4.1.1 Antenna structure

The antenna structure is depicted in Fig. 18. The dielectric substrate of the length L, the width W, and the height h with the relative permittivity ε_r, and the loss tangent tan(δ) is on its both sides covered by metal sheets. The U-slot antenna with the length $L_{\text{slot-x}}$ in x-direction and $L_{\text{slot-y}}$ in y-direction is printed with the (GCPW) transition at the end of the shorted waveguide at the distance L_{viaX} from its short end in the x-direction, and from the solid wall of HMSIW at the distance L_{viaY} in the y-direction. The slot is located at the distance $L_{\text{GWC-SLOT}}$ from the GCPW. The slot is shorted by two shorts S_1 and S_2.

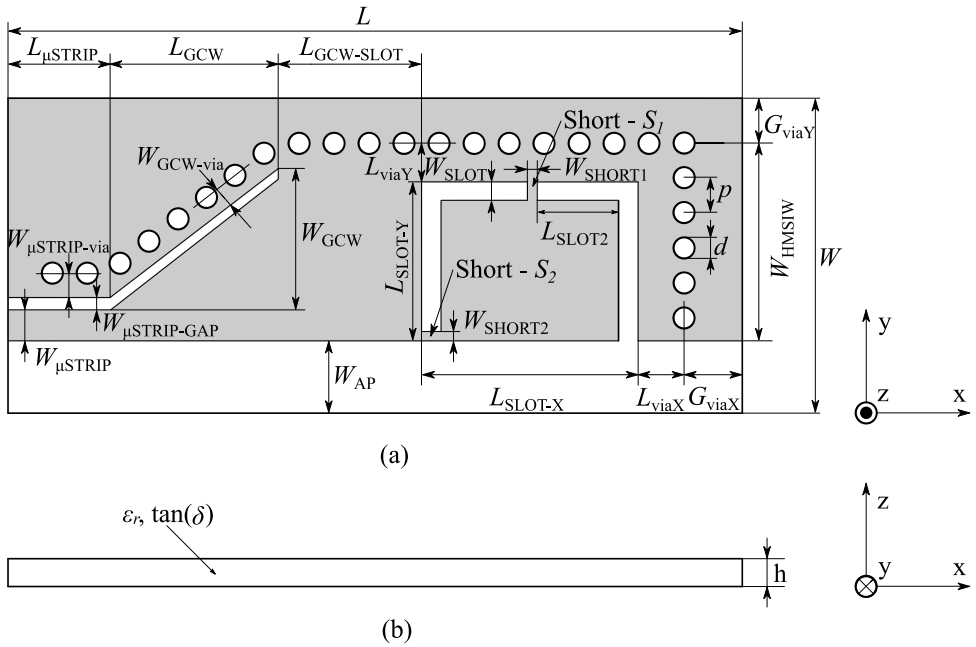

Fig. 18. Top (a) and side (b) view of the linearly polarized antenna (the bottom side of the antenna is fully coated by metal).

4.1.2 Simulated Results

The linearly polarized antenna was simulated and tuned in CST Microwave Studio (MWS) by the time domain solver for the operating frequency band of 10 GHz. In order to reduce computing time during calculation the simulation of the antenna, vias of HMSIW were substituted by a solid wall made of the PEC (perfect electrical conductor). The waveguide operates in the fundamental mode $TE_{0.5;0}$ with the cutoff frequency of 5.99 GHz. The antenna is designed on the dielectric substrate ARLON Cuclad 217 with relative permittivity $\varepsilon_r = 2.17$, tangent loss $\tan(\delta) = 0.0009$ and height $h = 1.524$ mm. This substrate is chosen due to low losses. The physical dimensions of the slot antenna are summarized in Table 4.

The simulated reflection coefficient is depicted in Fig. 19. The antenna achieves the minimum of the reflection coefficient at 10 GHz with reflection coefficient – 24.01 dB. The simulated impedance bandwidth of the antenna is 3 % for the reflection coefficient less than –10 dB. The simulated radiation patterns of the antenna in the E-plane (xz-plane) and H-plane (yz-plane) are shown in Fig. 20. The maximum of radiation is perpendicular to the antenna plane, but it is shifted by 5 degrees due to parasitic radiation of the GCPW-HMSIW transition. The simulated gain of the antenna is 6.55 dBi and the level of the cross-polarization is about -18 dB in the broadside direction. The propagation of surface currents and electric filed in the substrate (Fig. 21 and 22) indicates that the antenna radiated linearly polarized wave.

Table 4. Dimensions of the antenna.

Dimension	[mm]	Description	Dimension	[mm]	Description
L	31.2	length of the substrate	W_{GCW}	5.2	width of the GCPW
$L_{\mu STRIP}$	6.4	length of the μstrip line	W_{SLOT}	1.1	width of the slot
L_{GCW}	3.8	length of the GCPW	W_{SHORT1}	0.5	width of the short S_1
$L_{GCW\text{-}SLOT}$	3.8	distance between the GCPW and the slot	W_{SHORT2}	0.4	width of the short S2
$L_{SLOT\text{-}X}$	12.4	slot length in x-direction	G_{viaX}	3.0	distance between the HMSIW and the end of the substrate in x-direction
$L_{SLOT\text{-}Y}$	7.1	slot length in y-direction	G_{viaY}	3.0	distance between the HMSIW and the end of the substrate in y-direction
L_{SLOT2}	4.7	distance between the slot and the short S_2	W_{HMSIW}	8.4	width of the HMSIW
L_{viaX}	1.7	distance between the slot and the row of vias in x-direction	$W_{\mu STRIP}$	1.9	width of the μstrip line
L_{viaY}	1.3	distance between the slot and the row of vias in y-direction	W_{AP}	3.0	width of the aperture
W	14.4	width of the substrate	h	1.524	width of the dielectric substrate
$W_{\mu STRIP\text{-}GAP}$	0.7	gap between the μstrip line and the HMSIW	d	1.4	diameter of the via
$W_{\mu STRIP\text{-}via}$	1.3	distance between the μstrip line and the wall of vias	p	2.58	distance between vias
$W_{GCV\text{-}via}$	1.1	gap between the GCPW and the HMSIW			

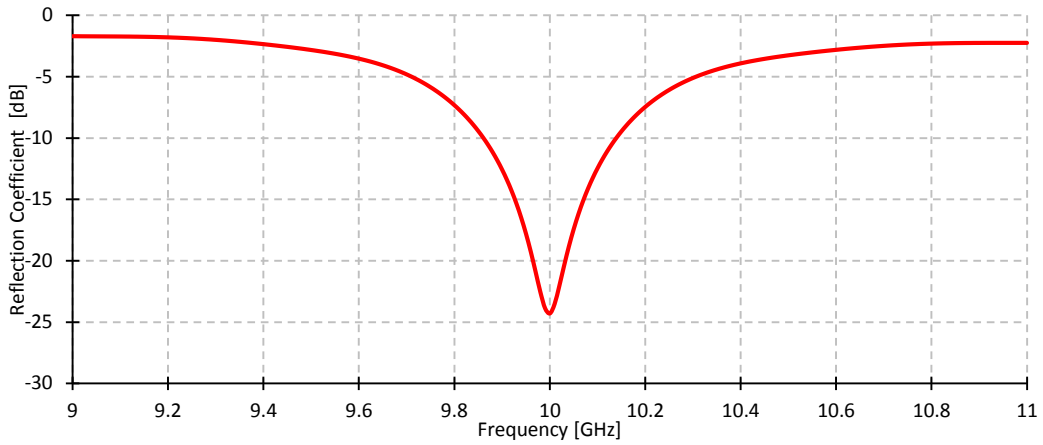

Fig. 19. Simulated reflection coefficient of the linearly polarized antenna.

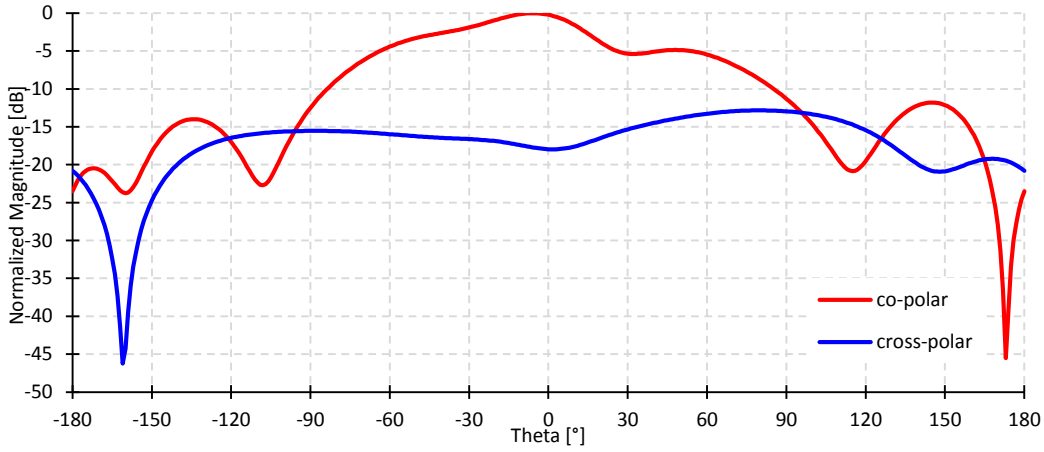

(a)

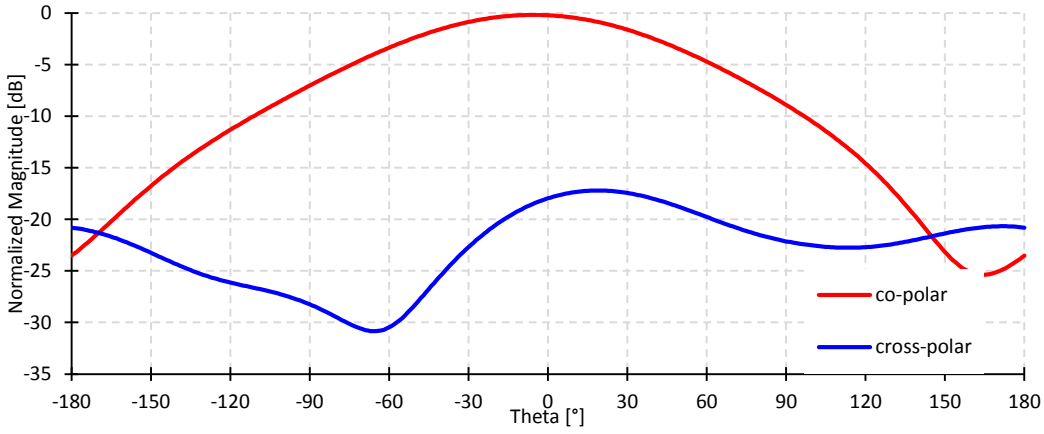

(b)

Fig. 20. Simulation of normalized magnitude of the antenna in (a) E-plane and (b) H-plane.

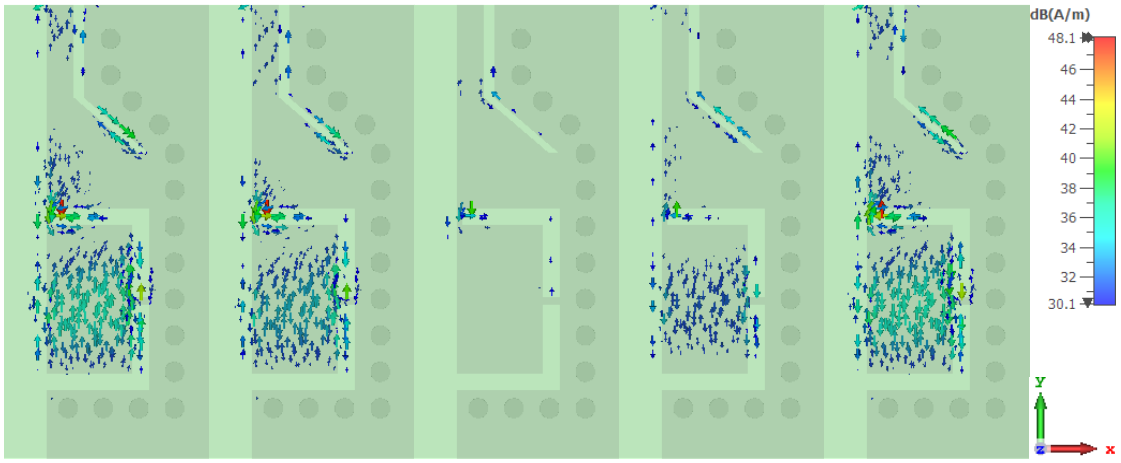

(a) (b) (c) (d) (e)

Fig. 21. Propagation of Surface currents: (a) phase = 0° and (b) phase = 45°, (c) phase = 90°, (d) = phase 135° and (e) phase = 180°.

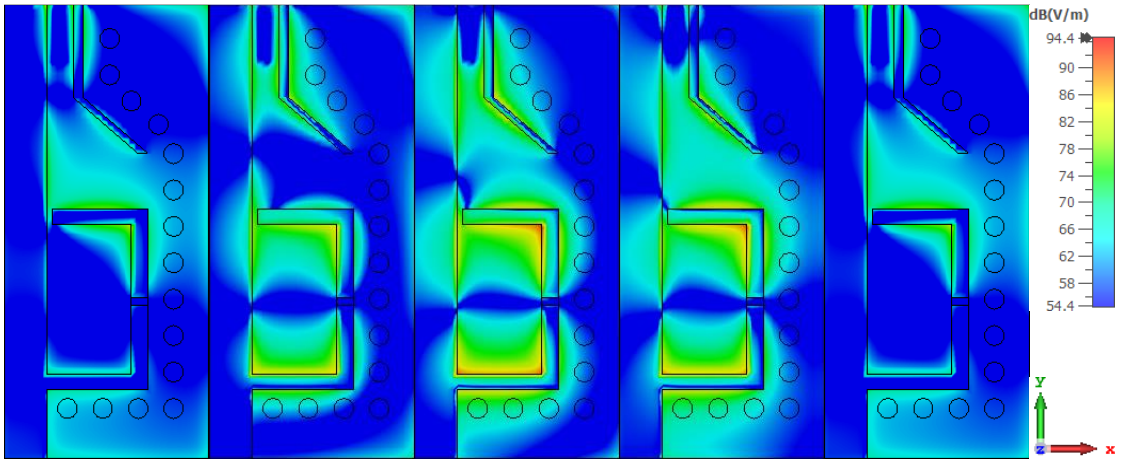

(a) (b) (c) (d) (e)

Fig. 22. Distribution of electric field intensity in substrate (magnitude): (a) phase = 0° and (b) phase = 45°, (c) phase = 90°, (d) = phase 135° and (e) phase = 180°.

4.1.3 Experimental Verification

This section provides a measured results of the antenna [58]. The antenna dimensions are summarized in Table 4. The antenna was fabricated by a low-cost etching PCB process. The antenna is equipped with soldered SMA coaxial connector to carry out a conventional coaxial measurement. The manufactured sample of the antenna is depicted in Fig 23.

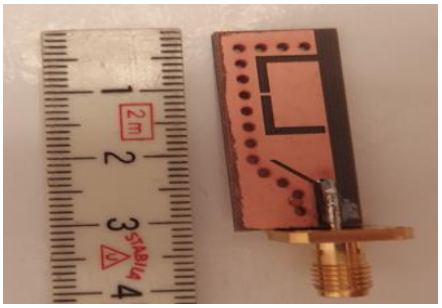

Fig. 23. Fabricated sample of the proposed HMSIW U-slot antenna.

The reflection coefficient was measured in a laboratory environment, the radiation patterns for the Theta range from –90° to 90° were measured in an anechoic chamber. For the measurement, Rohde&Schwarz vector network analyzer ZVA67 was used. The measured reflection coefficient is shown in Fig. 24. It is in relatively good agreement in comparison to the simulated one. The measured reflection coefficient is about 80 MHz shifted to lower frequencies due to the manufacturing tolerance. The fabricated sample of the antenna achieves the impedance bandwidth of 3.2 % for the reflection coefficient less than – 10 dB.

The normalized radiation patterns in two orthogonal cutting planes are depicted in Fig. 25. The measurement was done in an anechoic chamber for the Theta range from -90° to 90°. In the E-plane, the radiation pattern is shifted about 10° in comparison to the simulated results due parasitic radiating of GCPW and manufacturing tolerance. In the H-plane, the simulated and measured values are in good agreement. The simulated and measured gain of the antenna is 6.55 dBi and 6.01 dBi, respectively. The measured level of cross-polarization is – 24 dB in the broadside direction.

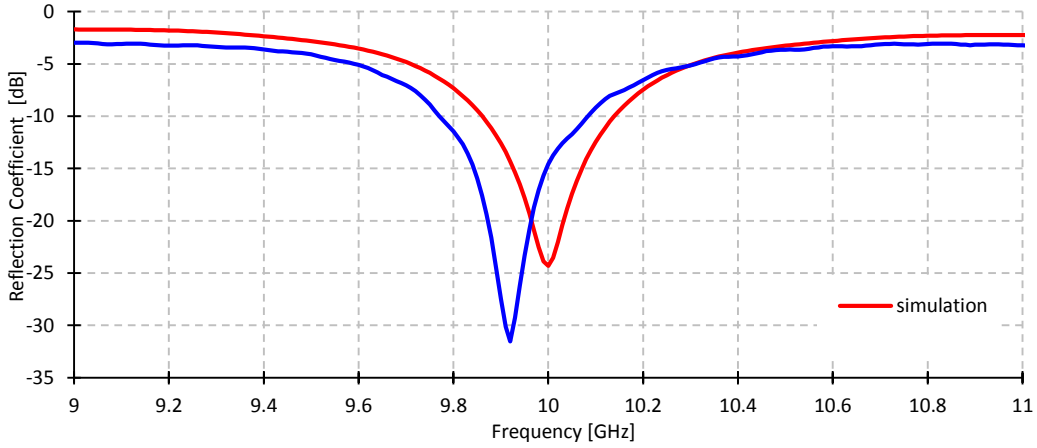

Fig. 24. Reflection coefficient of the proposed antenna.

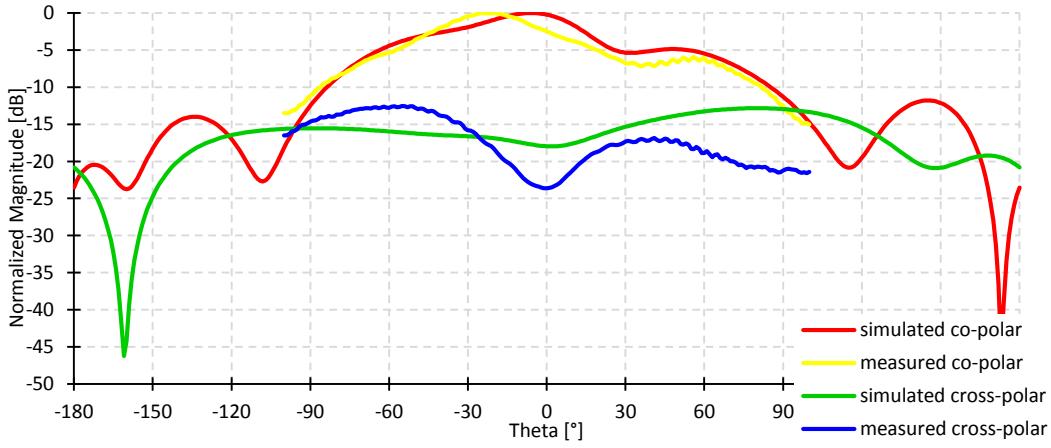

(a)

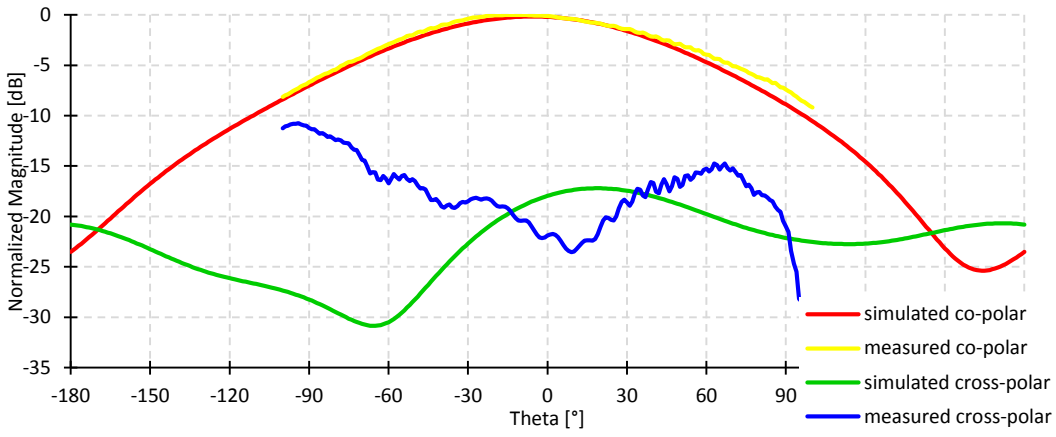

(b)

Fig. 25. Normalized radiation patterns of the proposed antenna in (a) E-plane and (b) H-plane.

4.1.4 Characteristic Modal Analysis

In order to better understand to the behavior of the antenna especially at higher frequencies, a characteristic modal analysis (CMA) is carried out. The investigated antenna was tuned at 10 GHz and the CMA was performed with the help of CST MWS. The antenna was investigated considering finite size of the lossless dielectric substrate, however, the ground was considered as infinite matching the boundary condition $E_t = 0$. The dimensions of the investigated antenna are shown in Table 4.

The CMA was performed in the frequency range from 3 GHz to 18 GHz. The first ten modal significances (MSs) in comparison to the reflection coefficient are shown in Fig. 26. Based on the well-known theory of the CMA [62], all modes that are above 0.8 can be effectively excited at a given frequency. Based on the results, the antenna operates in the mode #5. At the lower frequencies, only 4 modes could be exited. Thus, the antenna could operates with a more narrow frequency band at a lower frequency. On the other hand, at higher frequencies, more modes can be excited close to each other, so that the antenna could operates with a wider impedance bandwidth. The resonating frequencies of every mode are listed in Table 5.

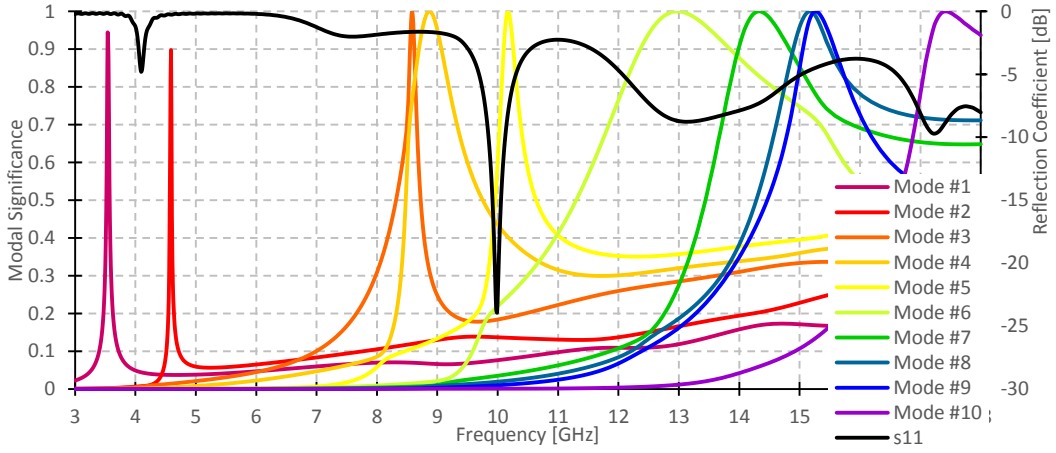

Fig. 26. CMA – Modal significance.

Table 5. Resonant frequency of the modes.

mode #	1	2	3	4	5	6	7	8	9	10
f_r **[GHz]**	3.54	4.59	8.58	8.87	10.17	12.98	14.33	15.17	15.27	17.43

Modal surface currents can generally tell which mode is suitable for the excitation and which is not. Based on the modal surface currents, antenna radiation patterns can be calculated. The usual requirement for such a kind of antenna is that a suitable mode should be able to create a radiation pattern whose maximum is perpendicular to an antenna plane. This requirement is fulfilled by the exciting mode #2 or #5, where J_n represents the modal surface current of the mode n (Fig. 27). It is obvious that the part of the modal surface currents J_4, J_6, J_8, J_9 and J_{10} are out of the antenna area bounded by the HMSIW. These modes are not suitable for the excitation because they are bounded to the outer dimensions of the substrate (W and L depicted in Fig. 18). That means the maximum of the modal significance of these modes are varies with the outer dimensions of the substrate.

The calculated radiation patterns are depicted in Fig. 28. F_n represents the radiation patterns of the mode n. Thanks to the distributions of the modal surface currents J_2 and J_5, the maximum radiation is in a direction which is perpendicular to the antenna plane (F_2 and F_5 in Fig. 28) Based on the reflection coefficient depicted in Fig. 26, only the mode F_5 is used.

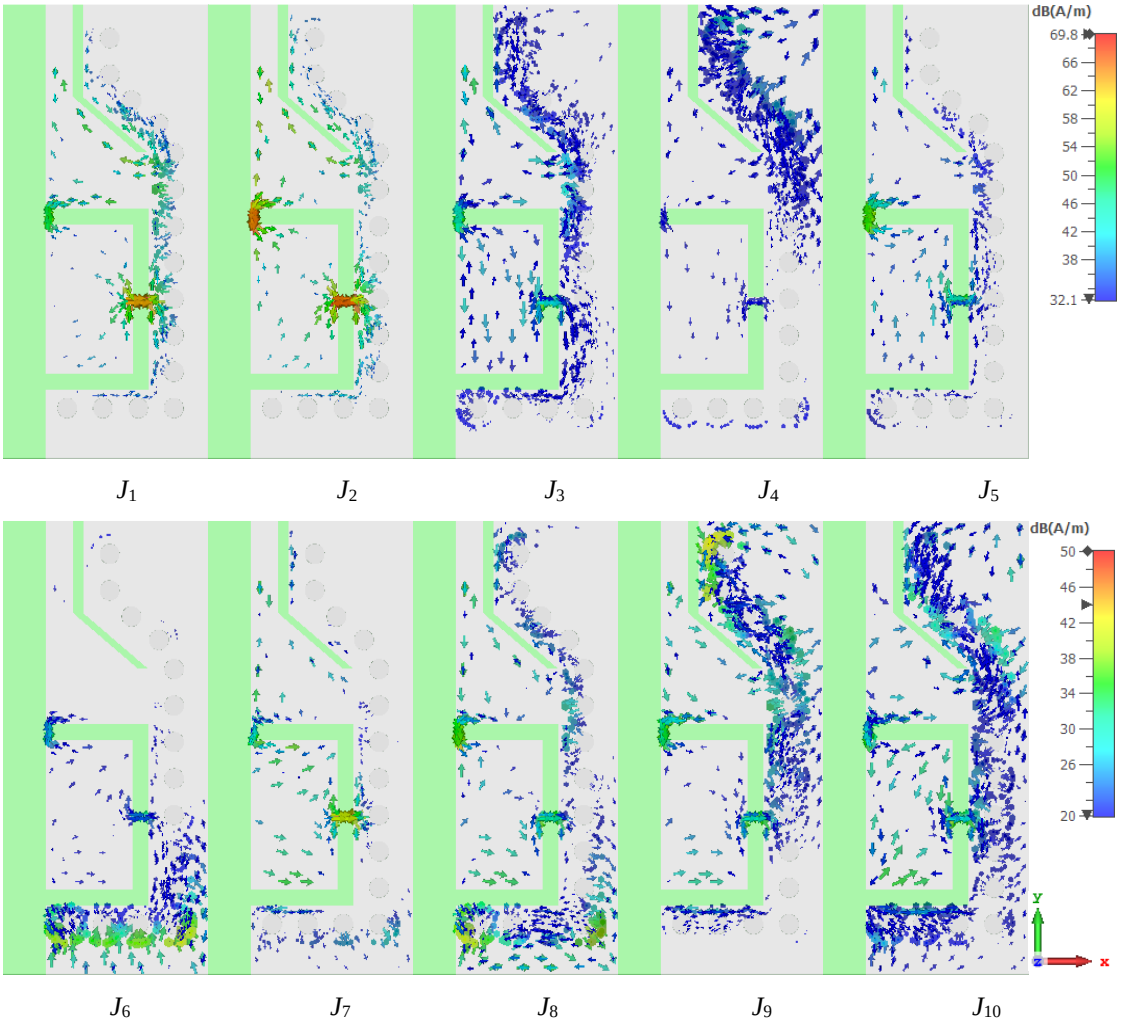

Fig. 27. CMA – Modal surface currents.

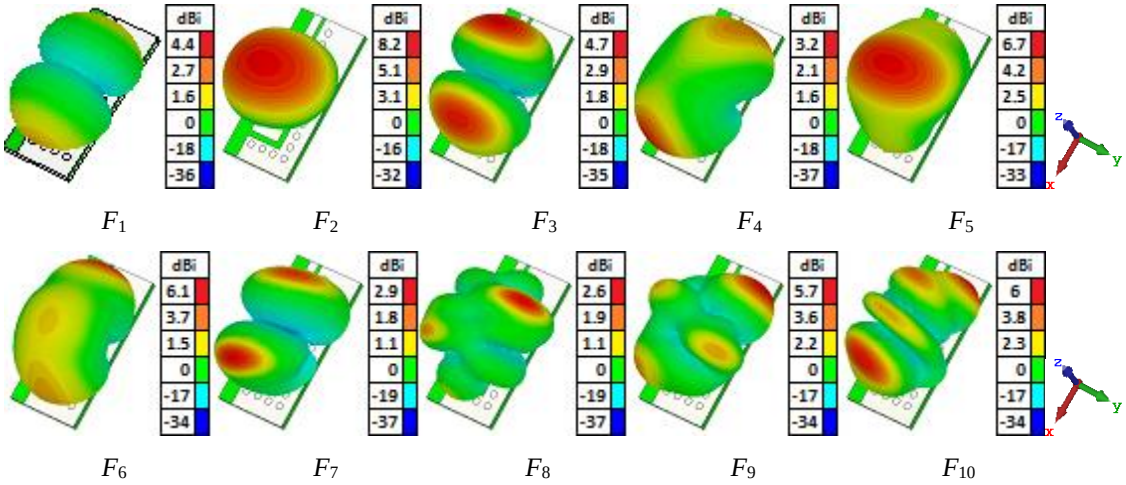

Fig. 28. CMA – Radiation patterns.

4.1.5 Parametric Study

Now, the parametric study of the antenna is carry out to demonstrate the effect of antenna geometrical parameters on the reflection coefficient, co-polarization and cross-polarization. During this study all parameters given in Table 4 are considered as a constant and only the following selected parameters are varied: the length of the antenna in the x-direction L_{slot_x}, the length of the antenna in y-direction L_{slot_y}, the width of the slot W_{slot}, and the distance L_{viaX} between the slot antenna and the shorting wall of the HMSIW. These parameters are swept with the step size of 0.25 mm to mainly consider a manufacturing inaccuracies that might occurred during the manufacture process.

The results of parametric study are depicted in Fig. 29 – 32. Obviously, the length L_{slot_x} greatly affects the impedance matching and the operating frequency while the co-polarization and the cross-polarization are affected minimally. Decreasing the slot length $L_{SLOT\text{-}X}$ leads to the improvement of the impedance matching and the shift of the reflection coefficient minimum towards higher frequencies. Decreasing of the length L_{slot_y} leads to the deterioration of the impedance matching and the level of cross-polarization in both planes in broadside direction. The level of co-polarization is affected minimally. The variation of the slot width W_{slot} strongly affects the impedance matching and the operating frequency. The influence on the level of the cross-polarization is small and the influence on the level of the co-polarization is minimal. Varying of the distance L_{viaX} between the antenna and the wall of vias slightly affects impedance matching of the proposed antenna. It has zero effect to the co-polarization and cross-polarization.

Considering the parametric study it can be concluded that the operating frequency dominantly depends on (the $L_{slot\text{-}X}$). Fine tuning and the impedance matching of the antenna can be carried out by the length of the slot in y-direction and the width of the slot ($L_{slot\text{-}Y}$ and W_{slot}).

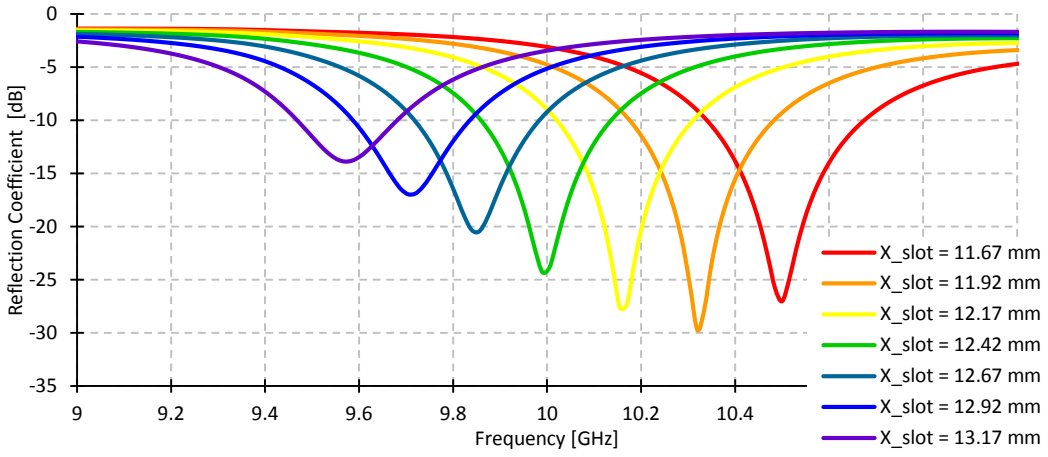

(a)

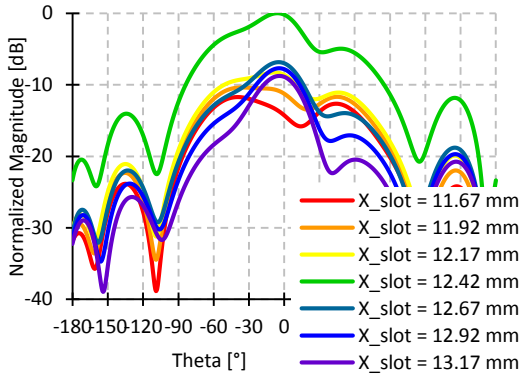

(b)

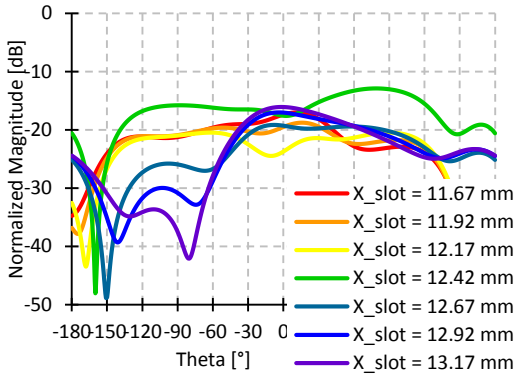

(c)

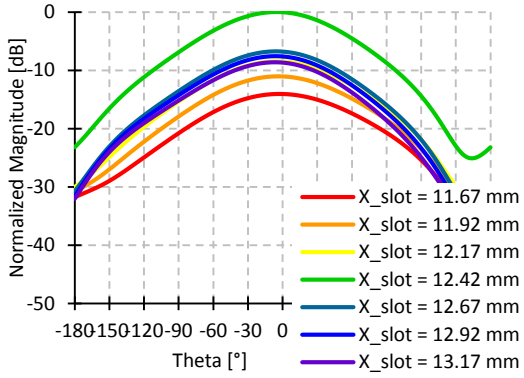

(d)

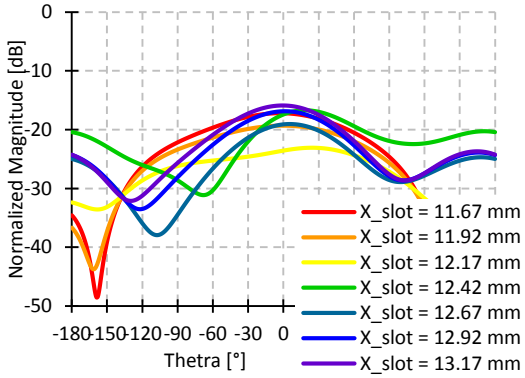

(e)

Fig. 29. Variation of the length L_{slot_x}.

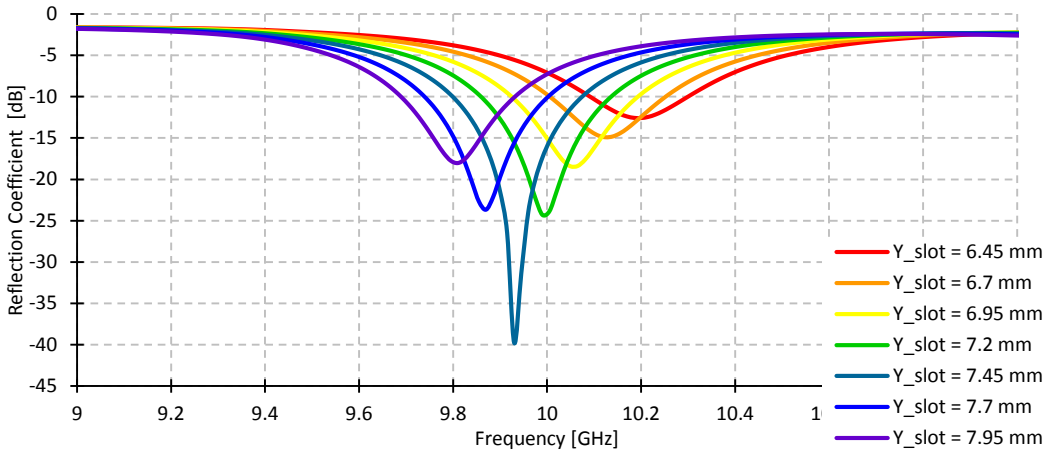

(a)

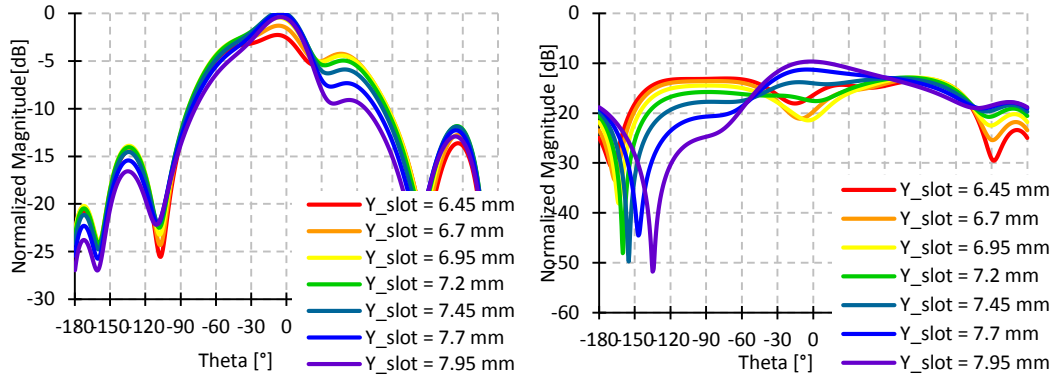

(b)

(c)

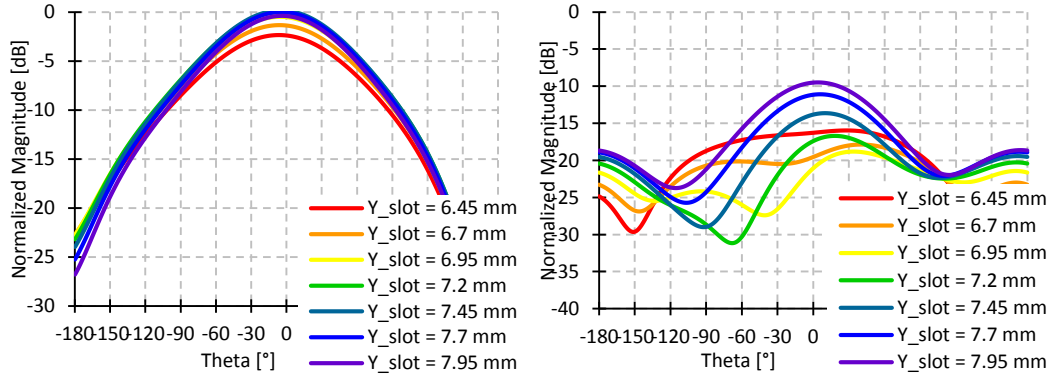

(d)

(e)

Fig. 30. Variation of the length L_{slot_y}.

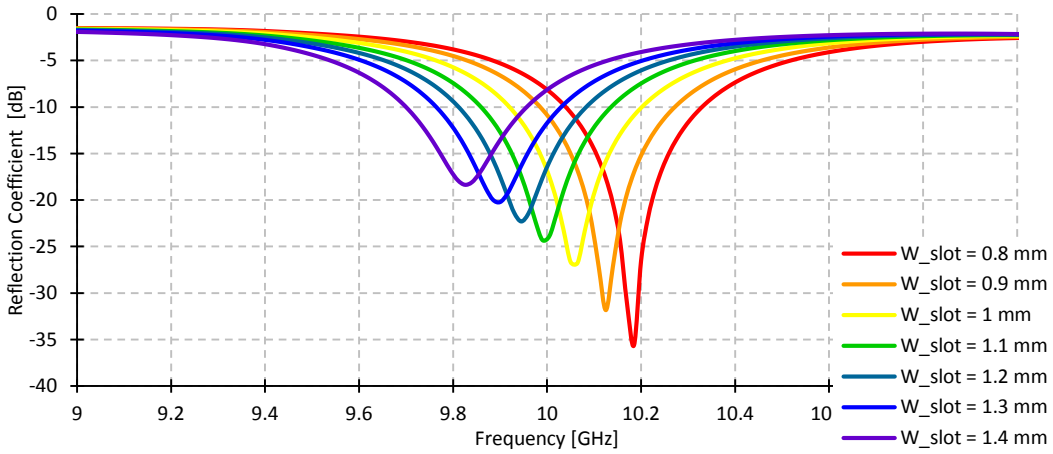

(a)

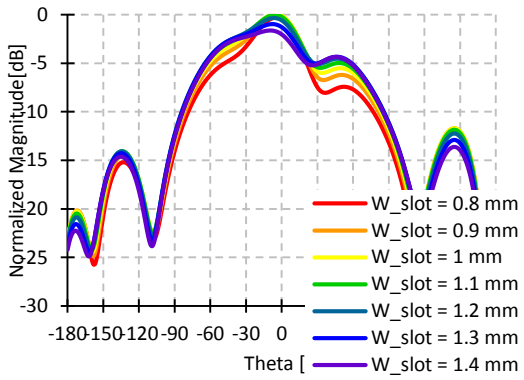

(b)

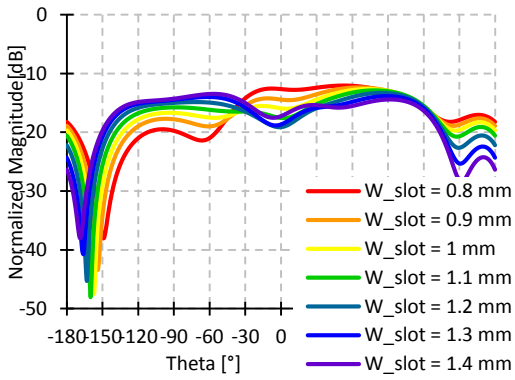

(c)

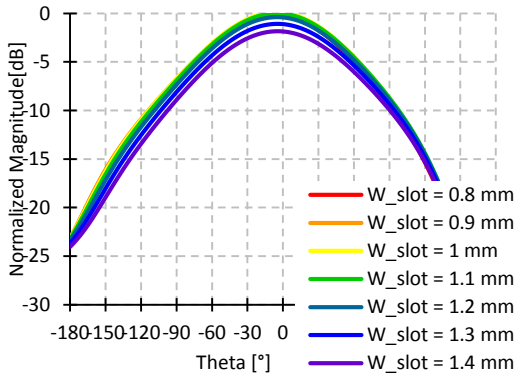

(d)

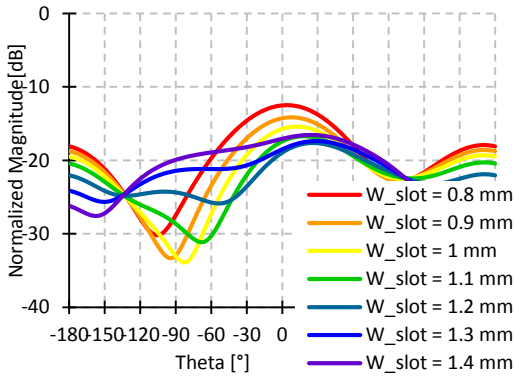

(e)

Fig. 31. Variation of the length W_{slot}.

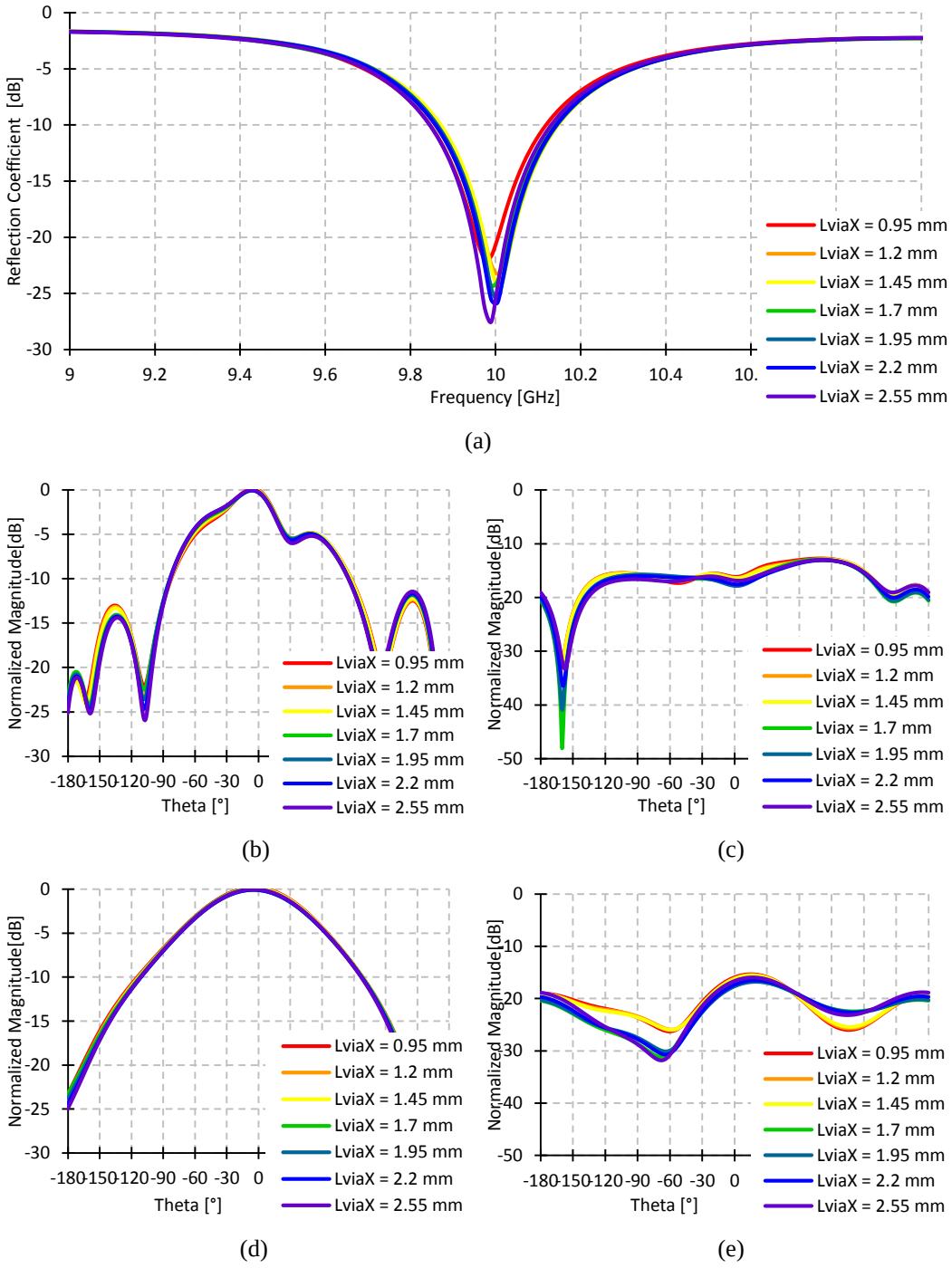

Fig. 32. Variation of the shift of the short S1.

4.1.6 Design Guide

Based on the above study, a design guide can be proposed. The antenna operating frequency depends mainly on the length $L_{SLOT\text{-}X}$ of the antenna in the x-direction. The length of the slot $L_{SLOT\text{-}Y}$ in the y-direction (Fig. 33) and the width of the slot W_{SLOT} slightly influences the operating frequency. However, they have significant effect on the impedance matching of the antenna. The distance L_{viaX} between the slot antenna and the shorting wall of the HMSIW slightly influences the operating frequency and the reflection coefficient. Therefore, the design guide is created only from the viewpoint of the reflection coefficient. The dielectric substrates listed in Table 6 were used to create the

design guide. It was created by tuning the antenna on dielectric substrates for the operating frequency f_o = 2 – 19 GHz with a step of 1 GHz.

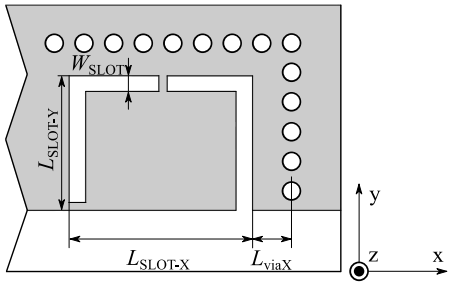

Fig. 33. The selected parameters for the design guide.

Table 6. Dielectric substrates used for design guide.

Substrate	**ε_r [-]**	**tg(δ)**	***h* [mm]**
FoamClad	1.25	0.0035	1.86
CuClad 217	2.17	0.0009	0.79
Arlon25N	3.38	0.0025	0.76
Arlon 600	6.15	0.003	1.58

The first step of the design process begin with choosing an appropriate dielectric substrate. Generally, the appropriate dielectric substrate for antennas should have lower values of the relative permittivity to support maximum radiation, low losses, desired height and stable properties.

The second step of the design process is determining the physical dimensions L_{SLOT-X}, L_{SLOT-Y}, L_{viaX}, W_{SLOT} and the width of the HMSIW. For this purpose, the physical dimensions can be easily deducted from Fig. 34(*a* – *e*). The equations were created by gradual retuning of the antenna on the substrates listed in Table 6. The frequency step of each tuning was 1 GHz. After tuning, the change of the dimensions of the antenna with respect to the nominal value is extracted and the trend link as the $k_x(f)$, $k_y(f)$, $k_f(f)$ and W_{HMSIW} are noted in the Table 7. The curves mentioned in Fig. 34(*a* – *e*) are based on the equations (1 – 4)

$$L_{slot-X} = 0.6\lambda_m k_x(f), \quad [mm, mm, -] \quad (1)$$
$$L_{slot-Y} = 0.35\lambda_m k_y(f), \quad [mm, mm, -] \quad (2)$$
$$L_{viaX} = 0.4\lambda_m k_f(f), \quad [mm, mm, -] \quad (3)$$
$$W_{slot} = 0.045\lambda_m, \quad [mm, mm, -] \quad (4)$$

where λ_m is a wavelength at an operating frequency in a dielectric substrate and k_x(f), k_y(f) and k_f(f) are correction factors. The correction factors are expressed numerically in Tab 7.

Table 7. Correction factors $k_x(f)$, $k_y(f)$ and $k_f(f)$ and width W_{HMSIW}.

Substrate	f_o [GHz]	h [mm]	$k_x(f)$	$k_y(f)$	$k_f(f)$	W_{HMSIW} [mm]
FoamClad	2 – 19	1.86	$-0.00064\,f_o$ $+1.0615$	$-0.0019f_o$ $+0.9418$	$-0.0026f_o +$ 0.414	$158.01f_o^{-1.085}$
CuClad 217	2 – 19	0.79	$-0.0025\,f_o +$ 1.0093	$-0.002f_o +$ 1.0908	$-$ $0.0012f_o+0.3141$	$82.991f_o^{-0.959}$
Arlon 25N	2 – 39	0.76	$0.0012\,f_o +$ 1.0285	$0.0016f_o +$ 1.1477	$-3.10^{-5}f_o +$ 0.9935	$70.91f_o^{-0.959}$
Arlon 600	2 – 40	1.58	$0.0006\,f_o +$ 1.0429	$0.0072f_o +$ 1.0237	$0.0052f_o +$ 0.7165	$63.09f_o^{-1.147}$

The final step of the design procedure deals with the fine tuning of the antenna at the desired operating frequency with the help of a local optimization procedure, e.g., Trust Region Framework or Nedler Mead Simplex Algorithm which are implemented in CST MWS. However, other local optimization procedures can also be exploited.

If the design process takes place on a different dielectric substrate than mentioned in Table 6, the following simplified design rules can be used in order to tune the designed antenna at the desired operating frequency. The length $L_{SLOT\text{-}X}$ and $L_{SLOT\text{-}Y}$ should be $0.6\lambda_m$ and $0.35\lambda_m$, respectively. The λ_m is the wavelength in the dielectric substrate at the design frequency. Obviously, the width of the slot W_{SLOT} depends on the portion of λ_m, e.g., $\lambda_m/45$. The distance L_{viaX} between slot antenna and shorting wall of HMSIW should be $0.3\lambda_m$. The width of the HMSIW W_{HMSIW} can be determined by the help of equations (8) – (13) published in [61]. Two conditions of the design of the HMSIW has to be met: the HMSIW operates in the fundamental mode $TE_{0.5,0}$ and the operating frequency of the antenna is approximately 1.5 times higher than the cut-off frequency of the fundamental mode $TE_{0.5,0}$. However, for the finalization of the design, a local optimization procedure should be used.

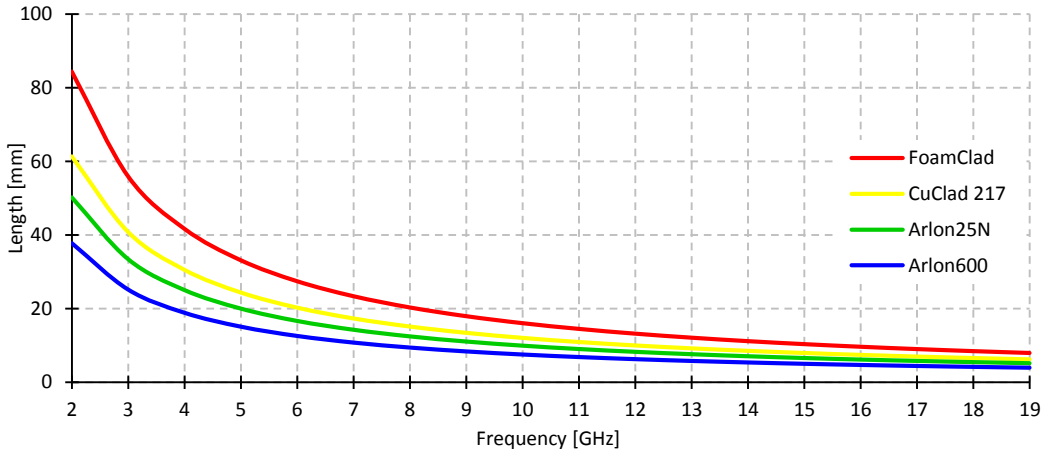

(a)

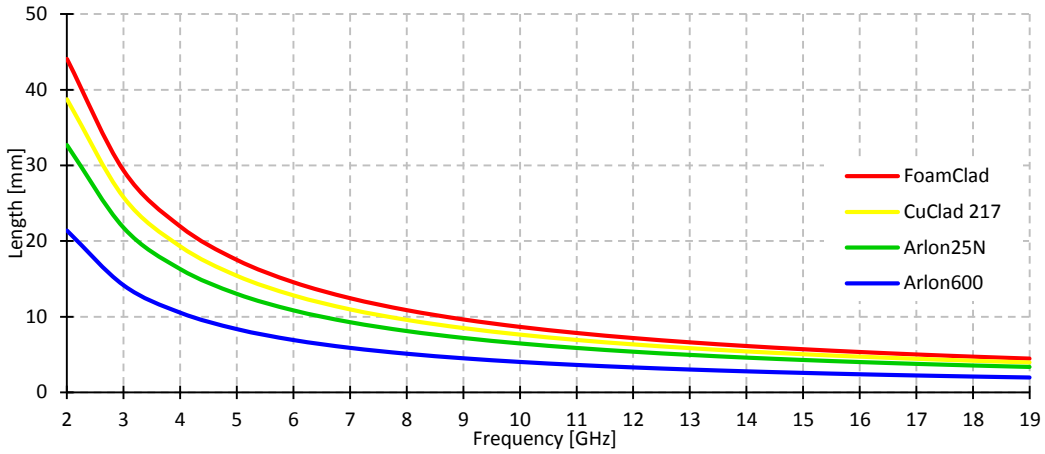
Length [mm]
Frequency [GHz]
FoamClad
CuClad 217
Arlon25N
Arlon600

(b)

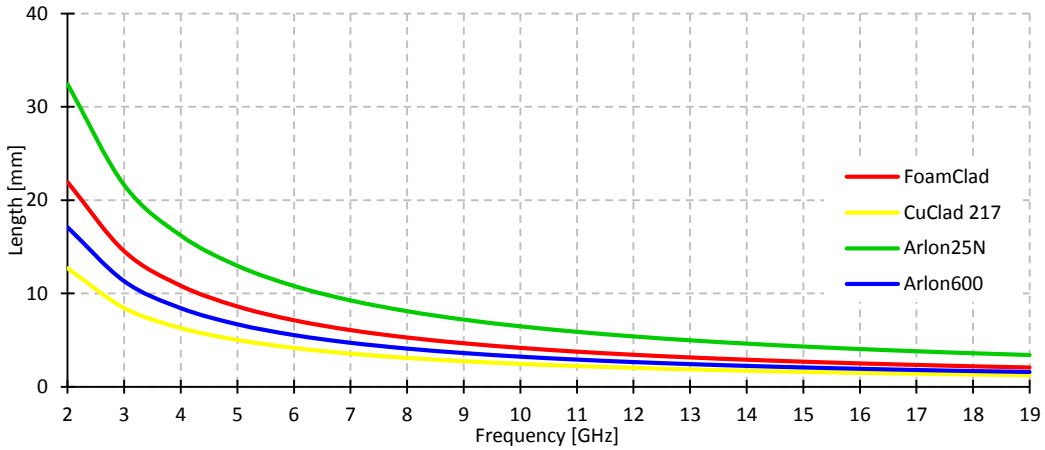
Length [mm]
Frequency [GHz]
FoamClad
CuClad 217
Arlon25N
Arlon600

(c)

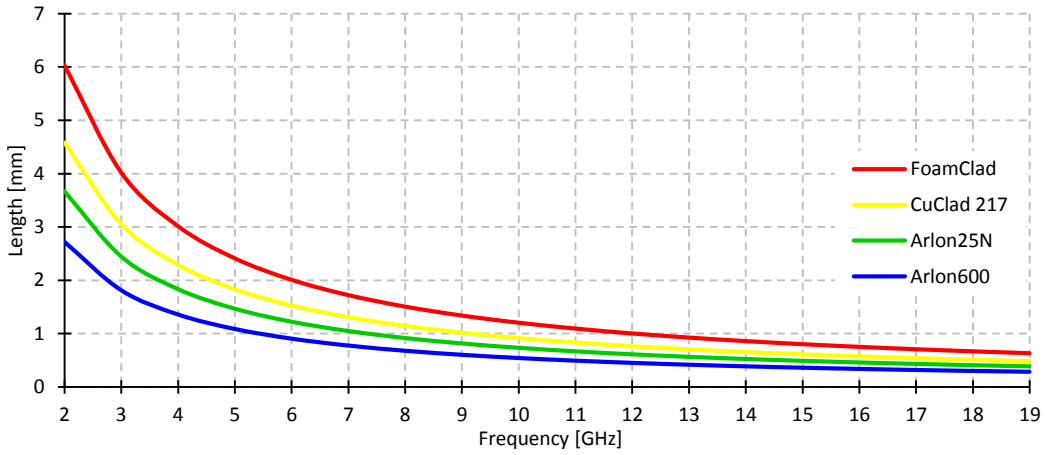
Length [mm]
Frequency [GHz]
FoamClad
CuClad 217
Arlon25N
Arlon600

(d)

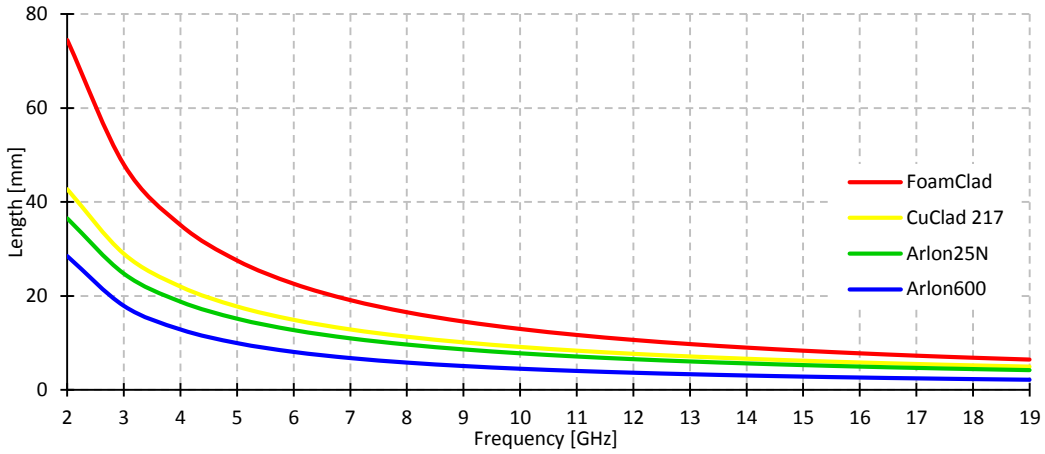

(e)

Fig. 34. Physical dimension of (a) $L_{SLOT\text{-}X}$, (b) $L_{SLOT\text{-}Y}$, (c) L_{viaX}, (d) W_{SLOT}, (e) W_{HMSIW}.

4.1.7 Experimental Verification

To verify the proposed antenna design guide experimentally, several antennas were designed by the proposed design guide at operating frequency mentioned in Table 8. The operating frequencies were chosen randomly from the frequency range f_o = 2 – 19 GHz. The antennas were designed using the time domain solver of CST MWS. The optimization technique called Trust Region Framework was used to optimize the antenna for a desired operating frequency band. After finishing optimization, the antennas were fabricated by a low-cost etching PCB process. Fabricated sample of the antennas are depicted in Fig. 35.

Table 8. Operating frequency of the antennas.

Substrate	f_o [GHz]
FoamClad	10
CuClad 217	12
Arlon25N	8
Arlon 600	7

The antenna reflection coefficients were measured in a laboratory environment and are shown in Fig 36. In the case of Fig. 36(*b*) and (*c*), there is a good agreement between the measured and simulated results. On the other hand, the measured coefficient depicted in Fig. 36(*a*) and (*d*) are slightly different in comparison to the simulated ones. In case *a*, the dielectric substrate FoamClad is easily bendable. Therefore, the measured minimum of reflection coefficient is slightly shifted to the lower frequencies. In case *d*, the reflection coefficient is shifted thanks to the inaccurate manufacture process.

The radiation patterns for the Theta range from –90° to 90° were measured in an anechoic chamber. For the measurement, Rohde&Schwarz vector network analyzer ZVA67 was used. In Figs. 37 – 40 the normalized radiation patterns in two orthogonal planes are depicted. The measurement was done in an anechoic chamber for the Theta range from -90° to 90°. The measured gain in comparison to the simulates one of the antennas is presented in Table 9. The measured patterns might be slightly shifted due to parasitic radiation of the GCPW and manufacturing tolerance.

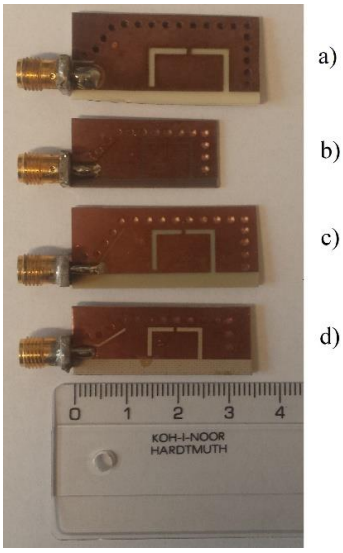

Fig. 35. Fabricated sample of the antennas: (a) FoamClad, (b) CuClad 217, (c) Arlon 25N, (d) Arlon 600.

Table 9. Measured and simulated gain in E-plane.

Substrate	Measured peak gain [dBi]	Simulated peak gain [dBi]
FoamClad	7.4	7.5
CuClad 217	6.7	7.6
Arlon25N	5.6	5.6
Arlon 600	5.7	5.8

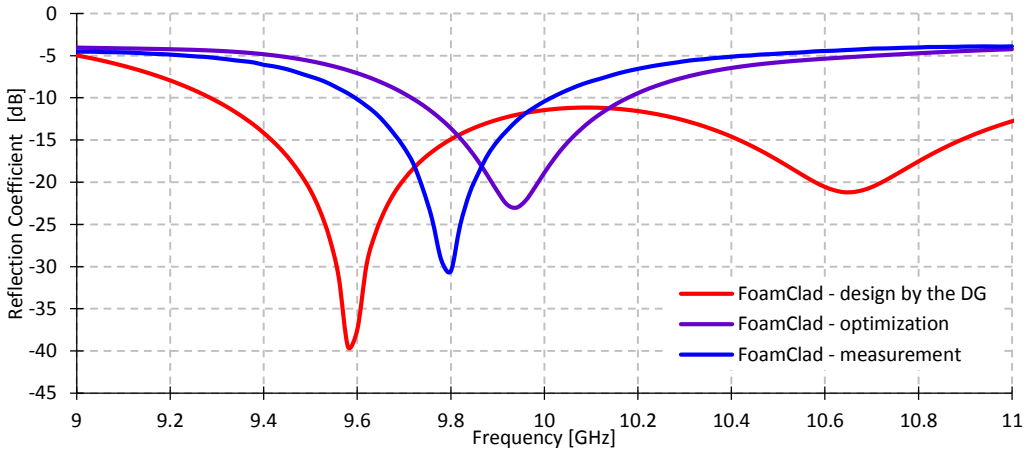

(a)

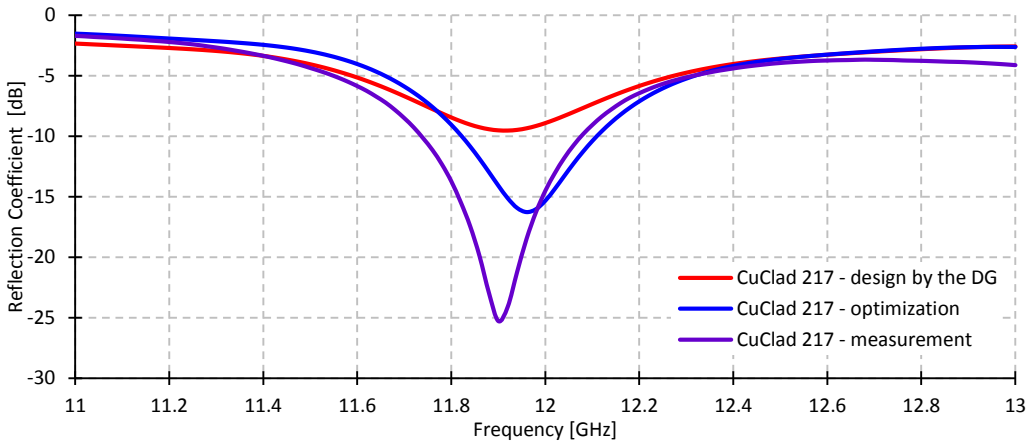

(b)

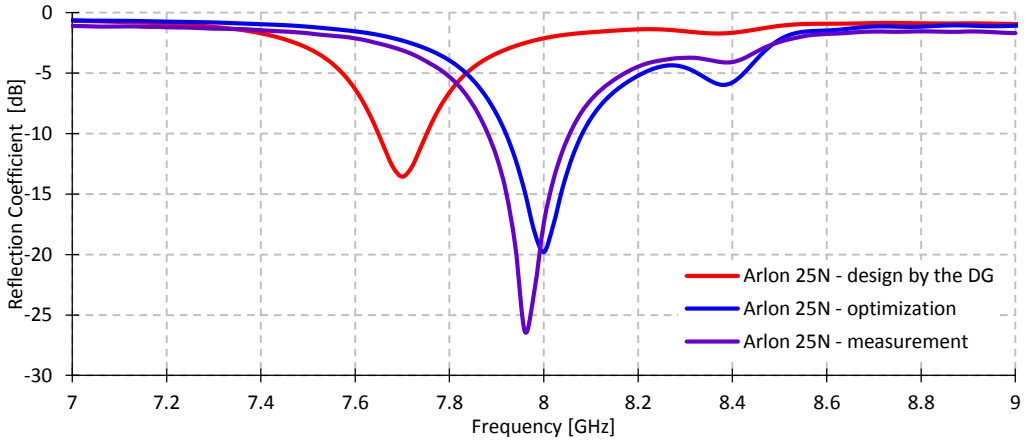

(c)

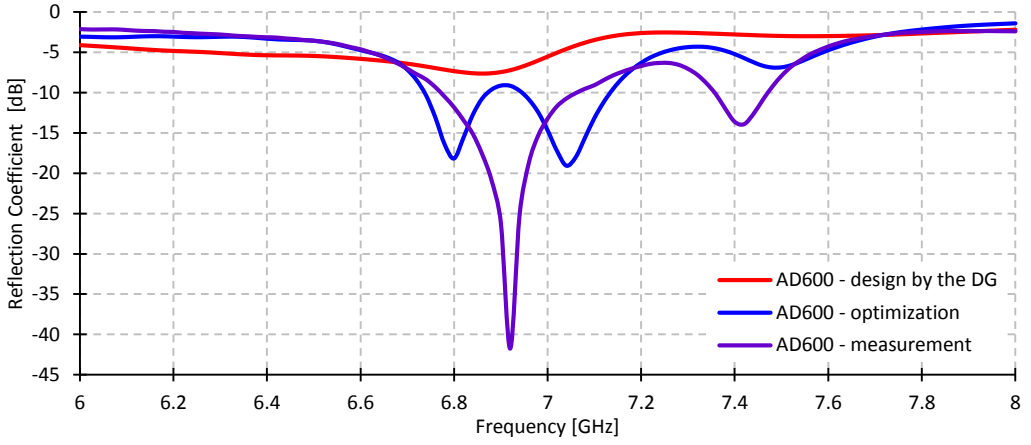

(d)

Fig. 36. Reflection coefficient (a) FoamClad, (b) CuClad 217, (c) Arlon25N, (d) Arlon 600.

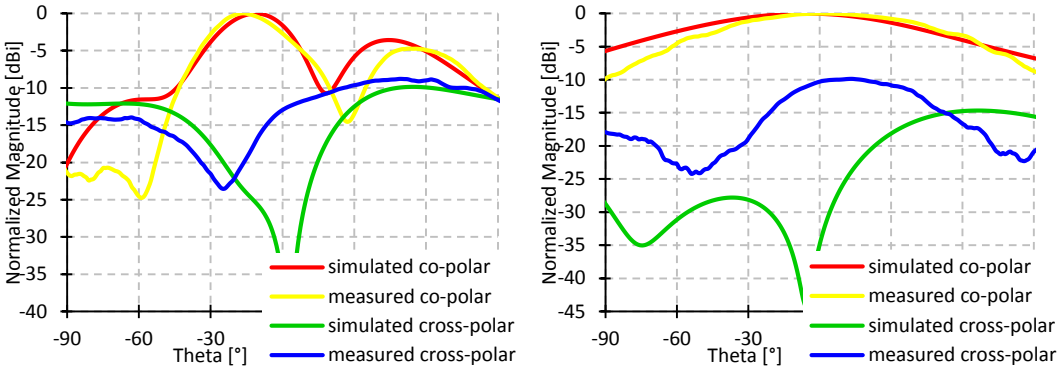

(a) (b)

Fig. 37. Normalized magnitude measured at 10 GHz, substrate FoamClad: (a) E-plane, (b) H-plane.

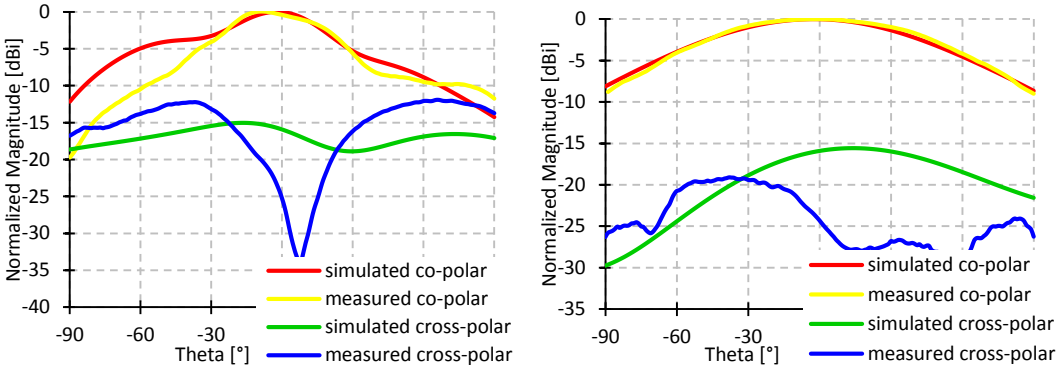

(a) (b)

Fig. 38. Normalized magnitude measured at 12 GHz, substrate CuClad 217: (a) E-plane, (b) H-plane.

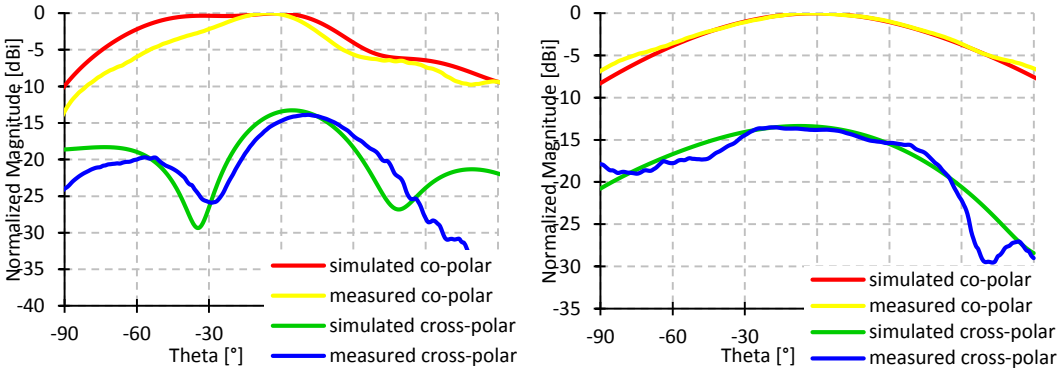

(a) (b)

Fig. 39. Normalized magnitude measured at 8 GHz, substrate Arlon25N: (a) E-plane, (b) H-plane.

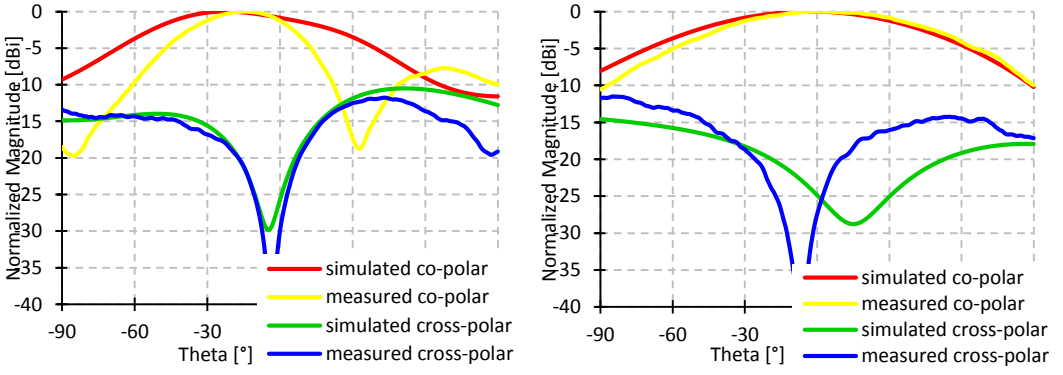

(a) (b)

Fig. 40. Normalized magnitude measured at 7 GHz, substrate Arlon600: (a) E-plane, (b) H-plane.

4.1.8 Summary

This section described behavior of the HMSIW linearly polarized U-slot antenna. Based on the results of the parametric study, the design guide was created. The design guide was verified by designing of several antennas. The characteristic modal analysis of the antenna were investigated in the wide frequency range.

The behavior of the proposed antenna is interesting especially at higher frequencies – thanks to the presence of more excitable modes the proposed antenna can achieve a wider impedance bandwidth.

In comparison to published antennas presented in Table 10, the proposed HMSIW linearly polarized U-slot antenna achieves a higher gain and a wider impedance bandwidth. In addition, it has also compact size.

Table 10. The proposed antenna in comparison to other HMSIW antennas (λ_0 is wavelength in vacuum).

	Operating frequency [GHz]	**S11<-10 dB [%]**	**Gain [dBi]**	**Antenna size**
Proposed antenna	10	3.2	6	$1.04\lambda_0 \times 0.48\lambda_0$
Slot antenna [7]	4.9	1.1	–	$0.31\lambda_0 \times 2.48\lambda_0$
E slot [19]	7.6	1	4.6	–
Z-slot [21]	15.5	3.5	5.6	$0.12\lambda_0 \times 1.55\lambda_0$
Cavity-backed [9]	8.5	4.9	6.7	$0.48\lambda_0 \times 1.0\lambda_0$
Dual band U-slot [24]	5.8/7	2.2/2.4	5.9/5.1	$1.09\lambda_0 \times 0.28\lambda_0$
Cavity-backed slot [12]	2.4	1.7	4.1	$0.23\lambda_0 \times 0.35\lambda_0$
Triangular antenna [16]	5.3	0.9	5.6	$0.7\lambda_0 \times 0.7\lambda_0$
Semi-circular antenna [16]	5.2 sim	1.1 sim	5.3 sim	$1.04\lambda_0 \times 1.04\lambda_0$
Semi-hexagonal antenna [17]	5.6	1.2	5.3	$1.12\lambda_0 \times 1.12\lambda_0$
Triangular slot [15]	4.5	0.2	2.3	$0.9\lambda_0 \times 0.9\lambda_0$
Semi-circular slot [13]	4.8 sim	0.9 sim	4.9 sim	$0.96\lambda_0 \times 0.96\lambda_0$
Semi-hexagonal slot [17]	4.9	0.8	3.4	$0.98\lambda_0 \times 0.98\lambda_0$
Low-profile patch [13]	8.1	10	7.5	$0.63\lambda_0 \times 0.58\lambda_0$
Aperture-coupled DRA [23]	60	24	5.5	$0.44\lambda_0 \times 1.78\lambda_0$
Horn antenna [30]	27.3	1.2	5.9	$1.7\lambda_0 \times 1.7\lambda_0$
Dual-band slot [22]	8.25/9.5	2.1/1.2	5	–

4.2 Circularly Polarized HMSIW U-Shape Slot Antenna

In this chapter, a circularly polarized HMSIW U-shape slot antenna [59] is proposed and described. It is based on the SIW version of the antenna published in [64], where the author utilizing two methods of feeding: the first one is a direct feeding with a pair of two inductive vias and the second one is feeding by a coaxial probe. The first mentioned method is suitable for integration with other SIW-based circuits and the second is suitable when the SIW antenna is used as an individual antenna.

The excitation of a circularly polarized wave can be carried out relatively easily by adding a single via into the antenna structure. The below proposed HMSIW antenna radiated left-handed circularly polarized (LHCP) wave and is fed by a coaxial probe. The right-handed circularly polarized (RHCP) antenna can be obtained from that antenna by mirroring the antenna with respect to its longitudinal axis.

4.2.1 Antenna structure

The antenna structure [61] is depicted in Fig. 41. The dielectric substrate of the length L, the width W, and the height h with the relative permittivity ε_r, and the loss tangent tan(δ) is on its both sides covered by metal sheets. The HMSIW is created by a row of vias and both its end are shorted. The slot with length L_{slotX} in x-direction and L_{slotY} in y-direction is etched at the end of the waveguide at the distance L_{viaX} from its short end in the x-direction, and from the solid wall of HMSIW at the distance L_{viaY} in the y-direction. The width of the slot is W_{slot}. The slot is shorted by the short S_1. A shorting via is placed into the antenna area bounded by the slot in distance X_{via} in x-direction and Y_{via} in y-direction from the edge of the slot. The antenna is equipped by a HMSIW-to-SMA transition.

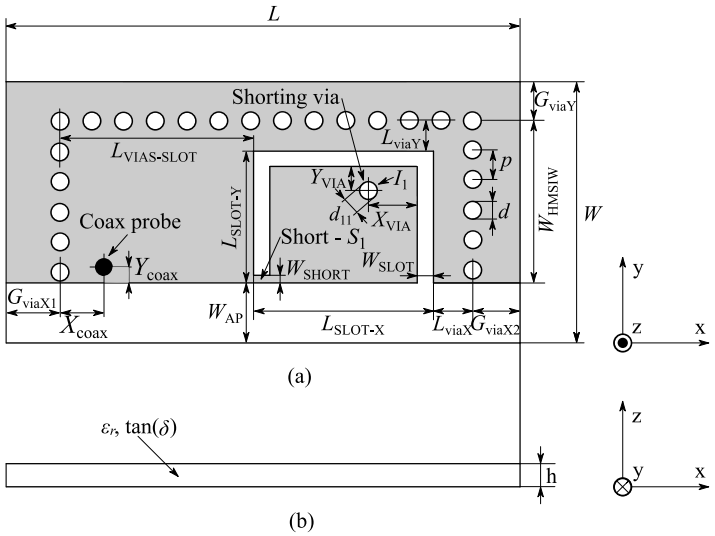

Fig. 41. Top (a) and side (b) view of the circularly polarized antenna (the bottom side of the antenna is fully coated by metal).

4.2.2 Simulated Results

The proposed antenna is designed for the operating frequency of 10 GHz on the dielectric substrate ARLON Cuclad 217 with relative permittivity ε_r = 2.17, tangent loss tan(δ) = 0.0009, and height h = 1.524 mm with the help of time domain solver of CST MWS. In order to reduce computing time during calculation the simulation of the antenna, vias of HMSIW could be substituted by a solid wall made of PEC as it is mentioned above. The HMSIW operates in the fundamental mode $TE_{0.5;0}$. Physical dimensions of the antenna are noted in Table 11.

Table 11. Physical dimensions of the circularly polarized antenna.

Dimension	[mm]	Description	Dimension	[mm]	Description
L	37.5	length of the substrate	Y_{COAX}	0.8	position of the coax in y-direction
L_{SLOT-X}	14.6	slot length in x-direction	X_{VIA}	3.21	distance of the shorting via in x-direction
L_{SLOT-Y}	7.2	slot length in y-direction	Y_{VIA}	2.65	distance of the shorting via in y-direction
L_{viaX}	2.8	distance between the slot and the row of vias in x-direction	G_{viaX1}	4.2	distance between the HMSIW and the end of the substrate in x-direction
L_{viaY}	1.7	distance between the slot and the row of vias in y-direction	G_{viaX2}	7.5	distance between the HMSIW and the end of the substrate in x-direction
W	18.0	width of the substrate	G_{viaY}	6.1	distance between the HMSIW and the end of the substrate in y-direction
W_{HMSIW}	8.9	width of the HMSIW	H	1.524	height of the substrate
W_{SHORT}	0.3	width of the short	d_{I1}	1.4	diameter of the shorting via
W_{SLOT}	1.1	width of the slot	d	1.4	diameter of the vias
W_{AP}	3.0	width of the aperture	p	2.58	distance between vias
X_{COAX}	3.0	position of the coax in x-direction			

The simulated reflection coefficient is depicted in Fig. 42. The antenna achieves two resonances. The first one occurs at 9.92 GHz with reflection coefficient – 35.65 dB and the second one occurs at 10.42 GHz with reflection coefficient – 17.5 dB. The simulated impedance bandwidth of the antenna is 11.4 % for the reflection coefficient less than –10 dB. The minimum of the axial ratio is 0.51 at 9.98 GHz and the axial frequency bandwidth is 2.2 % for the AR less than 3 dB (Fig. 43). The normalized radiation patterns in two orthogonal cutting planes at the frequency of 10 GHz are depicted in Fig. 44. The maximum of the co-polarization is perpendicular to antenna plane and shifted about 6° and 4° in the xz- and yz-plane, respectively. The simulated gain is 5.87 dBi and level of cross-polarization is about of -30 dB at the broadside direction.

The shorting via I_1 mentioned above has crucial effect to the exciting of a circularly polarized wave. That fact is illustrated in Figs. 45 and 46. The electric field and surface currents are rotating around the slot; and the left-handed circular polarized (LHCP) wave is obtained. The right-handed circularly polarized (RHCP) wave can be obtained by mirroring the antenna with respect to the xz-plane.

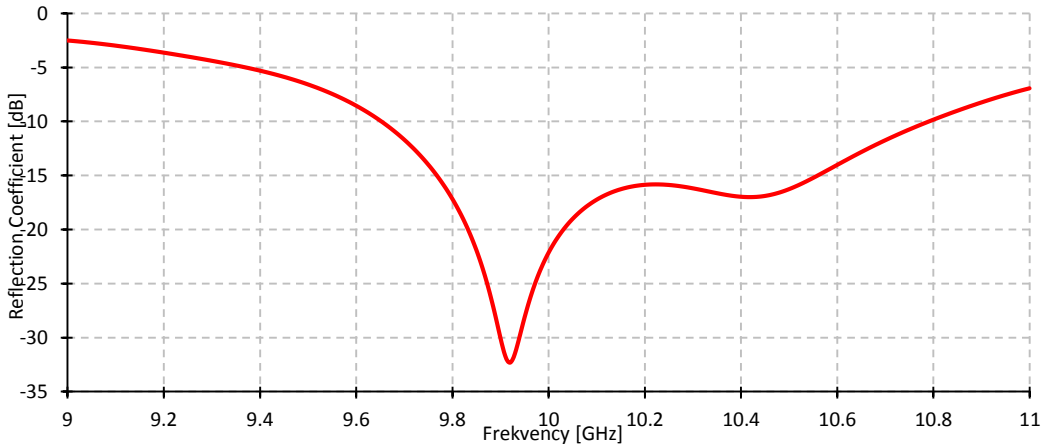

Fig. 42. Simulated reflection coefficient of the circularly polarized antenna.

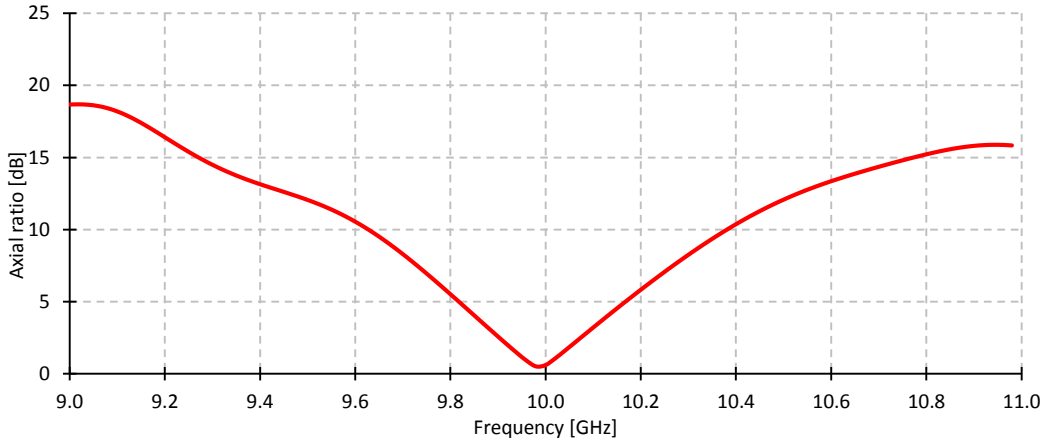

Fig. 43. Simulated axial ratio of the circularly polarized antenna.

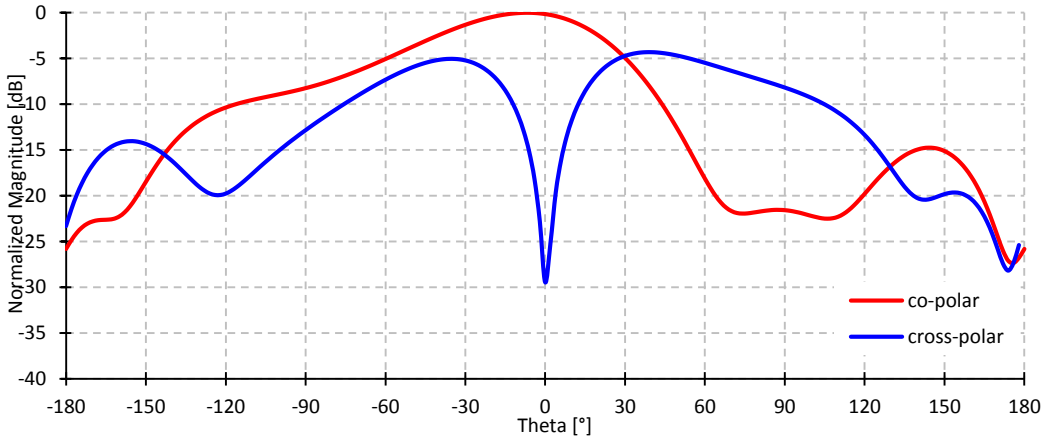

(a)

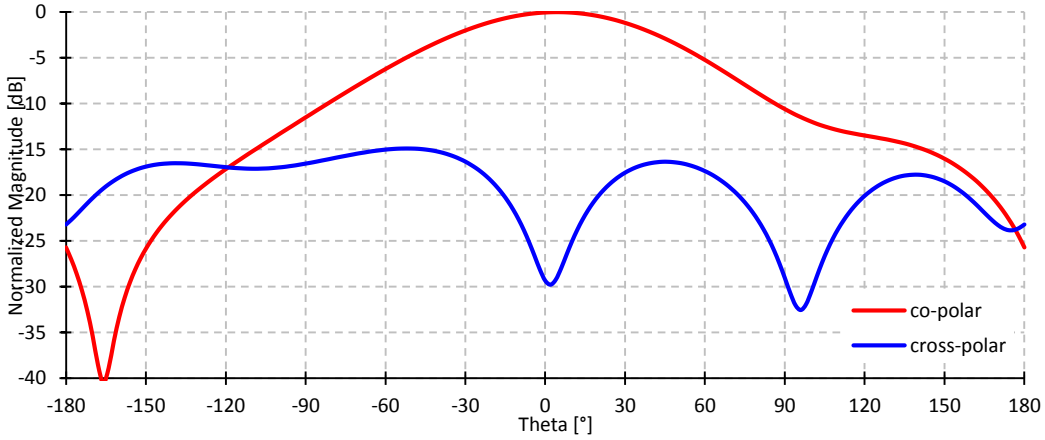

(b)

Fig. 44. Simulation of normalized magnitude of the antenna in (a) xz-plane and (b) yz-plane.

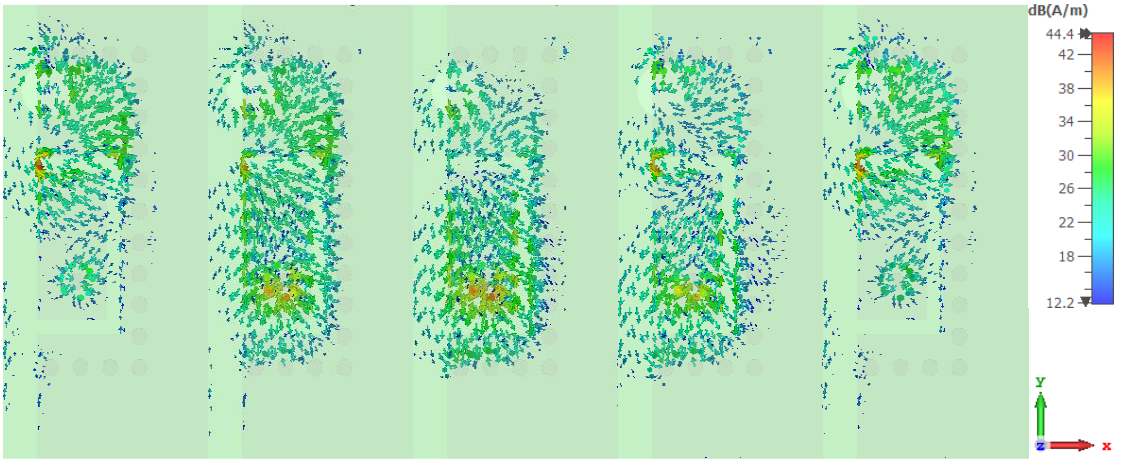

(a) (b) (c) (d) (e)

Fig. 45. Propagation of surface currents: (a) phase = 0° and (b) phase = 45°, (c) phase = 90°, (d) = phase 135° and (e) phase = 180°.

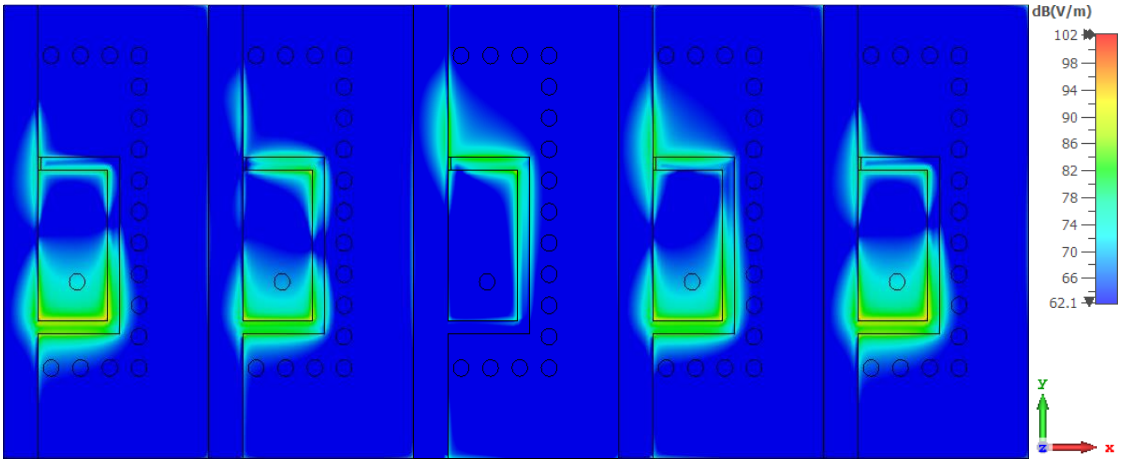

(a) (b) (c) (d) (e)

Fig. 46. Distribution of electric field intensity in substrate (magnitude): (a) phase = 0°, (b) phase = 45°, (c) phase = 90°, (d) phase = 135° and (e) = 180°.

4.2.3 Experimental Verification

This section provides a measured results of the antenna [59]. The antenna dimensions are summarized in Table 11. The antenna was fabricated by a low-cost etching PCB process. The antenna is equipped with soldered SMA coaxial connector to carry out a conventional coaxial measurement. The manufactured sample of the antenna is depicted in Fig 47.

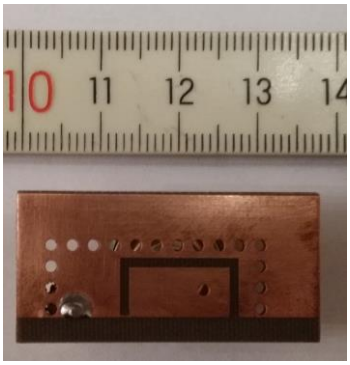

Fig. 47. Fabricated sample of the proposed HMSIW U-slot antenna.

The reflection coefficient was measured in a laboratory environment. The measured reflection coefficient is shown in Fig. 48. The impedance bandwidth is 11.9 % for reflection coefficient less than – 10 dB. The measured result is different in compassion to the simulated ones, especially in the minimum of the measured reflection coefficient. The difference is caused by the high sensitivity to the change of the physical dimensions of the proposed antenna. This topic is more discussed in the chapter 4.2.5. On the other hand, the measured axil ratio is in good agreement with the simulated one (Fig. 49). The minimum of the measured axial ratio is slightly shifted to the higher frequencies. The shift is about 60 MHz. The measured bandwidth of the axial ratio is 2.2 % for the axial ratio less than 3 dB. The measured minimum of the axial ratio is 0.22.

The radiation patterns for the Theta range from –90° to 90° were measured in an anechoic chamber. For the measurement, Rohde&Schwarz vector network analyzer ZVA67 was used. The radiation patterns in the xz-plane and the yz-plane are depicted in Fig. 50. The measured radiation patterns are in good agreement with the simulated ones. The radiation maximum is shifted about 16° in the zx- plane and 10° in the yz-plane comparison to the simulated ones due to the parasitic radiation of coax-to-HMSIW transition. The measured peak gain of the antenna is 6.0 dBi.

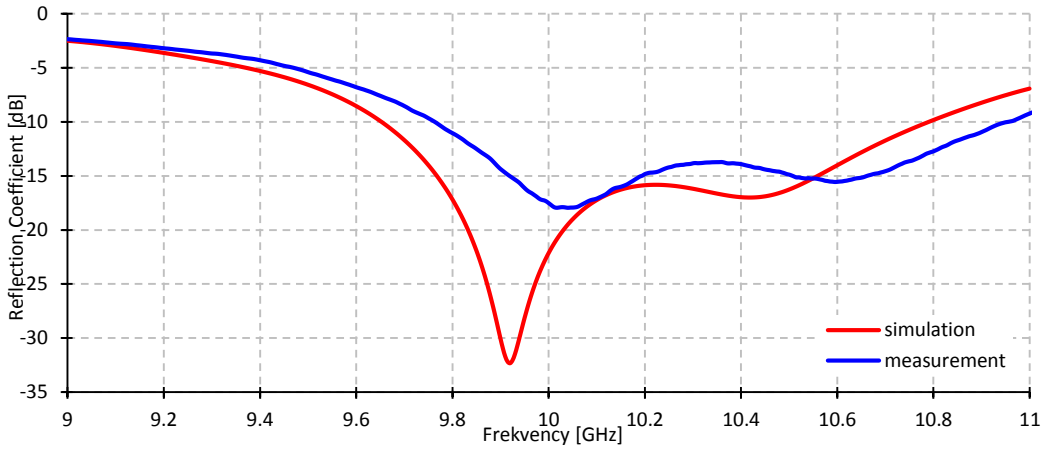

Fig. 48. Reflection coefficient of the proposed antenna.

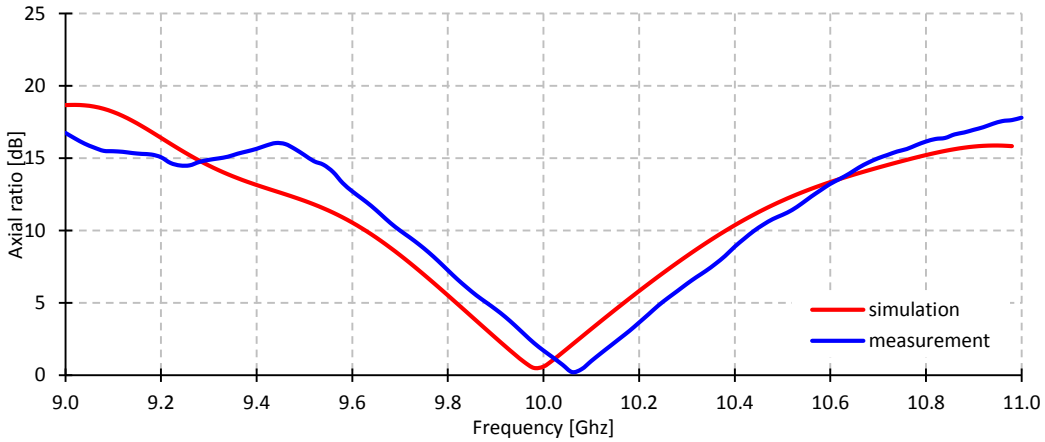

Fig. 49. Axial ratio of the proposed antenna.

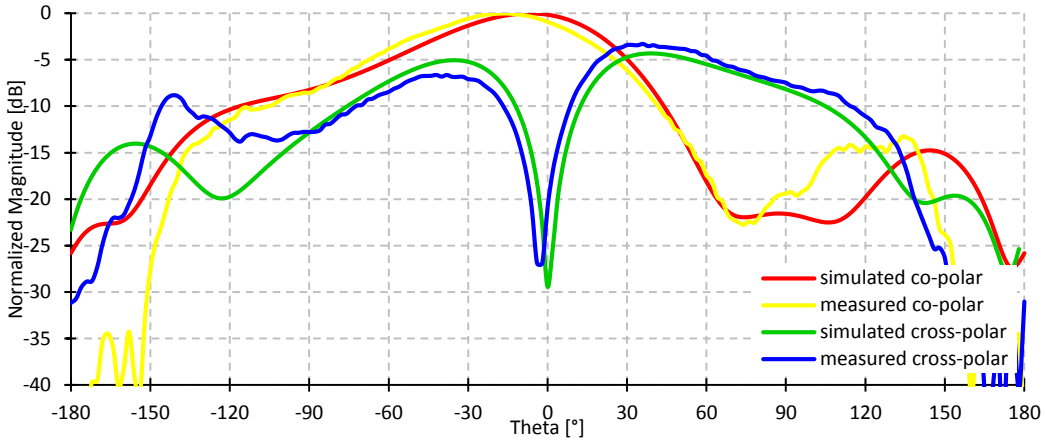

(a)

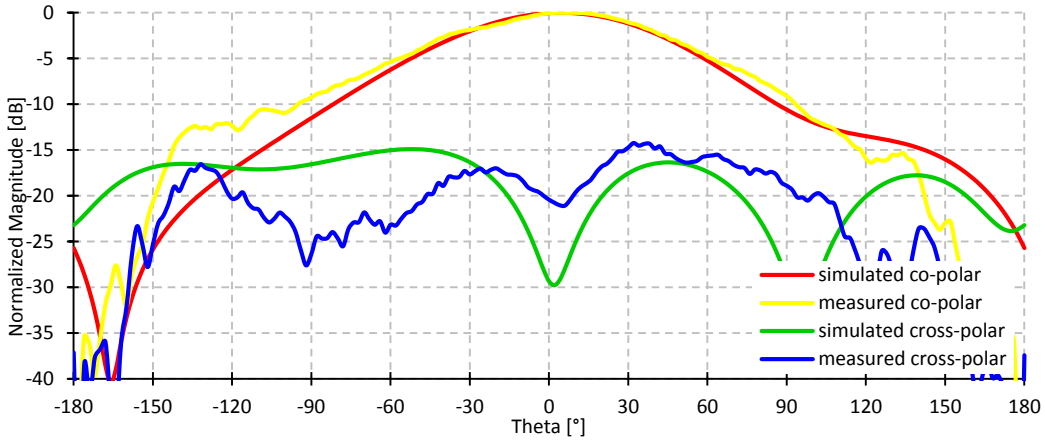

(b)

Fig. 50. Normalized radiation patterns of the proposed antenna in (a) xz-plane and (b) yz-plane.

4.2.4 Characteristic Modal Analysis

This section provides CMA which performed on the HMSIW circularly polarized antenna. The investigated antenna tuned for the frequency of 10 GHz was analyzed with the help of CST MWS. The CMA was performed on the finite lossless dielectric substrate with the infinite ground considering a boundary condition $E_t = 0$. The physical dimensions of the investigated antenna are shown in Table 11.

The CMA was performed in the frequency range from 3 GHz to 18 GHz. The first ten modal significances (MSs) in comparison to the reflection coefficient are shown in Fig 51. The resonating frequencies of each mode are listed in Table 12. In order to obtain a circular polarization, it is necessary to excite two orthogonal modes. Based on the reflection coefficient and modal significance, the antenna operates in the mode #7 and mode #6 or mode #5. The question is which of these modes have a major or minor contribution to the excited circular polarization. It is expected that the maximum of the modal significance of these modes corresponds to the minimum of the reflection coefficient but they are slightly shifted to the lower frequencies due to the principle of calculation of CMA (different calculation method and different fineness of the mesh in comparison to the time domain solver). The modal surface currents are depicted in Fig. 52, where J_n represents the modal surface current of mode n. Only in the case of J_5 and J_7 the modal surface currents are inside the antenna area bounded by the HMSIW. Therefore, it is expected that the mode #6 (J_6) has only minimal contribution to the radiation

performance if the antenna is by a coax-HMSIW transition as depicted in Fig. 41. The calculated radiation patterns of the polarized wave in the x- and in the y-direction are depicted in Fig. 53 and Fig 54, respectively. $F_{nx/y}$ represents the radiation patterns of the wave polarized in the x- or in the y- direction of mode *n*. Based on the results (Fig. 53 and Fig. 54), the maximum of the polarized wave (perpendicular to the antenna plane) in the x-direction of the radiation pattern F_{5x} and F_{7x} are 5.7 dBi and almost 0 dBi, respectively. Meanwhile the maximum of the polarized wave in the y-direction of the radiation pattern F_{5y} and F_{7y} are -16 dBi and almost 4.9 dBi, respectively. That indicates that the circular polarization is generated by the wave polarized in the x-direction of the mode F_{5x} and the wave polarized in the y-direction of the mode F_{7y}.

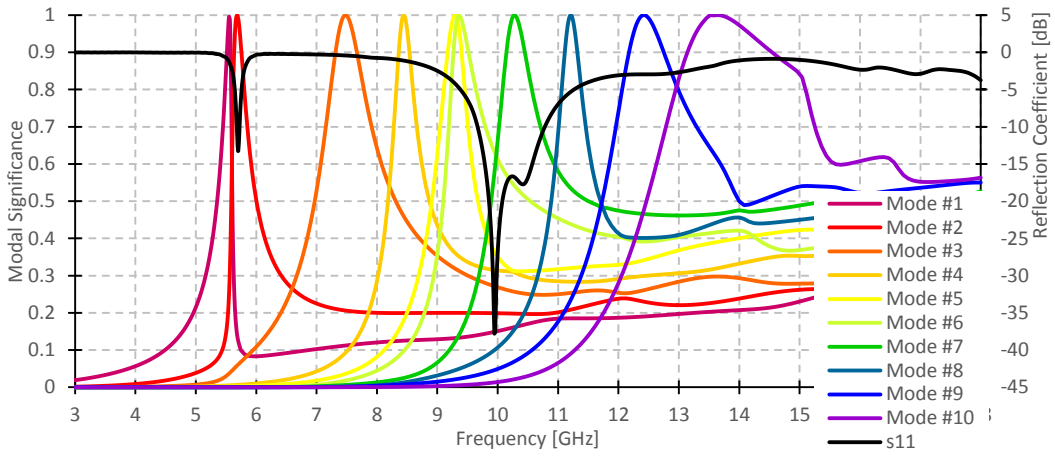

Fig. 51. CMA – Modal significance.

Table 12. Resonant frequency of the modes.

mode #	1	2	3	4	5	6	7	8	9	10
f_r **[GHz]**	5.55	5.69	7.49	8.45	9.30	9.36	10.28	11.21	12.42	13.53

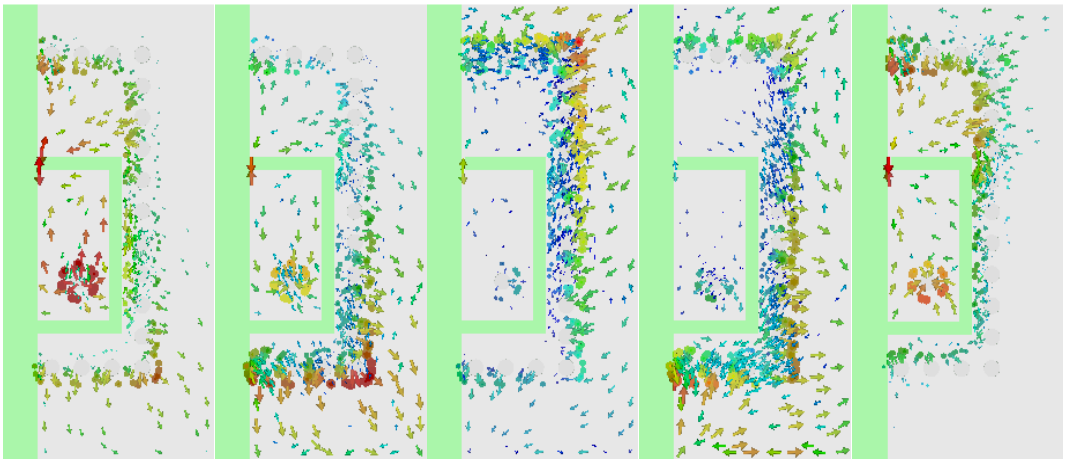

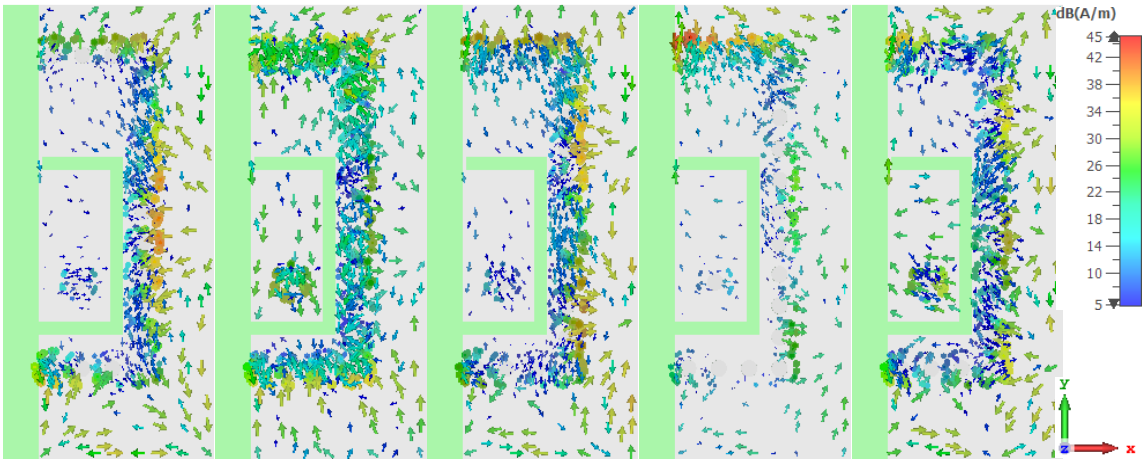

J_6 J_7 J_8 J_9 J_{10}

Fig. 52. CMA – Modal surface currents.

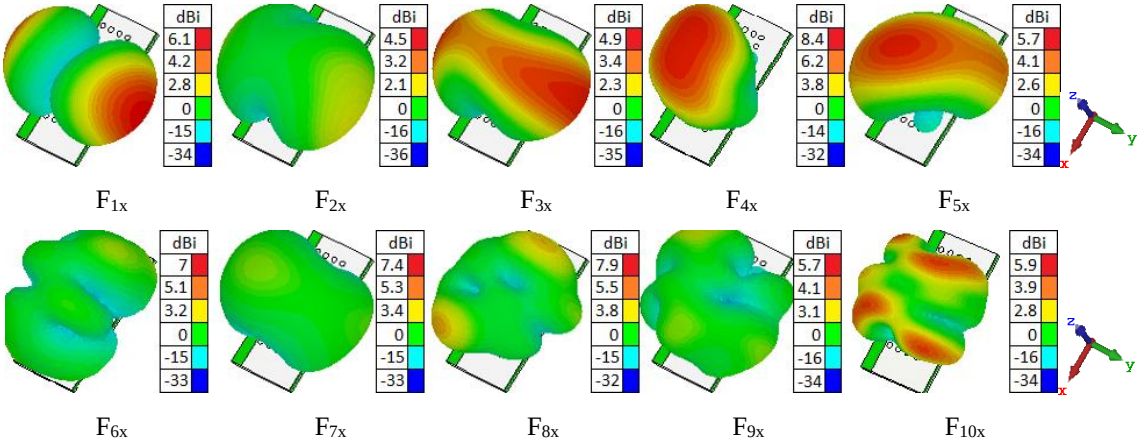

F_{1x} F_{2x} F_{3x} F_{4x} F_{5x}

F_{6x} F_{7x} F_{8x} F_{9x} F_{10x}

Fig. 53. CMA – Radiations patterns: polarization of the wave in the x-direction.

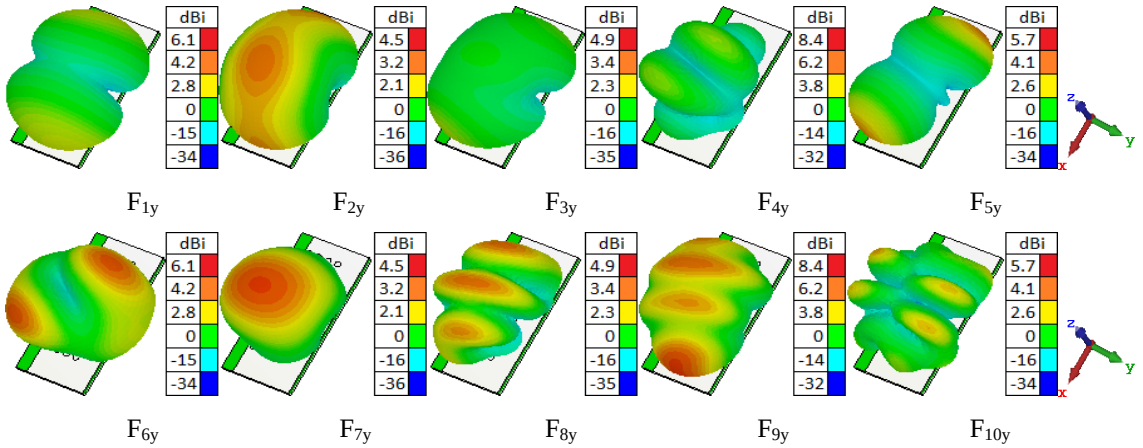

F_{1y} F_{2y} F_{3y} F_{4y} F_{5y}

F_{6y} F_{7y} F_{8y} F_{9y} F_{10y}

Fig. 54. CMA – Radiations patterns: polarization of the wave in the y-direction.

4.2.5 Parametric Study

The parametric study is a necessarily tool for an antenna design. Therefore, knowledge of the effect of a physical dimensions on the antenna parameters is essential. During the study, the effect of five parameters is investigated. The first two parameters are length of the slot $L_{SLOT\text{-}X}$ and $L_{SLOT\text{-}Y}$ in the x- and y- direction, respectively. The third one width of the slot W_{SLOT}. The fifth one and the last one are the position of the shorting via X_{via}

and Y_{via} in the x- and y-direction, respectively. The via I_1 is also moved diagonally from its original position, as shown in Fig. 55. The red circles indicate the possible positions of the via I_1 and the number in the circle indicates coordinate of the position. The other parameters are kept unchanged as noted in Table 11. The changing step is 0.25 mm.

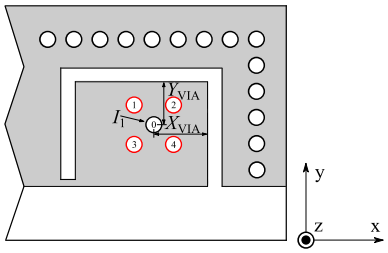

Fig. 55. Parametric study of the shorting via I_1. Physical dimensions for position **0** (original) are X_{via} = 3.21 mm and Y_{via} = 2.65 mm, for position **1** are X_{via} = 3.46 mm and Y_{via} = 2.40 mm, for position **2** are = X_{via} = 2.40 mm and Y_{via} = 2.71 mm, for position **3** are X_{via} = 2.90 mm and Y_{via} = 3.46 mm and for position **4** are X_{via} = 2.90 mm and Y_{via} = 2.96 mm.

The length $L_{SLOT\text{-}X}$ influences impedance matching and level of cross-polarization (Fig. 56(a), (d) and (f)). It has minimal effect to the co-polarization in both cutting planes and slightly influences frequency of the minimum of the axial ratio. On the other hand, the length $L_{SLOT\text{-}Y}$ affects operating frequency, axial ratio and the level of cross-polarization in the yz-plane (Fig. 57(a), (b) and (f)). The W_{slot} greatly influences impedance matching and frequency shift of the minimal of the axial ratio (Fig. 58(a) and (b)). It also has a significant influence on the radiation patterns (Fig. 58(c – f)). Variation of the via I_1 position in the x-direction (X_{via}) disrupts the surface currents in the area bounded by the slot. That effect is demonstrated in Fig. 59(a) and (b), where the operating frequency and the axial ratio are heavily shifted. The co-polarization in the xz-plane and the yz-plane (Fig. 59(c) and (e)) does not seem to be affected by the variation of the position of the via I_1 but the level of the cross-polarization (Fig. 59(d) and (f)) is strongly affected. On the other hand Variation of the via I_1 position in the y-direction (Y_{via}) minimally affects the shifting of the operating frequency and the axial ratio (Fig. 60(a) and (b)) and the co-polarization (Fig. 60(c) and (e)). The minimum of the cross-polarization is slightly shifted (Fig. 60(d) and (f)) to the upper levels. The main purpose for the investigating the effect of shifting of the via I_1 to the positions 1 to 4 (Fig.55) is to simulate inaccuracies that may occur during the manufacturing process. Based on the results depicted in (Fig. 61(a) – (f)), the operating frequency, the axial ratio and the minimum of the cross-polarization are heavily shifted. Therefore, a precisions manufacturing process is critical for successful antenna design.

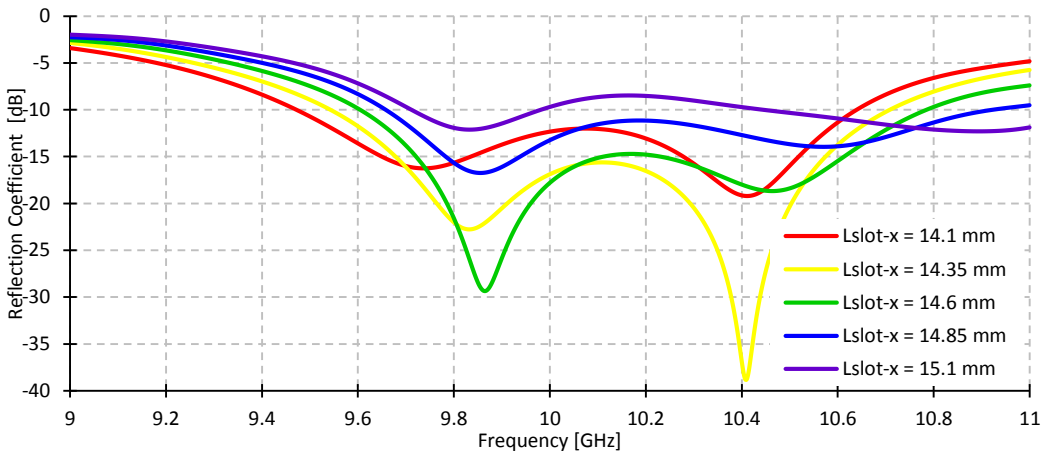

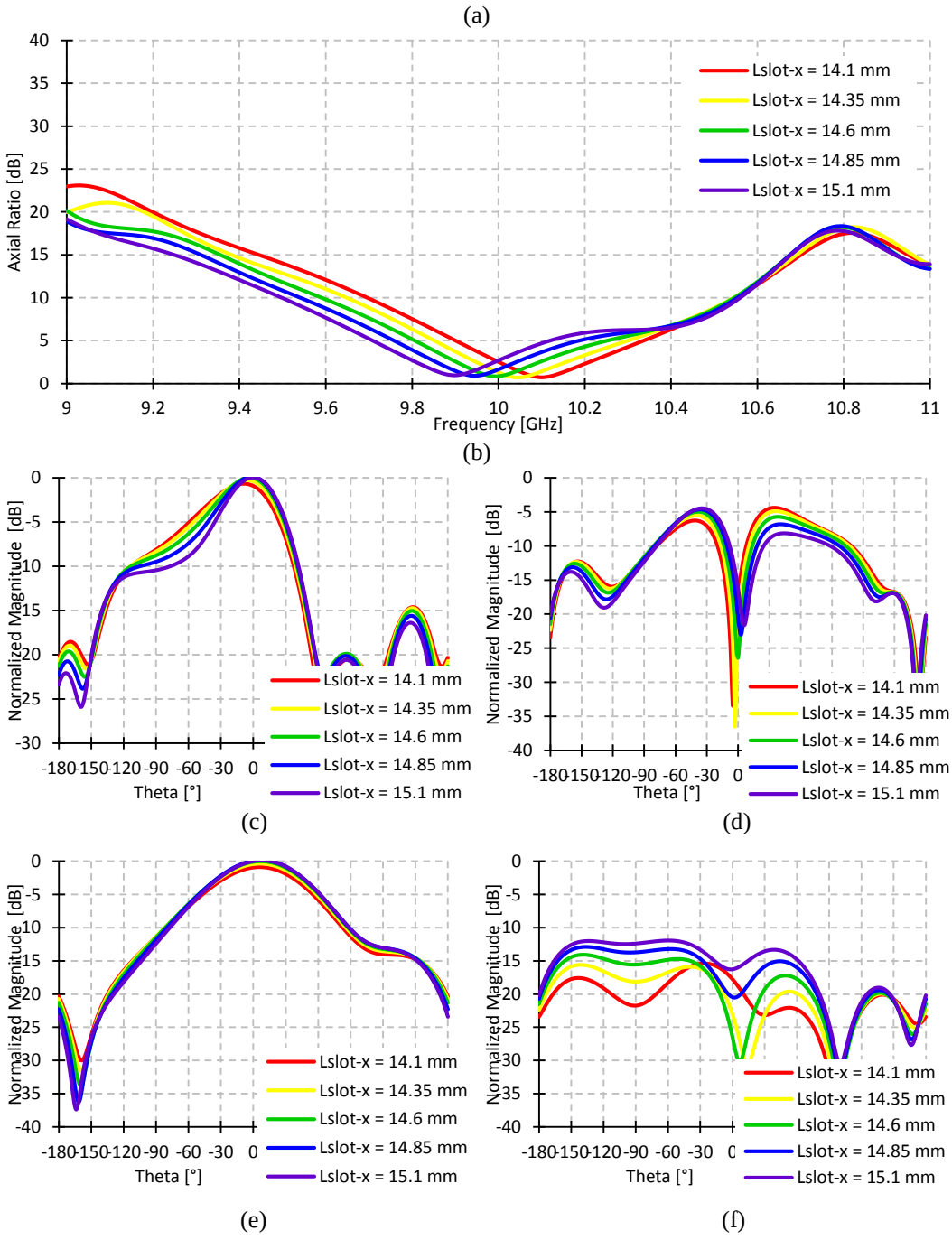

Fig. 56. Variation of the length $L_{SLOT\text{-}X}$: (a) reflection coefficient, (b) axial ratio, (c) co-polar in xz-plane, (d) cross-polar in xz-plane, (e) co-polar in yz-plane and (f) cross-polar in yz-plane.

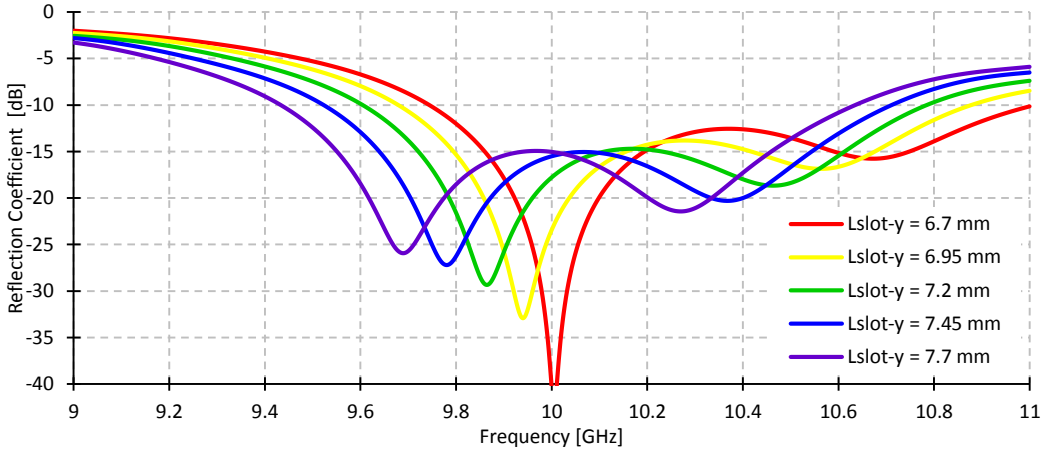

(a)

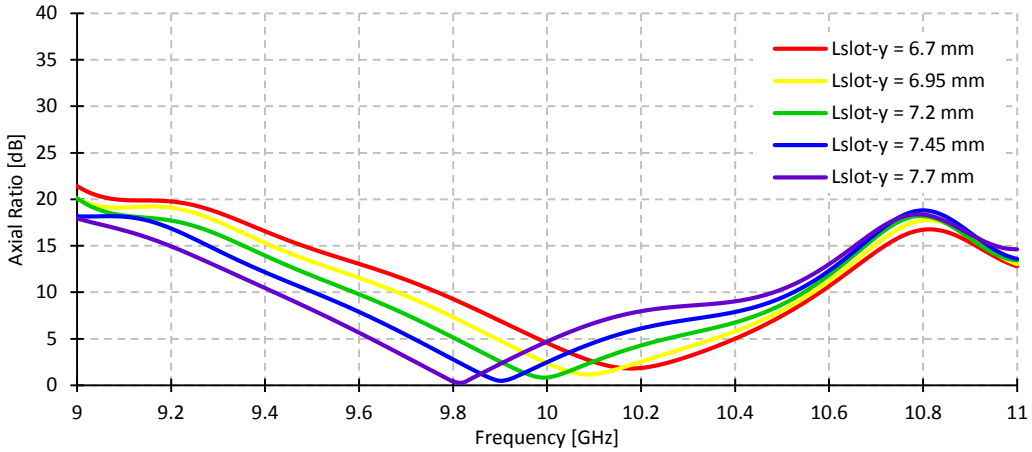

(b)

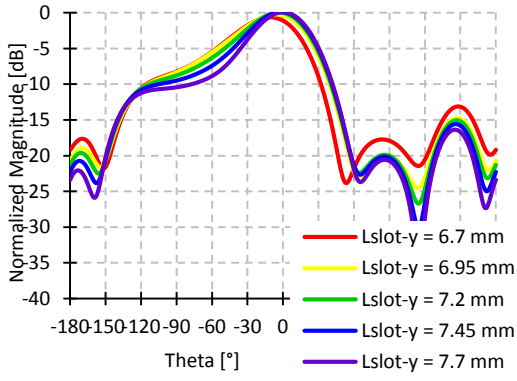

(c)

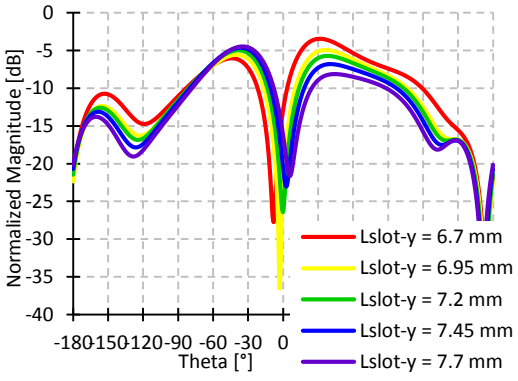

(d)

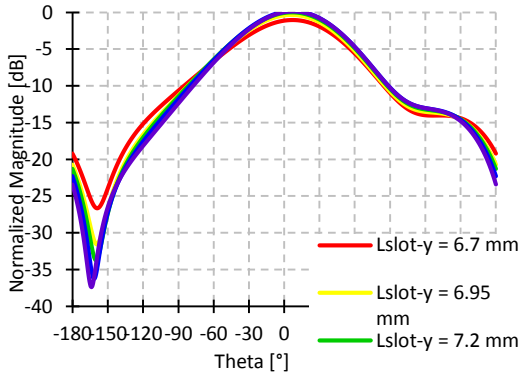

(e)

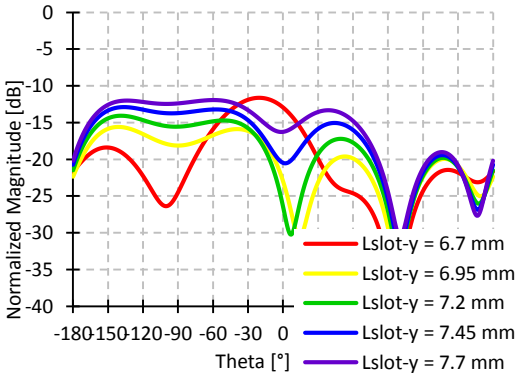

(f)

Fig. 57. Variation of the length $L_{SLOT\text{-}Y}$: (a) reflection coefficient, (b) axial ratio, (c) co-polar in xz-plane, (d) cross-polar in xz-plane, (e) co-polar in yz-plane and (f) cross-polar in yz-plane.

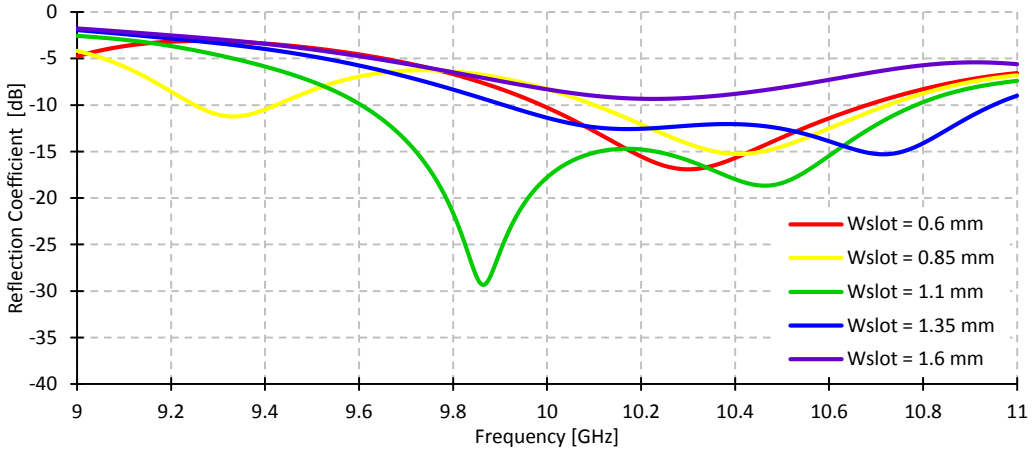

(a)

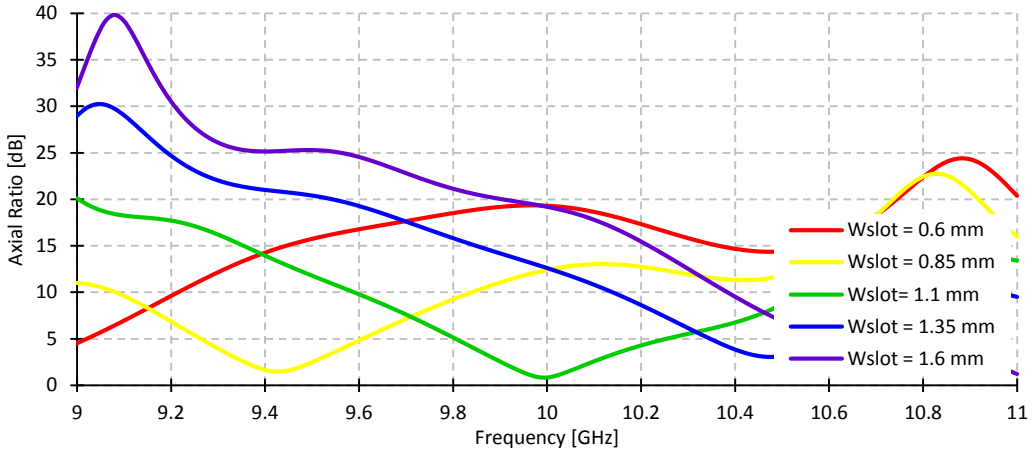

(b)

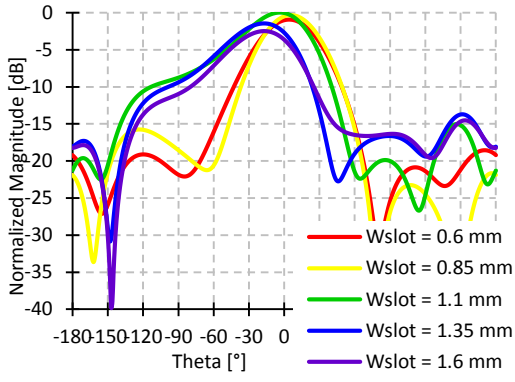

(c)

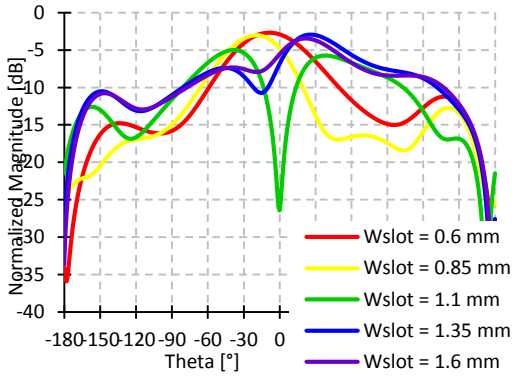

(d)

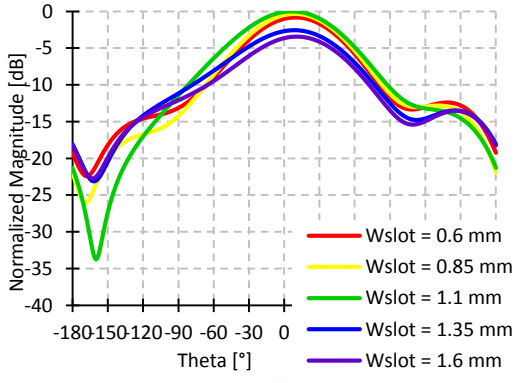

(e)

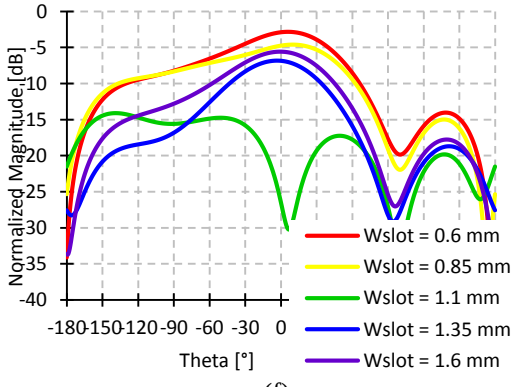

(f)

Fig. 58. Variation of the length W_{SLOT}: (a) reflection coefficient, (b) axial ratio, (c) co-polar in xz-plane, (d) cross-polar in xz-plane, (e) co-polar in yz-plane and (f) cross-polar in yz-plane.

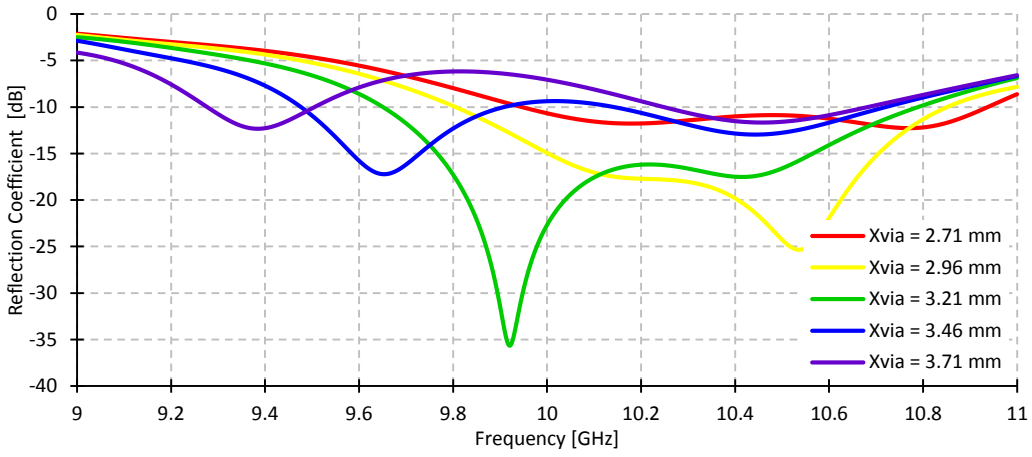

(a)

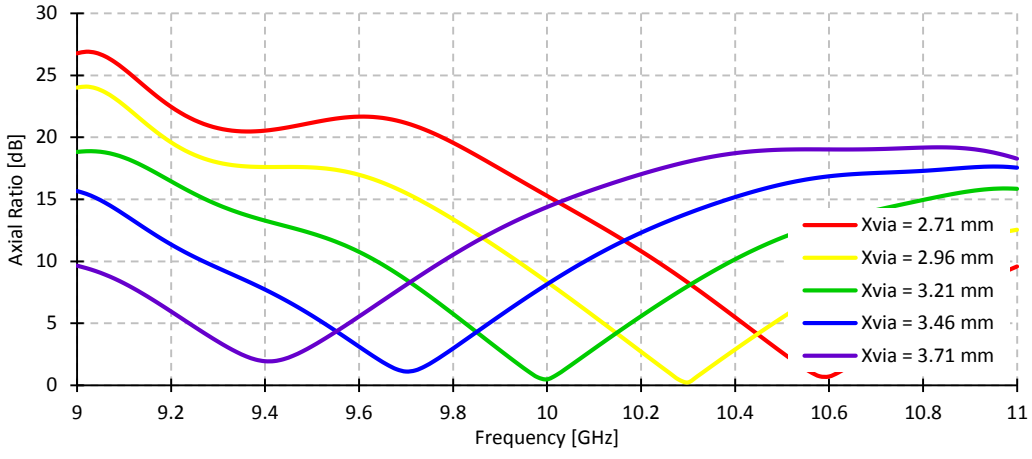

(b)

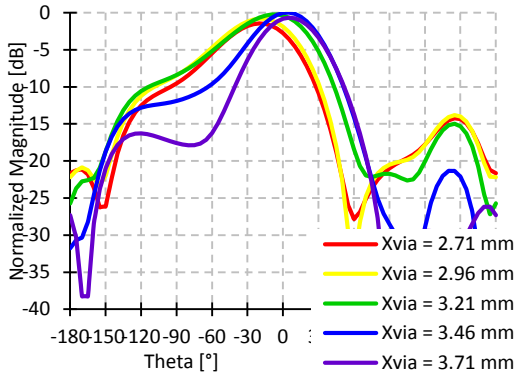

(c)

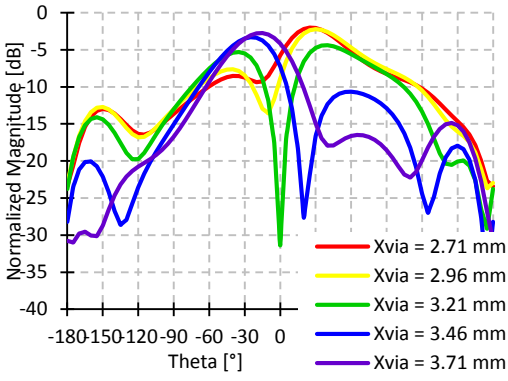

(d)

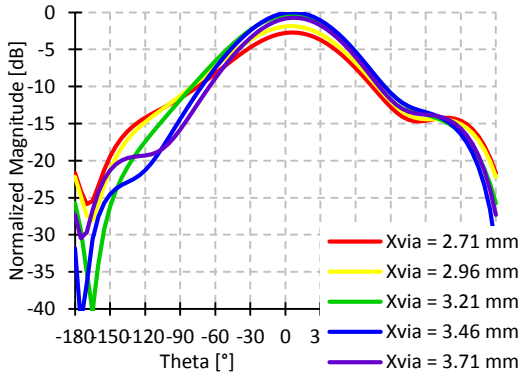

(e)

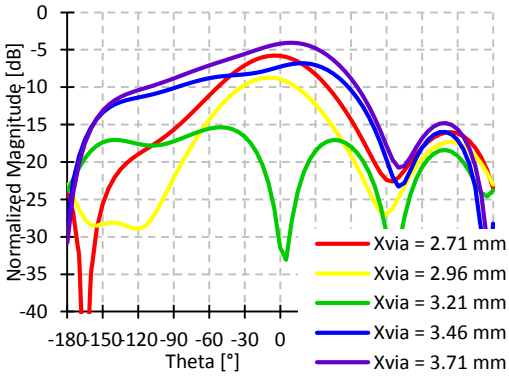

(f)

Fig. 59. Variation of via I_1 position in x-direction X_{via}: (a) reflection coefficient, (b) axial ratio, (c) co-polar in xz-plane, (d) cross-polar in xz-plane, (e) co-polar in yz-plane and (f) cross-polar in yz-plane.

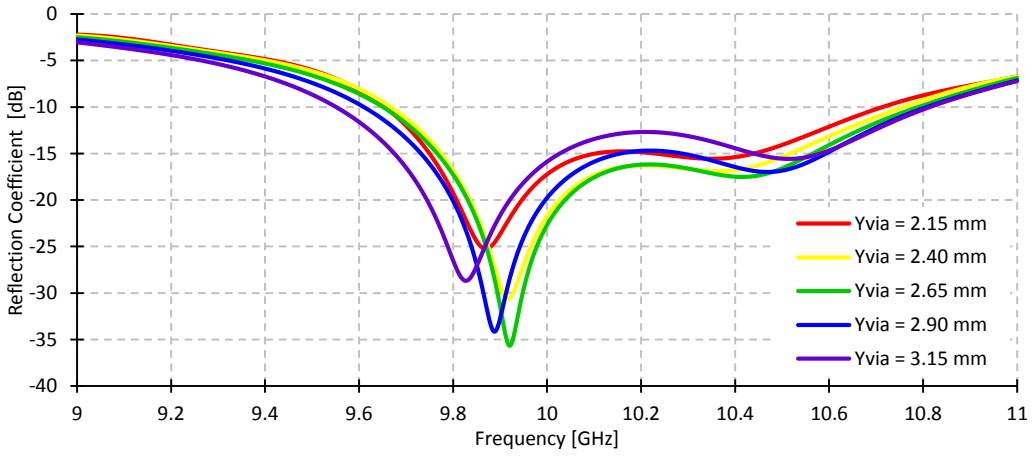

(a)

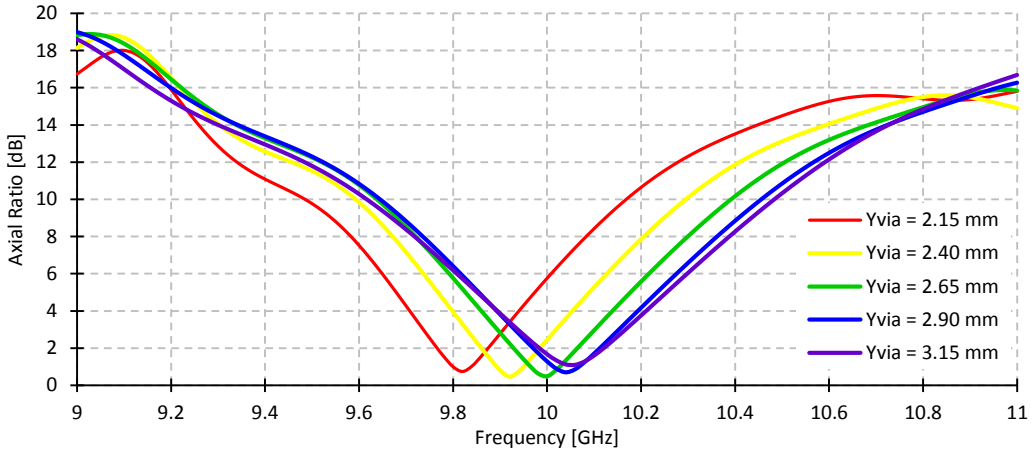

(b)

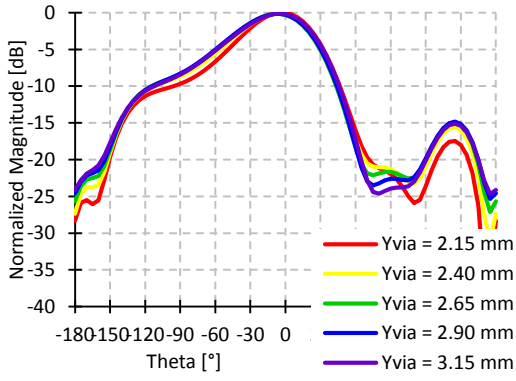

(c)

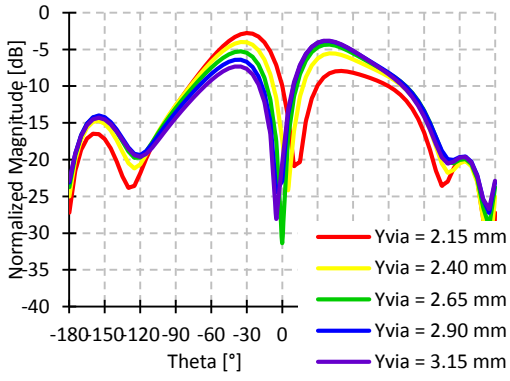

(d)

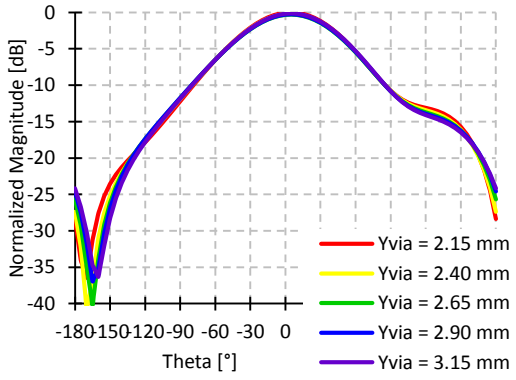

(e)

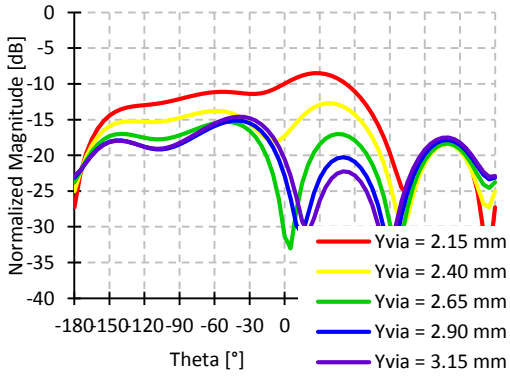

(f)

Fig. 60. Variation of via I_1 position in y-direction Y_{via}: (a) reflection coefficient, (b) axial ratio, (c) co-polar in xz-plane, (d) cross-polar in xz-plane, (e) co-polar in yz-plane and (f) cross-polar in yz-plane.

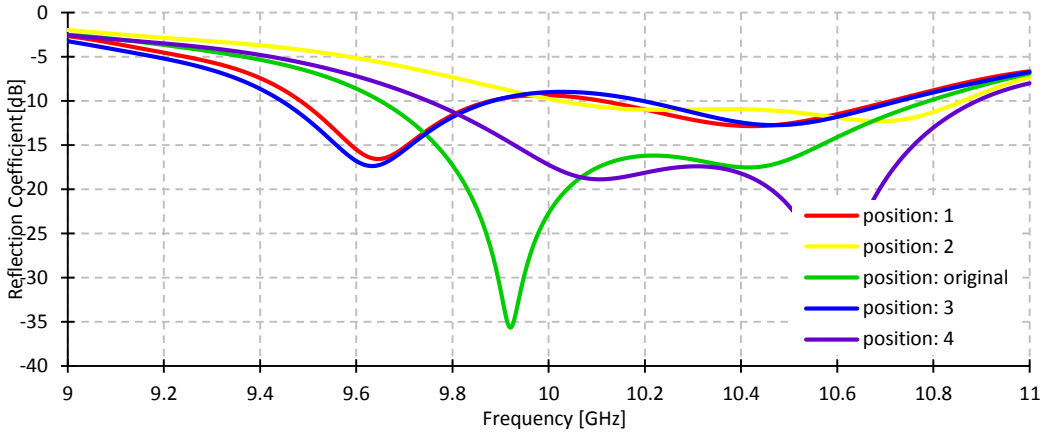

(a)

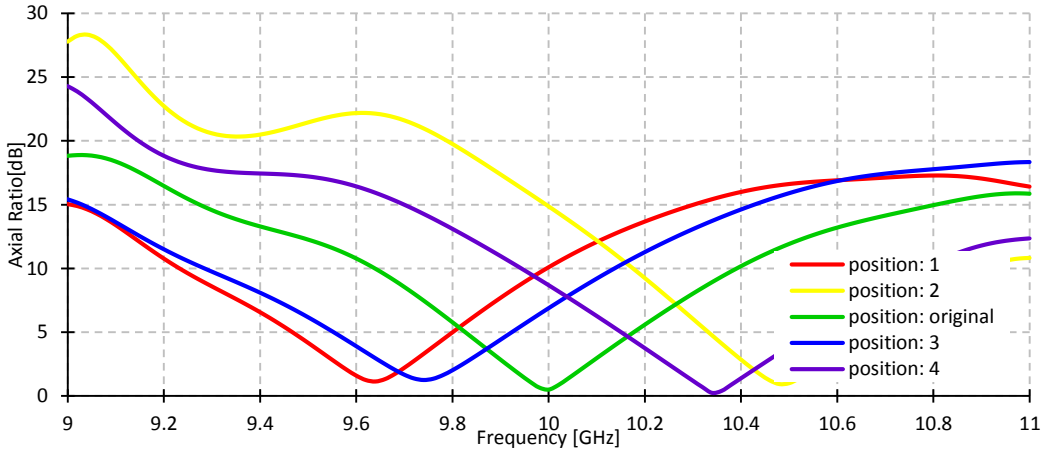

(b)

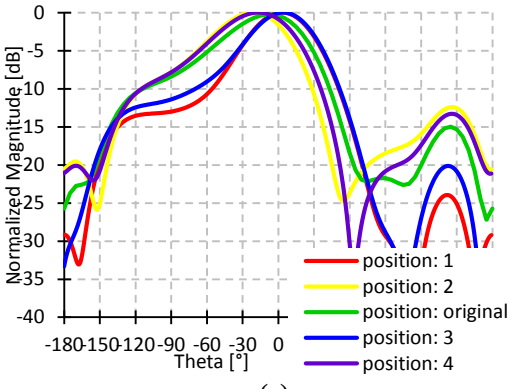

(c)

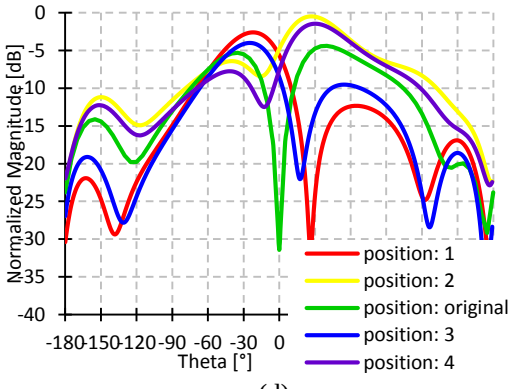

(d)

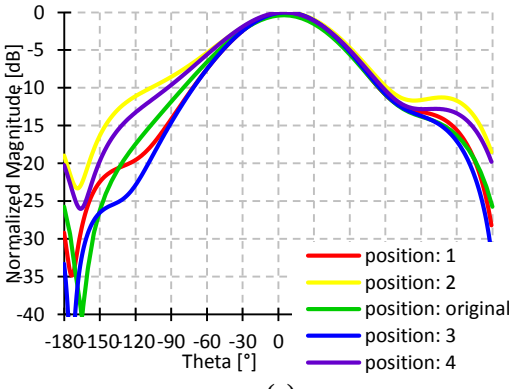

(e)

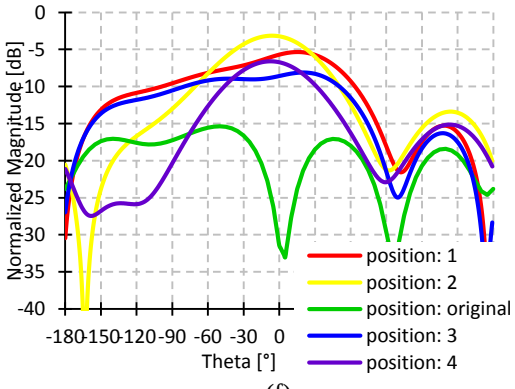

(f)

Fig. 61. Variation of via I_1 position 1 – 4: (a) reflection coefficient, (b) axial ratio, (c) co-polar in xz-plane, (d) cross-polar in xz-plane, (e) co-polar in yz-plane and (f) cross-polar in yz-plane.

4.2.6 Design Guide

A design guide of the circularly polarized HMSIW U-slot antenna is very similar to the linearly polarized antenna proposed in the chapter 4.1. The design guide should include the following steps [59]:

1. Appropriate choosing of a dielectric substrate. The dielectric substrate must have to have suitable electrical and mechanical properties that are stable in the real environment. Based on the experimental verification mentioned above, it is recommended to exploiting the ARLON CuClad 217.
2. Design of the HMSIW with respect to the relations (8) – (13) in [61]. The waveguide should operate in the fundamental mode $TE_{0.5,0}$. The operating frequency of the antenna should be approximately 1.5 times higher than the cut-off frequency of the fundamental mode.
3. Preliminary determination of the slot dimensions. The lengths $L_{SLOT\text{-}X}$ and $L_{SLOT\text{-}Y}$ of the slot should be lesser than λ_m and a half of λ_m in the x- and in the y-direction, respectively (λ_m is the wavelength in the dielectric substrate at the design frequency). The best initial lengths $L_{SLOT\text{-}X}$ and $L_{SLOT\text{-}Y}$ of the slot should be approximately $0.75\lambda_m$ and $0.4\lambda_m$ in the x- and in y-direction, respectively. The width of the slot W_{SLOT} should be only several hundredths of λ_m, e.g. $\lambda_m/20$. The shorting via I_1 should be placed in the right half of the area bounded by the slot. The best placing of the shorting via I1, for the optimization process of the antenna in the step 5, is in the distance $X_{via} \sim 0.15\lambda_m$ and $Y_{via} \sim \lambda_m/5$ from the edge of the slot.
4. Determination of the coax probe position. The coax probe should be placed in the distance approximately $\lambda_m/4$ from the shorted end of the HMSIW in the x-direction and as much as close the magnetic wall (open edge) of HMSIW in the y-direction. The gap between the coaxial probe and the slot should be $\lambda_m/4$.
5. Application of the optimization process. In order to tune the antenna for a desired operating frequency band, the optimization procedure with the combination of a full wave solver has to be applied.

4.2.7 Summary

This section described the HMSIW circularly polarized U-slot antenna [59]. The antenna was experimentally verified.

The proposed antenna achieves a wider impedance bandwidth, a higher gain and a wider axial ratio bandwidth in comparison to the other relevant compact size antennas (Table 13). Unfortunately, the parametric study showed a high sensitivity of the axis ratio on the position of the shorting via. This fact has to be considered during an antenna design process.

Table 13. Proposed CP U-shape slot antenna in comparison to the other CP HMSIW antennas (λ_0 is wavelength in vacuum).

	Operating frequency [GHz]	s11<-10 dB [%]	Peak gain [dBi]	AR<3 dB [%]	Antenna size
Proposed antenna	10	11.9	6.0	2.2	0.64 λ_0 x 0.24 λ_0
Antenna with dielectric aperture [23]	60	4.5	5.5	4.0	0.73λ_0 x 0.22λ_0
Cavity-backed antenna [10]	8.67	6.0	4.2	0.7	1.07λ_0 x 0.46λ_0
Hybrid antenna [13]	7.9	10	6.8	1	1.45λ_0 x 1.45λ_0
Semi-circle antenna [20]	29	12.8	5.5	2.3	0.65 λ_0 x 0.34λ_0
Dual-band antenna [22]	9.5/8.25	2.1(sim)/1.2(sim)	5.0	1.7	0.35λ_0 x 0.84λ_0

4.3 Reconfigurable HMSIW U-Shape Slot Antenna

A rapid development of microwave wireless applications urges an antenna with polarization diversity. A polarization reconfigurable antenna can dynamically change its radiating characteristics, thus effectively increasing performance of wireless communication systems. The switching between polarizations is carried out by electronically controlling of components built into the antenna. The main disadvantage of these antennas is the necessity to compromise between the possibility of polarization switching and the deterioration of the antenna performance.

In this chapter, a reconfigurable HMSIW U-slot antenna is proposed and described [60].

4.3.1 Antenna Structure - Concept

The concept of reconfigurable HMSIW U-shape slot antenna is based on linearly and circularly HMSIW U-shape slot antennas mentioned above. The geometry of proposed antenna is shown in Fig. 62. The reconfigurable antenna radiating LHCP or LP. To generate LHCP wave, the shorting via is located between the area bounded by the slot and HMSIW bottom wall. The additional short S_2 switch the antenna between the radiation of a circularly and linearly polarized wave. If the short S_2 is present, the antenna generates LP. On the other hand, if the short S_2 is not present, the antenna generates LHCP. The reconfigurable antenna is equipped by a HMSIW-to-SMA transition.

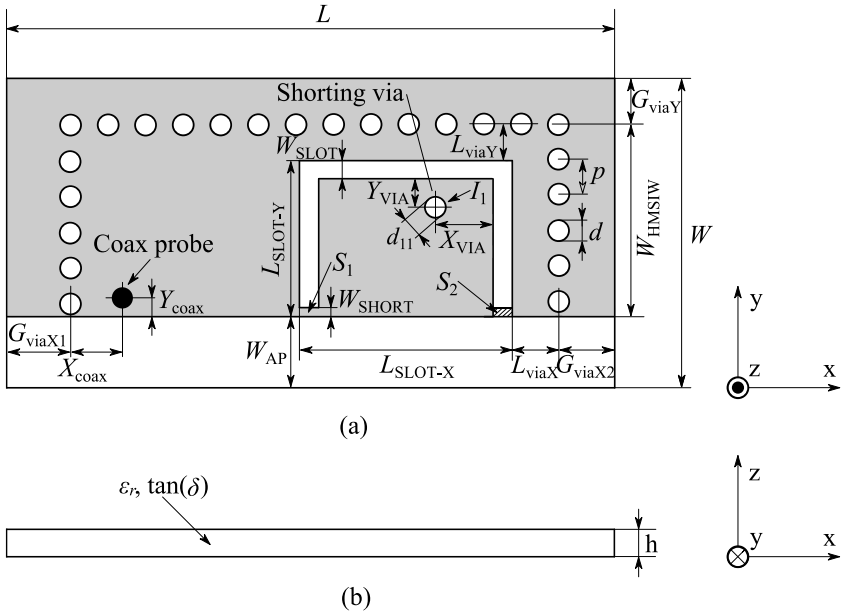

Fig. 62. Top (a) and side (b) view of the reconfigurable HMSIW antenna (the bottom side of the antenna is fully coated by metal).

4.3.2 Simulated Results – Concept

The operating frequency of the proposed antenna is 10 GHz. The antenna was designed with the help of the time domain solver of CST MWS on the dielectric substrate ARLON CuClad 217 (ε_r = 2.17, tan(δ) = 0.0009 and h = 1.524 mm). The HMSIW operates in the fundamental mode $TE_{0.5;0}$. The physical dimensions are noted in the Table 14.

Two models of the antenna were used for the simulation. The first model operates in the LHCP mode and the second operates in the LP mode. The physical dimensions are the same for the both models.

The simulated reflection coefficient of the antenna in LHCP and LP mode is depicted in Fig. 63. The antenna achieves impedance bandwidth 11.9 % and 5.3 % (for s_{11} < - 10 dB) for LHCP and LP mode, respectively. The axial ratio of the LHCP antenna is depicted in Fig. 64. The minimum of AR is 0.19 dB at 10 GHz and the AR bandwidth is 2.4 % (for AR < 3 dB). The simulated radiation patterns for the antenna operating in the LHCP and LP mode are depicted in Fig. 65. The simulated peak gains for the LHPC and LP mode are 6.47 dBi and 6.61 dBi, respectively.

The distribution of the surface currents and the electric field intensity of the antenna operating in LP mode are depicted in Figs. 66 and 67, respectively. Based on the results, the linearly polarized wave is exited. The distribution of surface currents and electric field intensity of the antenna operating in the LHCP mode is depicted in Fig. 68 and 69. Obviously, now the antenna operates in the LHCP mode.

Table 14. Physical dimensions of the reconfigurable antenna concept.

Dimension	[mm]	Description	Dimension	[mm]	Description
L	37.5	length of the substrate	Y_{COAX}	0.8	position of the coax in y-direction
L_{SLOT-X}	14.85	slot length in x-direction	X_{VIA}	2.9	distance of the shorting via in x-direction
L_{SLOT-Y}	8.0	slot length in y-direction	Y_{VIA}	3.65	distance of the shorting via in y-direction
L_{viaX}	2.8	distance between the slot and the row of vias in x-direction	G_{viaX1}	4.2	distance between the HMSIW and the end of the substrate in x-direction
L_{viaY}	1.15	distance between the slot and the row of vias in y-direction	G_{viaX2}	7.5	distance between the HMSIW and the end of the substrate in x-direction
W	18.0	width of the substrate	G_{viaY}	5.85	distance between the HMSIW and the end of the substrate in y-direction
W_{HMSIW}	9.15	width of the HMSIW	H	1.524	height of the substrate
W_{SHORT}	0.3	width of the short	d_{I1}	1.4	diameter of the shorting via
W_{SLOT}	1.1	width of the slot	d	1.4	diameter of the vias
W_{AP}	3.0	width of the aperture	p	2.0	distance between vias
X_{COAX}	3.0	position of the coax in x-direction			

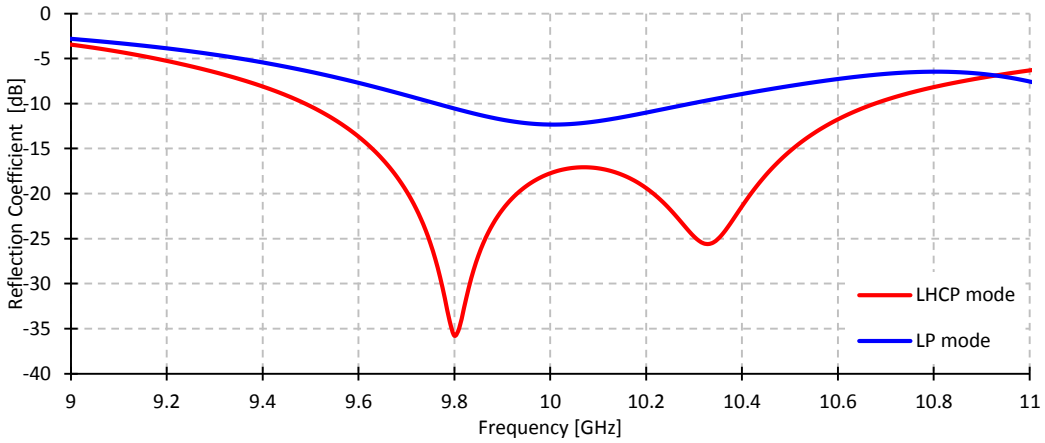

Fig. 63. Simulated reflection coefficient.

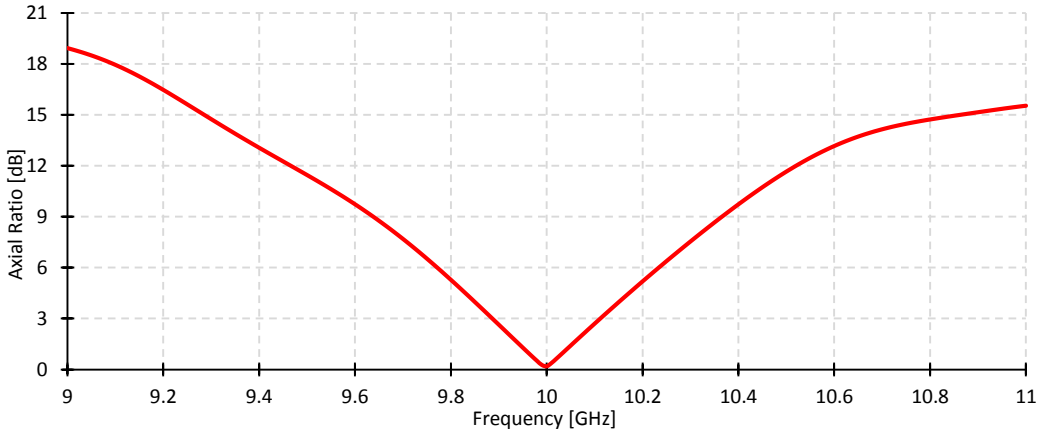

Fig. 64. Simulated axial ratio of LHCP mode.

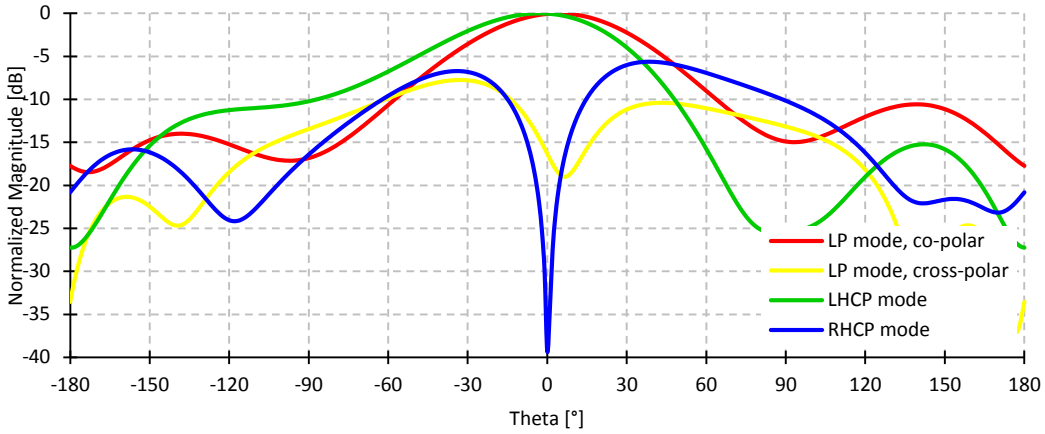

(a)

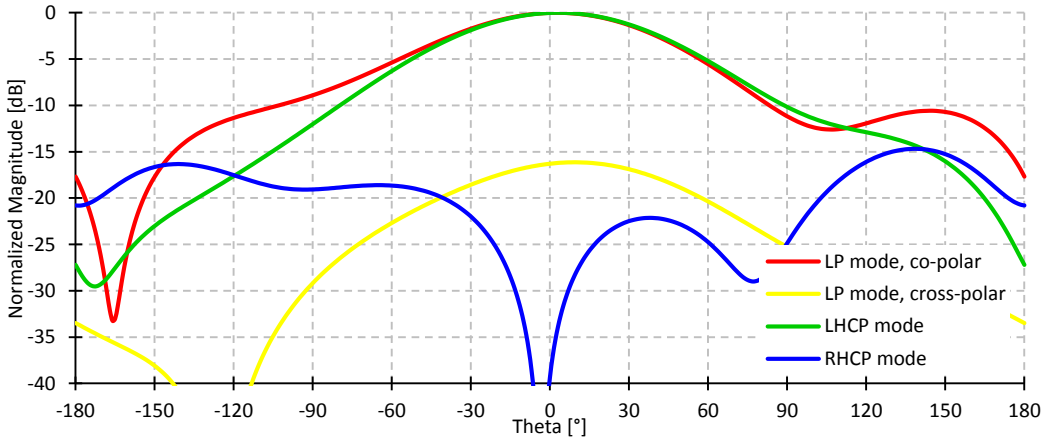

(b)

Fig. 65. Simulated radiation pattern for LHPC and LP mode in (a) xz-plane and (b) yz-plane.

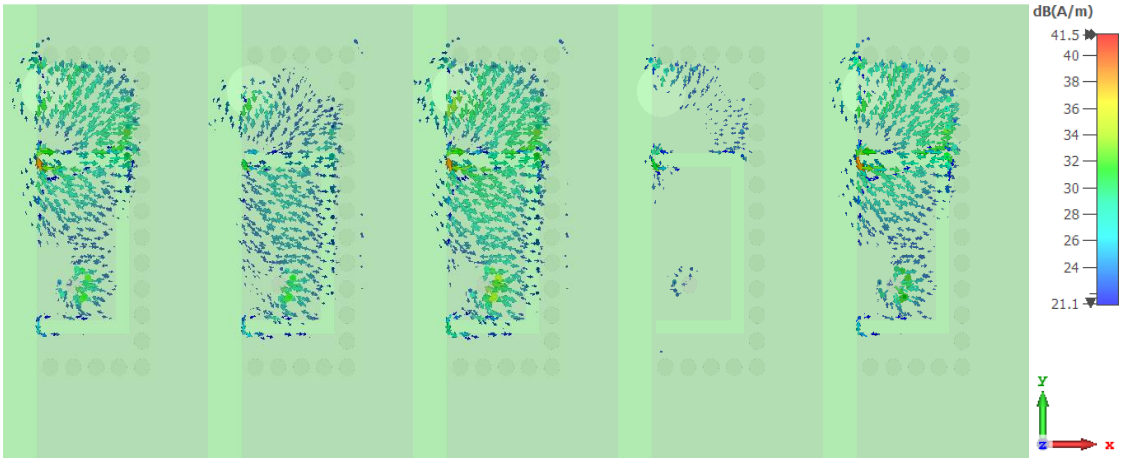

(a) (b) (c) (d) (e)

Fig. 66. Propagation of surface currents of antenna operating in LP mode: (a) phase = 0° and (b) phase = 45°, (c) phase = 90°, (d) = phase 135° and (e) phase = 180°.

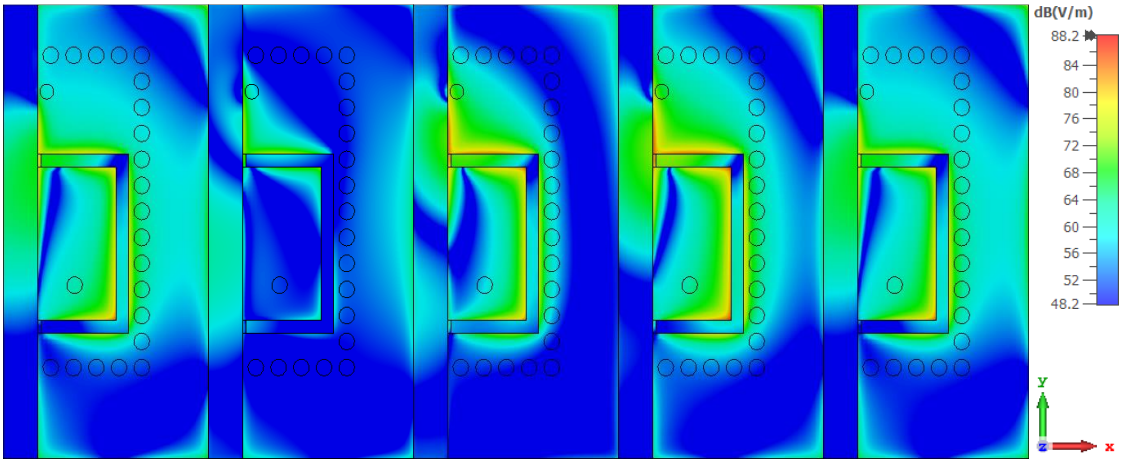

(a) (b) (c) (d) (e)

Fig. 67. Distribution of electric field intensity in substrate (magnitude) of antenna operating in LP mode: (a) phase = 0° and (b) phase = 45°, (c) phase = 90°, (d) = phase 135° and (e) phase = 180°.

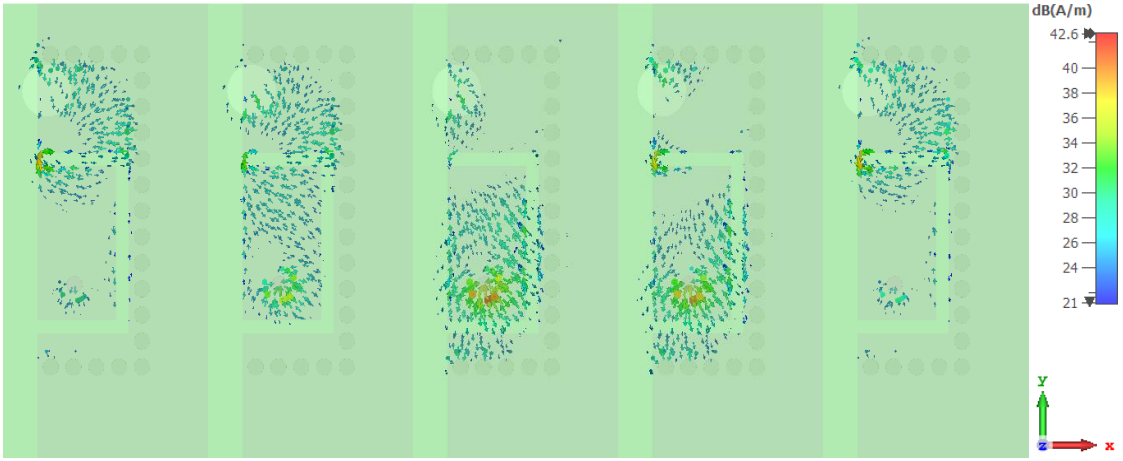

(a) (b) (c) (d) (e)

Fig. 68. Propagation of surface currents of antenna operating in LHCP mode: (a) phase = 0° and (b) phase = 45°, (c) phase = 90°, (d) = phase 135° and (e) phase = 180°.

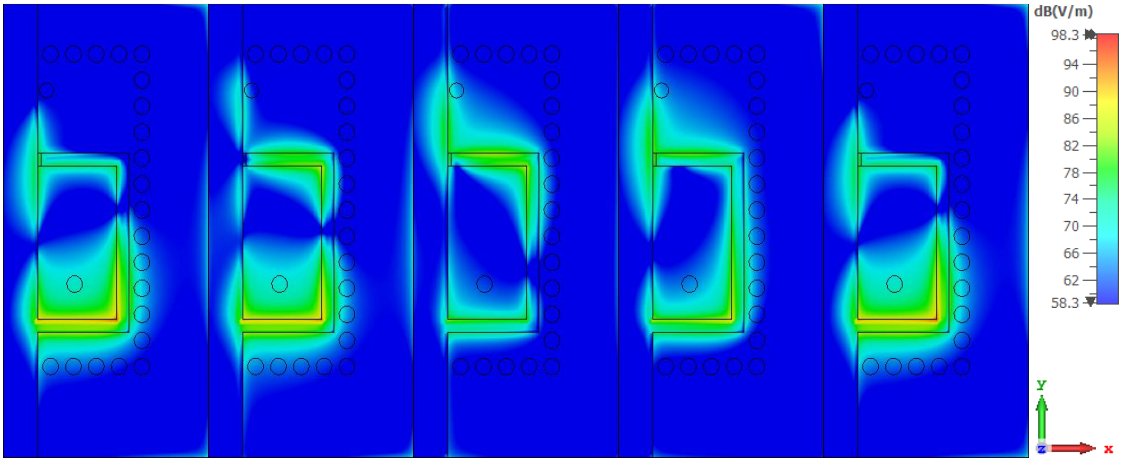

(a) (b) (c) (d) (e)

Fig. 69. Distribution of electric field intensity in substrate (magnitude) of antenna operating in LHCP mode: (a) phase = 0° and (b) phase = 45°, (c) phase = 90°, (d) = phase 135° and (e) phase = 180°.

4.3.3 Experimental Verification – Concept

To verify the proposed antenna concept, two samples of the antenna operating in the circular and linear polarization mode were fabricated (Fig.70) and measured. The reflection coefficient was measured in a laboratory environment, the radiation patterns for the Theta range from –90° to 90° were measured in an anechoic chamber. For the measurement, a Rohde&Schwarz vector network analyzer ZVA67 was used.

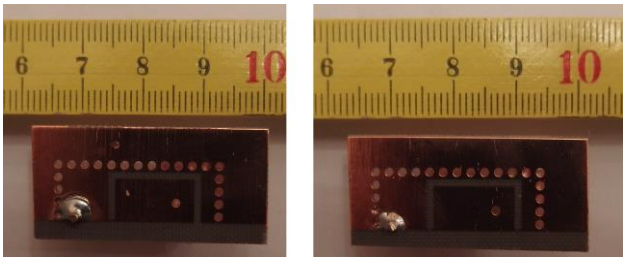

(a) (b)

Fig. 70. Fabricated sample of the antenna concept operating in (a) LHCP and (b) LP mode.

The measured reflection coefficient of the antennas operating in the LHCP and LP mode are depicted in Fig. 71. The measured impedance bandwidth (for s_{11}< -10 dB) of the antenna in the LHCP mode is 12.2%, and in the LP mode is 5.2%. The discrepancy between the simulated and measured data in mainly caused due to fabricated tolerances. In Fig. 72 the measured axial ratio of the antenna operating in the LHCP mode is depicted. The measured bandwidth of the axial ratio is 2.2 % (for AR < 3 dB) compared to the simulated value of 2.4%. The measured minimum of the axial ratio is 0.8 dB at the frequency of 9.94 GHz and the simulated one is 0.19 dB. The minimum of the measured axial ratio is shifted about 60 MHz to the lower frequencies in comparison to the simulated data. This discrepancy is mainly caused by a position of the shorting via I_1 since its position in the x-direction strongly influences the location of the axial ratio minimum along the frequency axis, as it was presented in the parametric study of the CP antenna in the chapter 4.2.

The normalized radiation patterns were measured in two orthogonal cutting planes (xz-plane and yz-plane) at the frequency 10 GHz. The radiation patterns of the antenna operating in the LP mode are in Fig. 73. The measured results are in good agreement with the simulated ones. The measured peak gain of the antenna at 10 GHz is 6.2 dBi. The measured radiation patterns for the antenna operating in the LHCP mode are depicted in Fig. 74. The simulated and measured radiation patterns are in good agreement. The measured peak gain of the antenna at 10 GHz is 5.4 dBi.

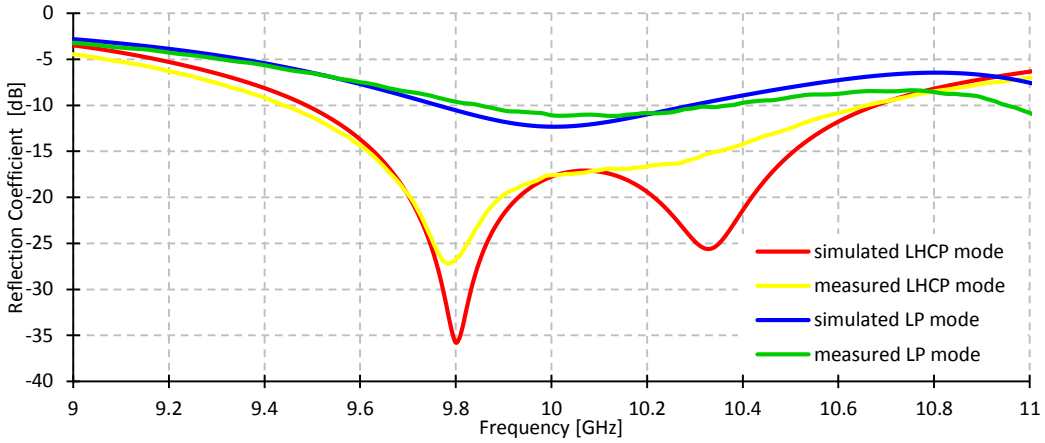

Fig. 71. Reflection coefficient.

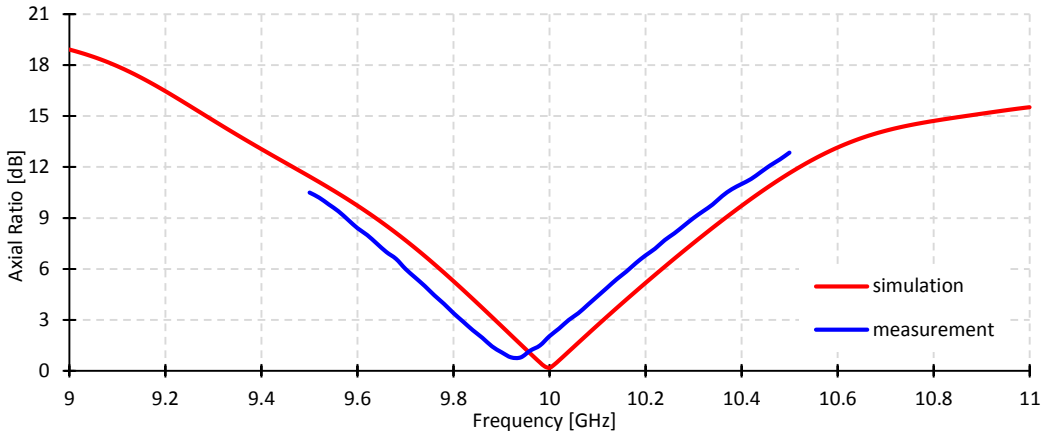

Fig. 72. Axial ratio of LHCP mode.

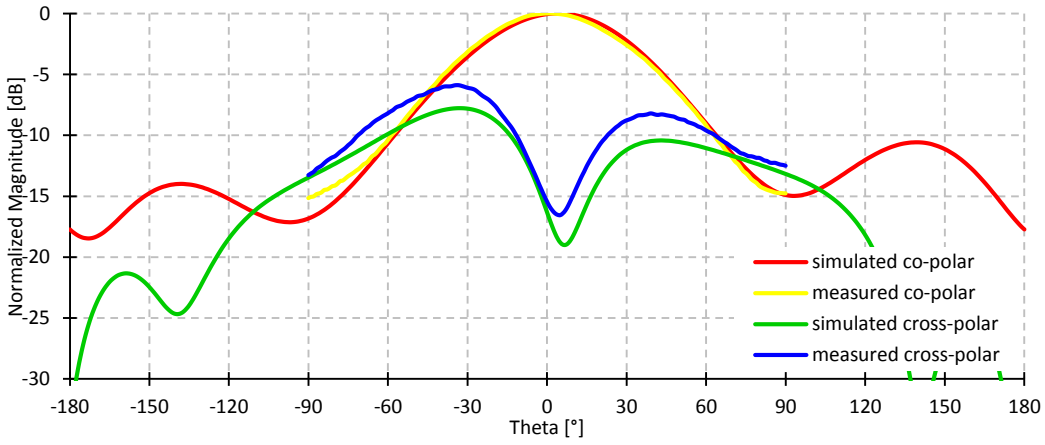

(a)

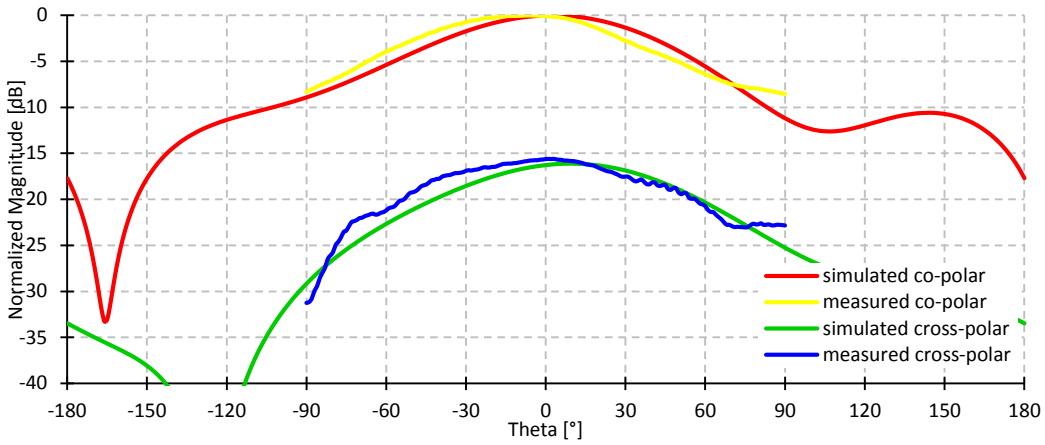

(b)

Fig. 73. Normalized radiation pattern of antenna operating in LP mode: (a) xz-plane (E-plane) and (b) yz-plane (H-plane).

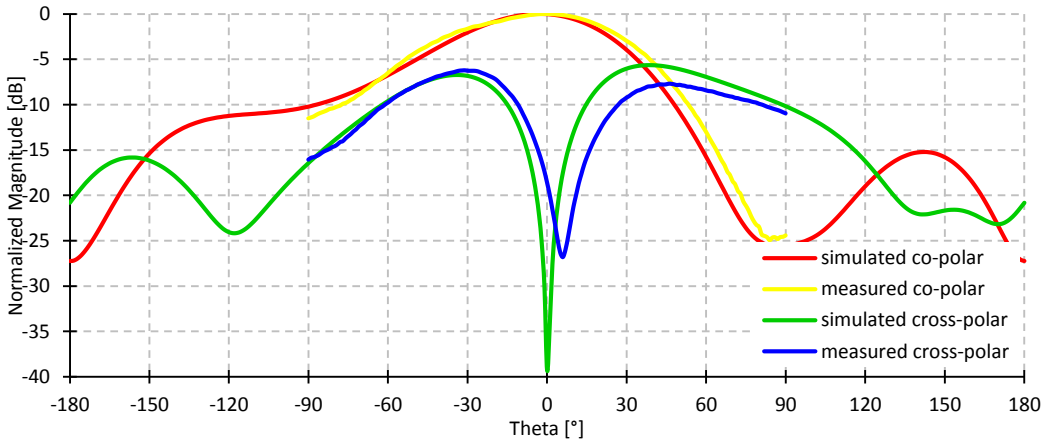

(a)

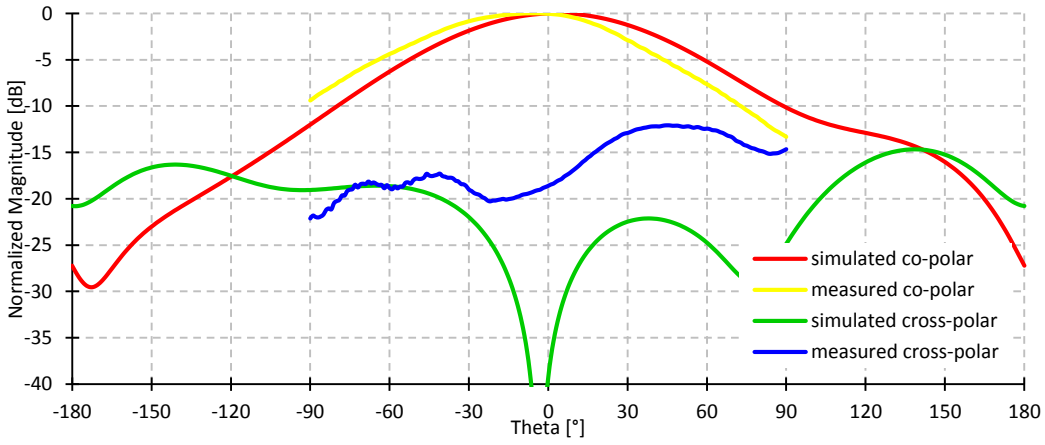

(b)

Fig. 74. Normalized radiation pattern of antenna operating in LHCP mode: (a) xz-plane and (b) yz-plane.

4.3.4 Antenna structure – Electronic Control

The antenna should be electronically controlled to achieve the desired polarization. The most advantageous solution was to substitute the short S_2 by a two separated PIN diodes. The circuit diagram of the solution is depicted in Fig. 75(a) and the implementation of the

solution is depicted in Fig. 75(b). If the diodes D_1 and D_2 are turned on, the LP is obtained, otherwise the LHCP is obtained. The diodes are glued on the board and they are fed by a direct current through via I_2. The power is supplied by a standard AA battery which is placed in a battery holder located on the back side of the board. In order to the separate the direct current from the high-frequency current, the inductor L_1 had to be used. The inductance of the inductor is 2 nH and the self-resonant frequency is at 16.3 GHz. An electronic load in the form of a resistor R_1 had to be used to reduce the current flowing through the two PIN diodes. The resistance of the resistor is 68 Ω. The specification of the PIN diodes and the inductor are summarized in the Table 15.

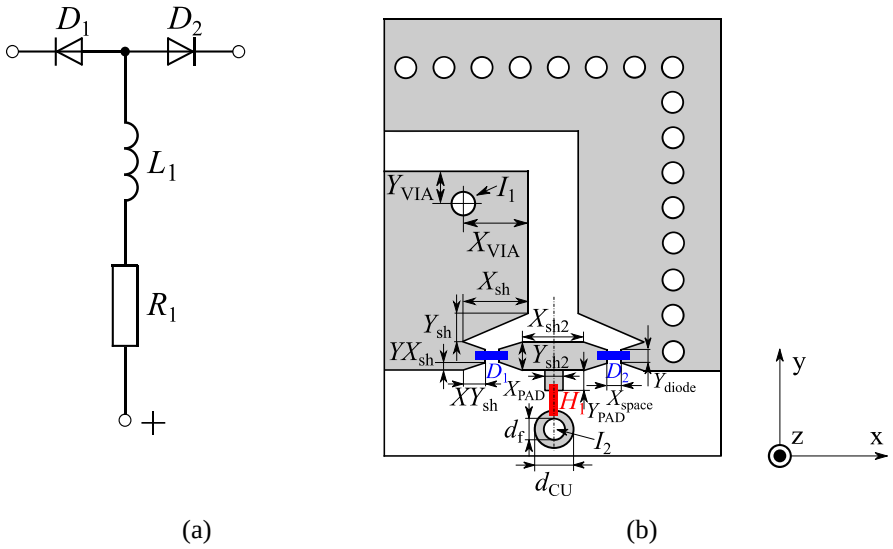

(a) (b)

Fig. 75. Implementation of the electronic switching control between LHCP and LP mode: (a) circuit diagram and (b) realization on the boar.

Table 15. Specification of the components used for the implementation of the electronic switching control between LHCP and LP.

Component	Value	Condition
	total capacitance C_T = 0.025 pF	-10 V, 1 MHz
PIN diode	series resistance R_S = 5.2 Ω	+10 mA, 1 GHz
MA4GP907 [65]	forward voltage V_F = 1.33 V	+10 mA
	reverse voltage current I_R = 10 µA (max)	V_R = -50 V
inductor	inductance L = 2 nH	
LQP03TQ2N0B02D [66]	self-resonant frequency F_s = 16.3 GHz	

4.3.5 Simulated Results – Electronic Control

The antenna was designed with the help of the time domain solver in CST Microwave Studio on the dielectric substrate ARLON CuClad217. The physical parameters of the antenna are almost the same as the reconfigurable antenna concepts defined in Table 14, however, the via I_1 had to be shifted in order to tune the antenna at the desired frequency, because the chamfering of the slot and the feeding network of the PIN diodes slightly influences the electric field in the slot. The physical parameters of the implementation of the electronic switching control are summarized in Tab. 16.

The simulated reflection coefficient of the antenna switched for LHCP and LP mode is depicted in Fig. 76. The 12.7 % and 6.5 % impedance bandwidth for the reflection coefficient less than – 10 dB are obtained for the LHCP and LP operating mode,

respectively. The simulated axial ratio for LHCP mode is depicted in Fig. 77. Its minimum is 0.67 dB at the frequency of 10 GHz, and the AR bandwidth is 2.4 % (for AR <3 dB). The simulated radiation patterns of the antenna operating in both modes in the xz-plane and yz-plane are shown in Fig. 78. The maximum of radiation is about 10 degrees shifted with respect to the direction which is perpendicular to the antenna plane due to parasitic radiation of the coax-HMSIW transition and the disturbetion of the surface currents caused by the electronic control. The simulated gain of the antenna for the LHCP and LP mode are 6.46 dBi and 7.04 dBi, respectively. For the LHCP and LP mode, the level of the cross-polarization is about -29 dB and -17.7 dB in the broadside direction, respectively.

The distribution of the surface currents and the electric field intensity for the LP mode of the antenna are depicted in Figs. 79 and 80, respectively. The results proves that the linearly polarized wave is excited. The distribution of surface currents and electric field intensity depicted in Figs. 81 and 82 indicate that in the CP mode the antenna radiates LHCP wave.

Table 16. Physical dimensions of antenna with electronic switching between LHCP and LP operating mode.

Dimension	[mm]	Description	Dimension	[mm]	Description
X_{via}	2.8	distance of the shorting via in x-direction	Y_{sh2}	0.8	node length in y-direction
X_{sh}	1.28	cutout length in x-direction	Y_{PAD}	0.4	pad length in y-direction
X_{sh2}	1.53	node length in x-direction	Y_{diode}	0.6	pad length for diode in y-direction
X_{PAD}	0.4	pad length in x-direction	XY_{sh}	0.4	chamfering of the cutout in x-direction
X_{space}	0.33	space between the node and the outer area	YX_{sh}	0.1	chamfering of the cutout in y-direction
Y_{via}	4.09	distance of the shorting via in y-direction	d_f	1.4	via diameter for feeding
Y_{sh}	0.4	cutout length in y-direction	d_{CU}	3	cooper diameter for inductor

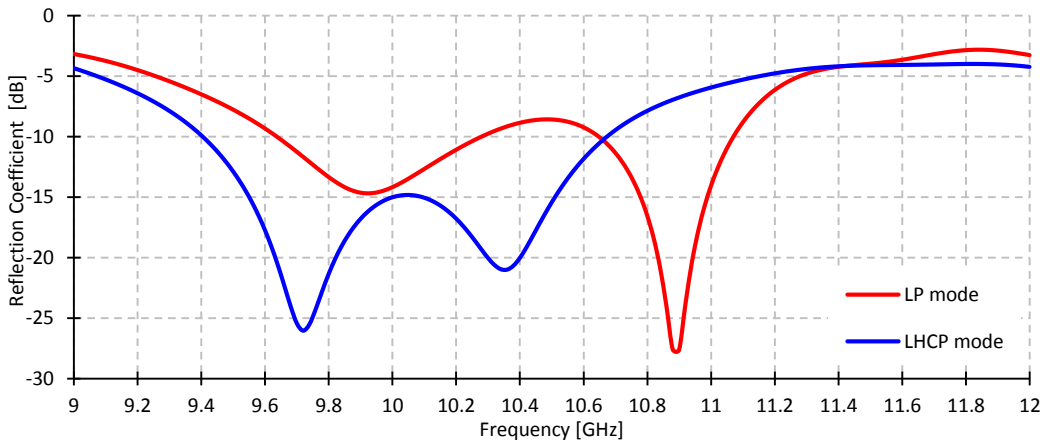

Fig. 76. Reflection coefficient.

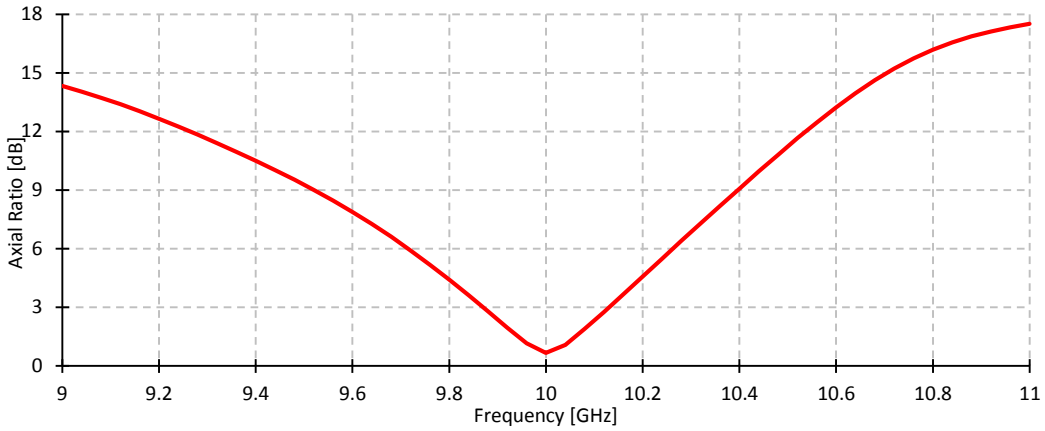

Fig. 77. Axial ratio of LHCP mode.

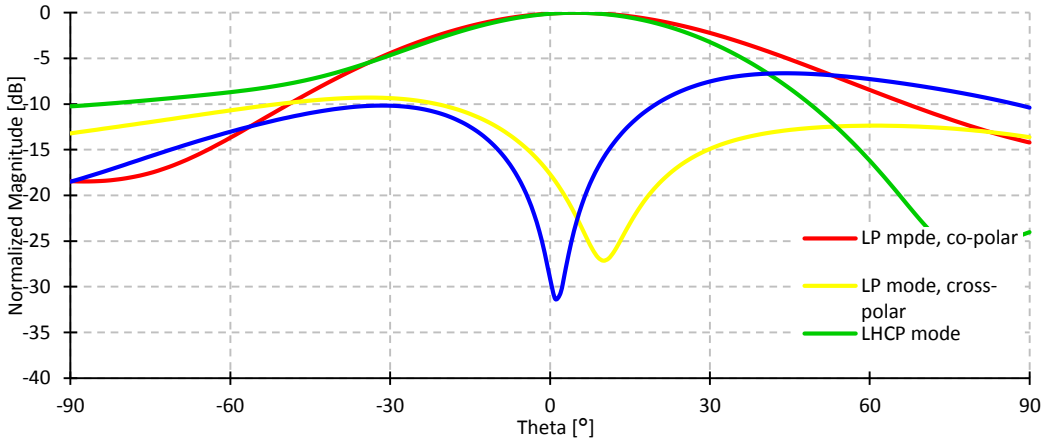

(a)

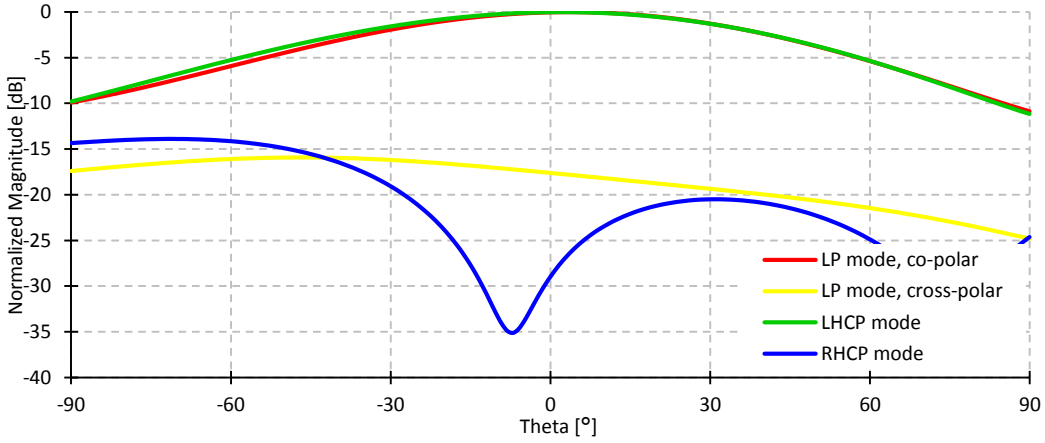

(b)

Fig. 78. Simulated radiation pattern for LHPC and LP mode in (a) xz-plane and (b) yz-plane.

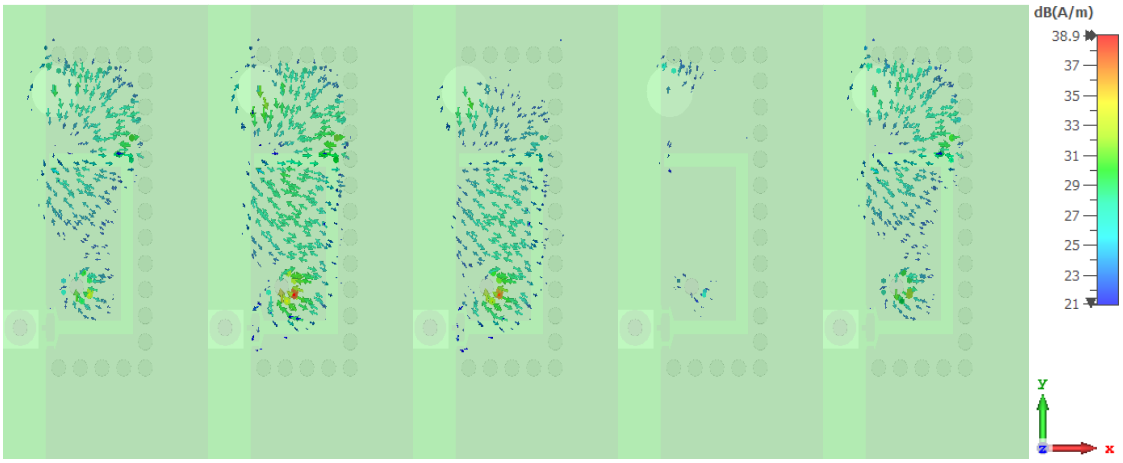

(a) (b) (c) (d) (e)

Fig. 79. Propagation of surface currents of antenna operating in LP mode (electronic components are set to "hidden"): (a) phase = 0° and (b) phase = 45°, (c) phase = 90°, (d) = phase 135° and (e) phase = 180°.

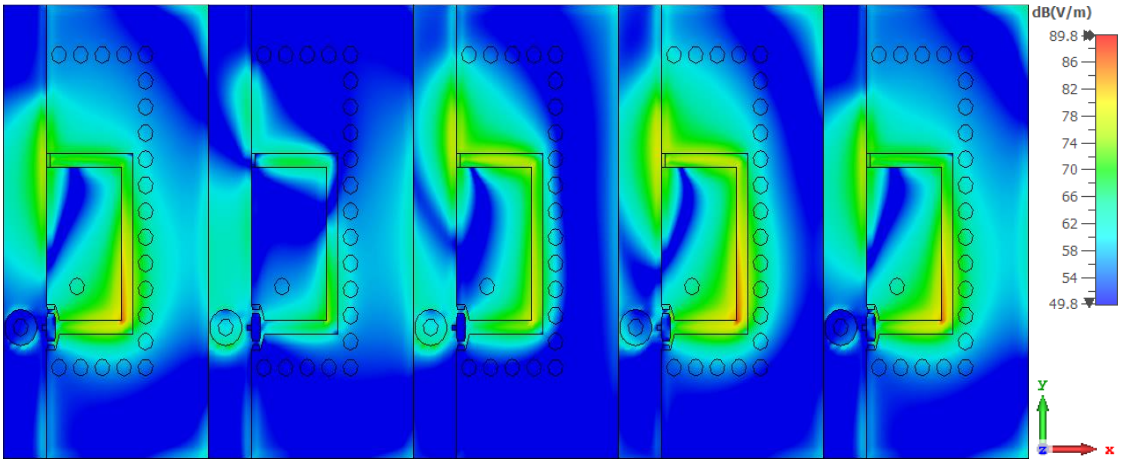

(a) (b) (c) (d) (e)

Fig. 80. Distribution of electric field intensity in substrate of antenna operating in LP mode (magnitude) (electronic components are set to "hidden"): (a) phase = 0° and (b) phase = 45°, (c) phase = 90°, (d) = phase 135° and (e) phase = 180°.

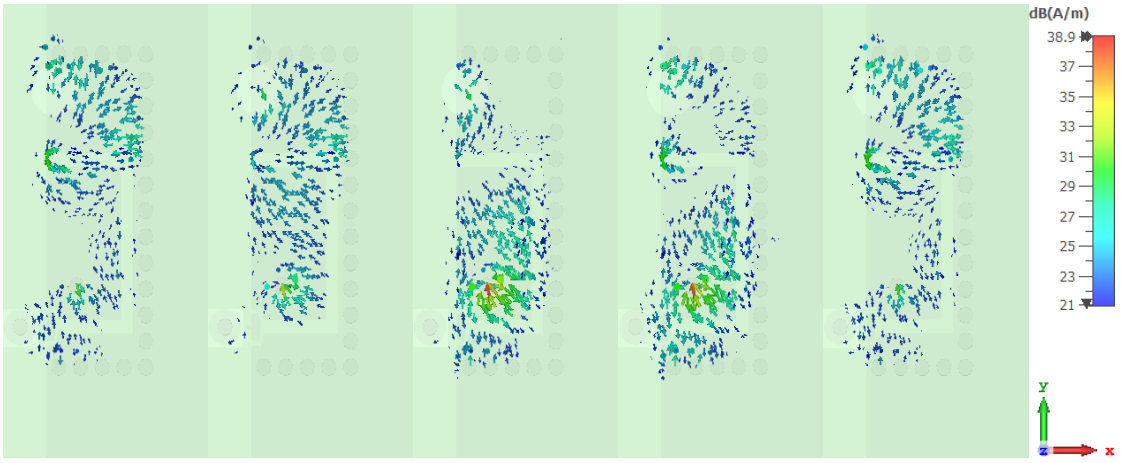

(a) (b) (c) (d) (e)

Fig. 81. Propagation of surface currents of antenna operating in LHCP mode (electronic components are set to "hidden"): (a) phase = 0° and (b) phase = 45°, (c) phase = 90°, (d) = phase 135° and (e) phase = 180°.

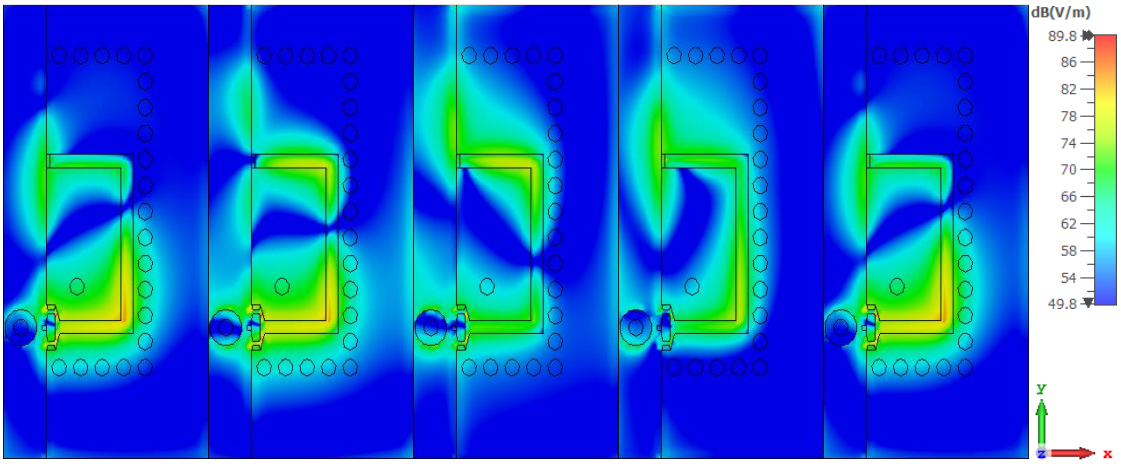

(a) (b) (c) (d) (e)

Fig. 82. Distribution of electric field intensity in substrate of antenna operating in LHCP mode (magnitude) (electronic components are set to "hidden"): (a) phase = 0° and (b) phase = 45°, (c) phase = 90°, (d) = phase 135° and (e) phase = 180°.

4.3.6 Experimental Results – Electronic Control

To verify the proposed antenna with the electronic control of the polarization mode, a sample of the antenna was fabricated (Fig. 83) and measured. The battery holder was not attached to the back of the board during photo shooting. The reflection coefficient was measured in a laboratory environment. The radiation patterns for the Theta range from –90° to 90° were measured in an anechoic chamber. For the measurement, Rohde&Schwarz vector network analyzer ZVA67 was used.

Fig. 83. Fabricated sample of the antenna with the electronic control of the polarization mode.

The measured reflection coefficient of the antennas operating in the LHCP and LP mode are depicted in Fig. 84 and Fig. 85. The measured impedance bandwidth (for s_{11}< -10 dB) of the antenna in the LHCP mode is 25.4%, and in the LP mode is 12.8%. In the LHCP mode, the measured reflection coefficient is in good agreement with the simulated one. In the LP mode, the measured reflection coefficient is shifted to the upper frequencies and the simulated second resonance is completely suppressed. That suppression might be caused by the disturbetion of the flow of the surface currents in the radiator by the implementation of the electronic control. The measured axial ratio for the LHCP mode is depicted in Fig. 86. The minimum of the axial ratio is noticeably shifted to the lower frequencies. Based on the parametric study of the LHCP antenna in the previous chapter, it is seems that the shift is caused by a slight displacement of the shorting via I_1. The minimum of the axial ratio is 0.55 dB at the frequency of 9.68 GHz and the AR frequency bandwidth is 2.5 % (for AR< 3 dB). The measured co-polar components (LHCP) of the radiation pattern are in good agreement with the simulated ones in both cutting planes (Fig. 87(a) and (b)). On the other hand, the measured minimum of the cross-polar component (RHCP) is shifted in the xz-plane (Fig. 87(a)). In the yz-plane, the measured

level of the cross-polar component is much higher than excepted (Fig. 87(b)). That might be caused by the displacement of the shorting via I_1, inaccuracies during the manufacture process or implementation of the electronic control of polarization or any combination of these inaccuracies. In LP mode, the co-polar and cross-polar components are in good agreement with the simulates ones (Fig. 88(a) and (b)). The measured peak gain in the LHCP and LP mode are 6.77 dBi and 7.09 dBi, respectively.

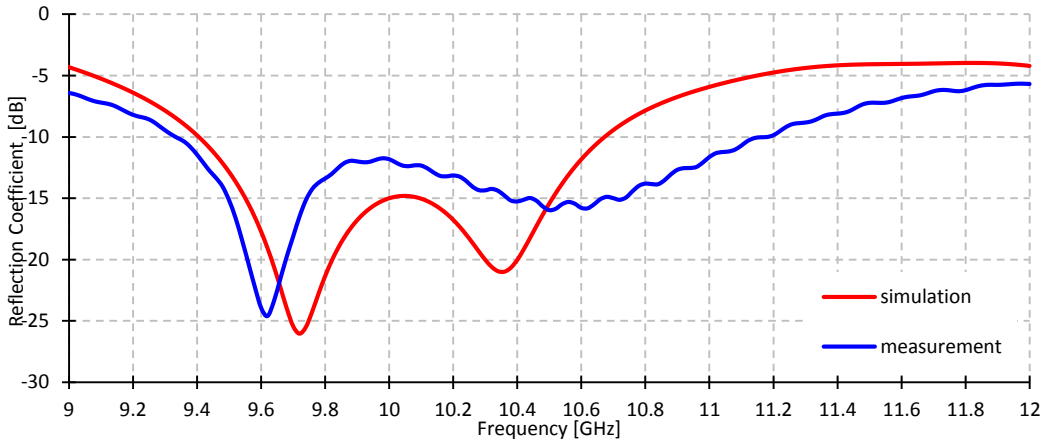

Fig. 84. Measured reflection coefficient of the antenna in LHCP mode.

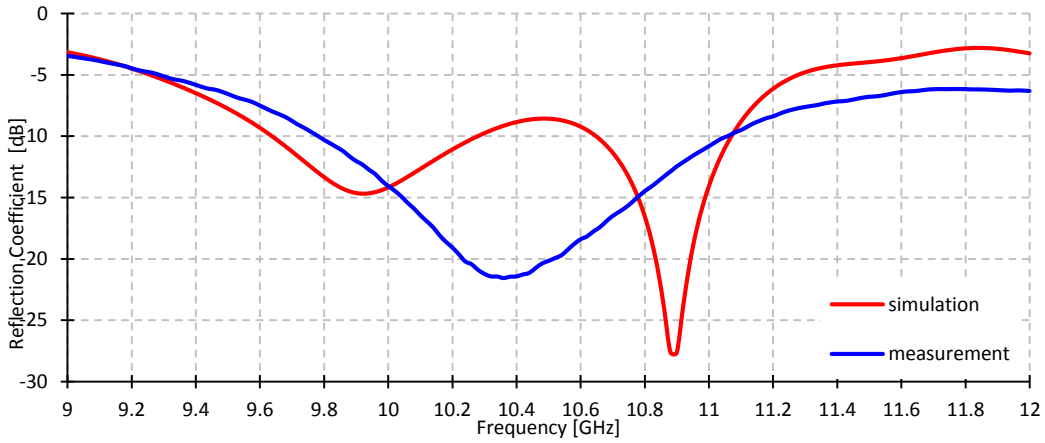

Fig. 85. Measured reflection coefficient of the antenna in LP mode.

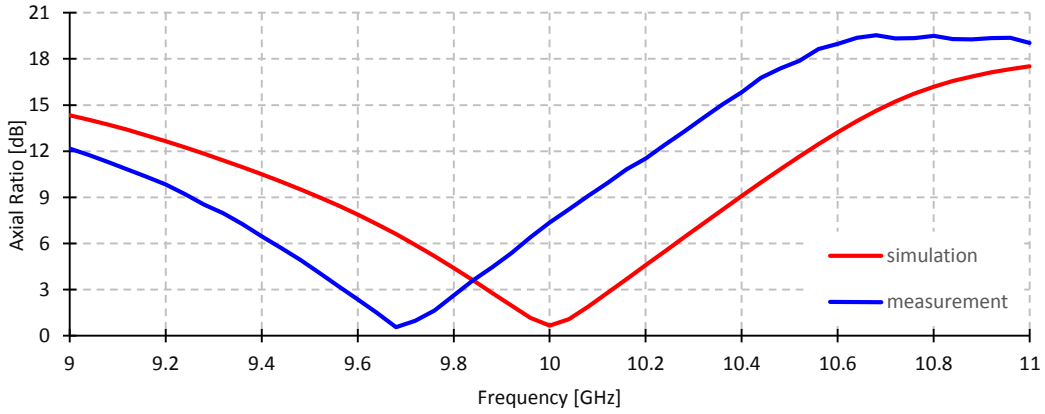

Fig. 86. Measured axial ratio of antenna in LHCP mode.

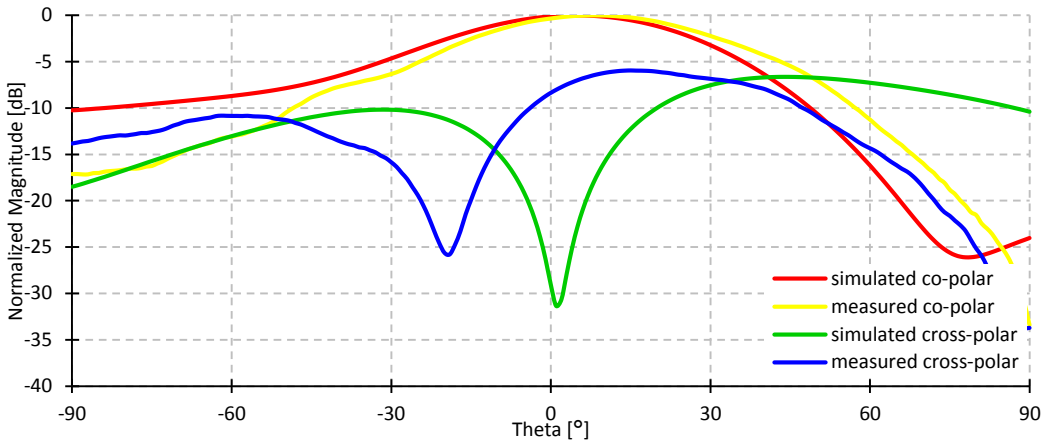

(a)

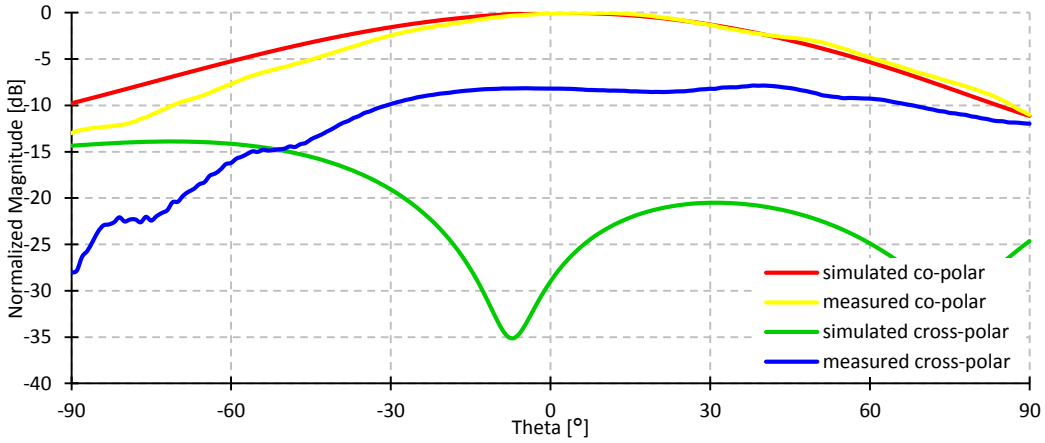

(b)

Fig. 87. Normalized radiation pattern for LHCP mode in: (a) xz-plane and (b) yz-plane.

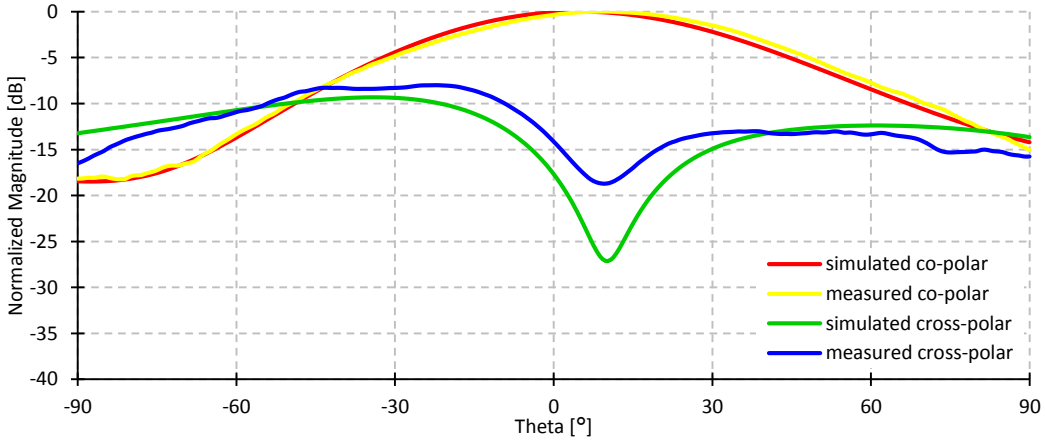

(a)

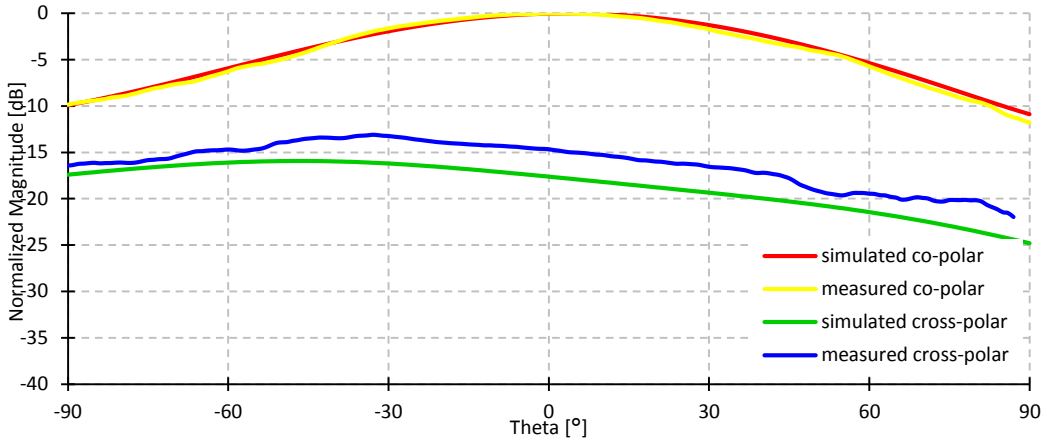

(b)

Fig. 88. Normalized radiation pattern for LP mode in: (a) xz-plane (E-plane) and (b) yz-plane (H-plane).

4.3.7 Summary

This section described the concept and the implementation of the electronic control of the reconfigurable HMSIW U-slot antenna. The reconfiguration supports switching between circular and linear polarization. The measured results of the antenna reconfigurable concept presented in the chapter 4.3.3. showed a promising way to a functional implementation of an electronic switching. The proposed electronic control described and studied in the chapters 4.3.4 – 4.3.6 was realized by the two PIN diodes and a feeding network. Unfortunately, the measured results of the antenna with implemented electronic control are a bit different in comparison to the simulated ones, especially the axial ratio. The differences between the measured a simulated results indicate that the electronic control disturbers the surface currents within the antenna more than was expected.

Summarized measured results are compared to the similar reconfigurable antennas (Table 17).

Table 17. Proposed polarization reconfigurable slot antenna in comparison to the other polarization reconfigurable antennas (f_o is operating frequency and λ_0 is wavelength in vacuum).

	Polarization	**f_o [GHz]**	**s_{11} at f_o [dB]**	**Impedance bandwidth [%] (s_{11}<-10 dB)**	**Peak gain [dBi]**	**Axial ratio BW [%] (AR<3dB)**	**Size of antenna**
Proposed antenna	LHCP/LP	10	-12.5/-14	25.4/12.8	6.77/7.09	2.5	$1.25\lambda_0 \times 0.6\lambda_0$
Novel reconfigurable antenna [32]	LHCP/RHCP	5.8	-17/-15	2.1/2	6/-	1/-	$0.33\lambda_0 \times 0.32\lambda_0$
Antenna with slotted ground [34]	LHCP/RHCP	2.5	-12/-12	4.8/4.8	5.7/5.7	2.8/2.8	$0.22\lambda_0 \times 0.22\lambda_0$
Antenna with switchable slots [46]	LHCP/RHCP	4.64	-17.5/-15	14/13.9	-/-	3/3	$0.62\lambda_0 \times 0.62\lambda_0$
Polarization diversity antenna [38]	LHCP/RHCP/LP	2.45	-11/-8/-6	2/1.6/1.9	-/-/-	1.27/1	$0.45\lambda_0 \times 0.45\lambda_0$
Single-feed antenna [33]	LHCP/RHCP/LP	2.48	-18/-15.5/-17	4/4/1.2	6/6/5.9	0.74/0.72	-
Antenna with agile polarization [36]	LHCP/RHCP/LP	5.4	-20/-18/-8	8.7/8.7/1.9	-/-/-	2.03/2.03	$0.63\lambda_0 \times 0.63\lambda_0$

5. Circularly polarized HMSIW Antenna Array

This chapter deals with the second objective of this thesis which is focused on exploitation of obtained knowledge from the first objective of this thesis, solved in detail in the chapter 4, for the design of antenna array. Here the attention will be concentrated on a circularly polarized antenna array based on the circularly polarized antenna element proposed and described in the chapter 4.2

5.1.1 Antenna array structure

The most important thing addressed during the antenna array design process is an organization of the basic radiators and its feeding network. From the viewpoint of the radiation pattern, those ones have significant influence on a shape of radiation pattern and consequently on a main beam of directional antennas. An antenna array could be organized as a planar array of $m \times n$ or a linear array with an organization of $1 \times n$, where m and n are number of the radiators in the y- and x-direction. A feeding network should assure desired excitation, an amplitude and phase, of a radiator in an antenna array. Amplitudes affect the shape of the main lobe and the shape of the lateral lobes, while phase affects mainly the direction of the main lobe.

The feeding network could be implemented in several ways. Let's take into consideration the antenna array with a linear organization and series feeding network. To assure a broadside radiation, the radiators of the antenna array should be fed by the same phase. However, for the considered antenna array with a linear organization of antenna radiators and series feeding network, that fact could imposes that the distance of the center of the radiators is larger than $\lambda_0/2$, where λ_0 is wavelength in the free space, so higher level of side lobes can be obtained. In addition, it the series feeding network has disadvantage in gradual reduction of the excitation amplitude due to radiation by radiators and losses in the feeding network.

More complex method for antenna array design is based on the Elliot's design procedure [84], [85]. This method is based on that all basic radiators in an antenna array should be self-resonant such that the sum of their normalized conductances is unity. In order to achieve that values, admittance of every basic radiator must be pure real. But the basic radiator does not achieve self-resonance on its own (or it is difficult to achieve), therefore, a matching via, which is additional tuning element, must be placed at an exacted position near the basic radiator. Then the pure admittance of the basic radiator could be obtained and the basic radiator is matched. The main advantage of this method is very low level of side-lobe level but on the other hand, the method could be relatively difficult to correctly carry out the extraction of the required values.

During the design process of the antenna array, it was decided to design RHCP antenna array with linear organization of 1×4 with the simple series feeding network. The main point of this effort is to show that the antenna could be used as a basic radiator in an antenna array.

The design process was consists of three steps. The first one was design of a HMSIW with coax-to-HMSIW transition. The second one was a design of the basic radiator. The design is carried out in the chapter 4.2. Thus, the diameters of the basic radiator were taken from the Table 11. In order to achieve RHCP, the LHCP antenna (whole board with the SMA connector) mentioned in the chapter 4.2 was simply mirrored with respect to the xz-plane. All the dimensions remained the same (Table 11). The last one was to determine the distance between radiators to assure the same excitation phase. Further, the center of

the coaxial probe should be located at the distance $\lambda_m/4$ (λ_m is the wavelength in the waveguide) from the shorted end of the HMSIW and at the distance $\lambda_m/4$ from the basic radiator in x-direction and as much as close the magnetic wall (open edge) of HMSIW in the y-direction.

The antenna array structure is depicted in Fig. 89. The L_e describes the distance between the basic radiators. Other description of the antenna structure is the same as it is in the chapter 4.2.1.

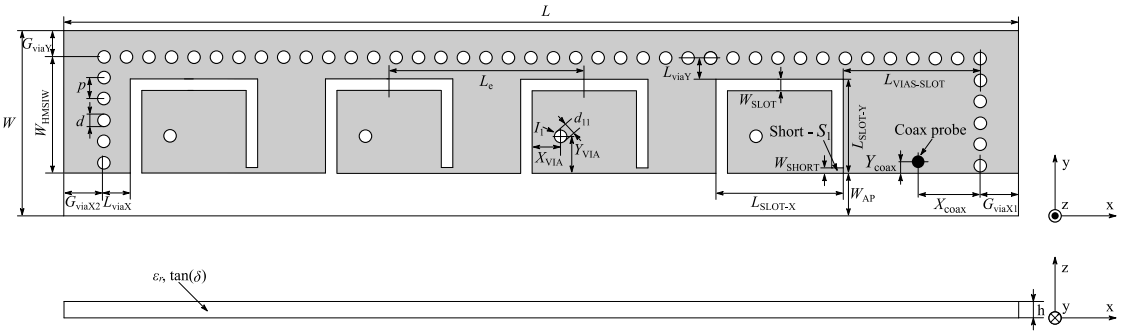

Fig. 89. Top (a) and side (b) view of the RHCP antenna array (the bottom side of the antenna is fully coated by metal).

5.1.2 Simulated Results

The antenna array was designed and simulated in CST MWS by the time domain solver for the operating frequency band of 10 GHz. In order to reduce computing time during calculation the simulation of the antenna, vias of HMSIW were substituted by a solid wall made of PEC. The waveguide operates in the fundamental mode $TE_{0.5;0}$ with the cutoff frequency of 5.99 GHz. The antenna is designed on the dielectric substrate ARLON Cuclad 217. During the optimization process, the dimensions of the basic radiator had to be slightly adjusted in order to get the best results. The via I_1 had to be shifted towards the lower right corner because it greatly disturbs surface currents, as it is described in the parametric study in the chapter 4.2.5. The final dimensions of the antenna array are summarized in Table 18.

The simulated reflection coefficient is depicted in Fig. 90. The minimum of the reflection coefficient is – 20 dB at 10 GHz. The impedance bandwidth is 17.4 % for the reflection coefficient less than – 10 dB. The axial ratio at 10 GHz reaches 0.77 dB and the corresponding axial ratio bandwidth is 1.7 % (for AR<3 dB) (Fig. 91). The normalized radiation patterns in two orthogonal cutting planes at the frequency 10 GHz are depicted in Fig. 92. The maximum of the radiation is perpendicular to the antenna plane. The simulated peak gain is 12.8 dBi. The surface currents and distribution of the electric field are depicted in the Figs. 93 and 94, respectively. As it was expected, the basic radiators are not excited with the same amplitude. That caused the higher level of side-lobe level (about -13 dB) and higher level of cross-polarization in the broadside direction. It is also clear that the more distant radiators are not excited with the same phase but the length λ_0 is respected.

Table 18. Dimensions of the antenna array.

Dimension	[mm]	Description	Dimension	[mm]	Description
L	127	length of the substrate	X_{VIA}	3.21	distance between the shorting via and edge of the slot in x-direction
L_{SLOT-X}	16.22	slot length in x-direction	Y_{VIA}	2.65	distance between the shorting via and edge of the slot in y-direction
L_{SLOT-Y}	7.16	slot length in y-direction	X_{COAX}	4.3	distance between the coax probe and row of vias in x-direction
L_{viaX}	3.7	distance between the last slot and the row of vias in x-direction	Y_{COAX}	0.8	distance between the coax probe and open edge of the HMSIW
L_{viaY}	1.7	distance between the slot and the row of vias in y-direction	G_{viaX1}	3	distance between the HMSIW and the end of the substrate in x-direction
Le	29.98	distance between the center of the radiators	G_{viaX2}	3	distance between the HMSIW and the end of the substrate in x-direction
$L_{VIAS-SLOT}$	9.8	distance between the first slot and the row of vias in x-direction	G_{viaY}	3	distance between the HMSIW and the end of the substrate in y-direction
W_{SLOT}	1.1	width of the slot	h	1.52	width of the dielectric substrate
W_{SHORT1}	0.4	width of the short S_1	d	1.4	diameter of the via
W_{HMSIW}	8.8	width of the HMSIW	d_{I1}	1.4	diameter of the shorting via
W_{AP}	3.0	width of the aperture	p	2.58	distance between vias

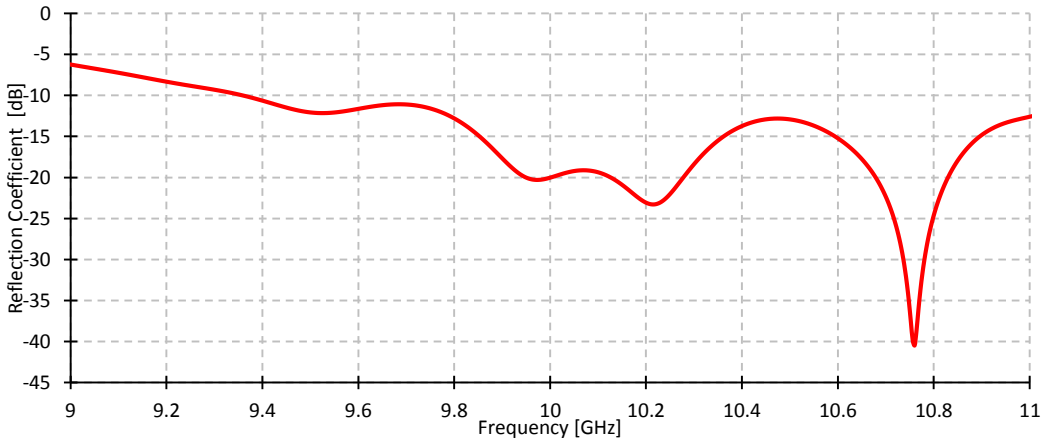

Fig. 90. Simulated reflection coefficient of the circularly polarized antenna array.

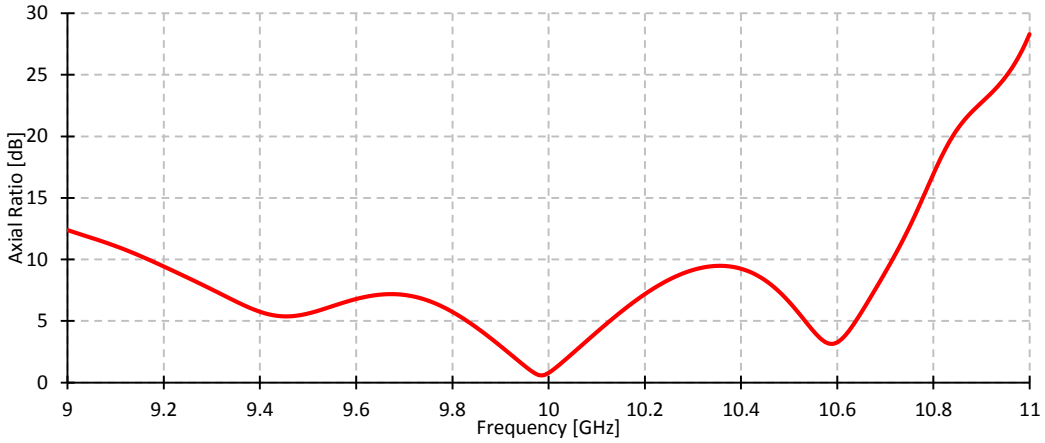

Fig. 91. Simulated axial ratio of the circularly polarized antenna array.

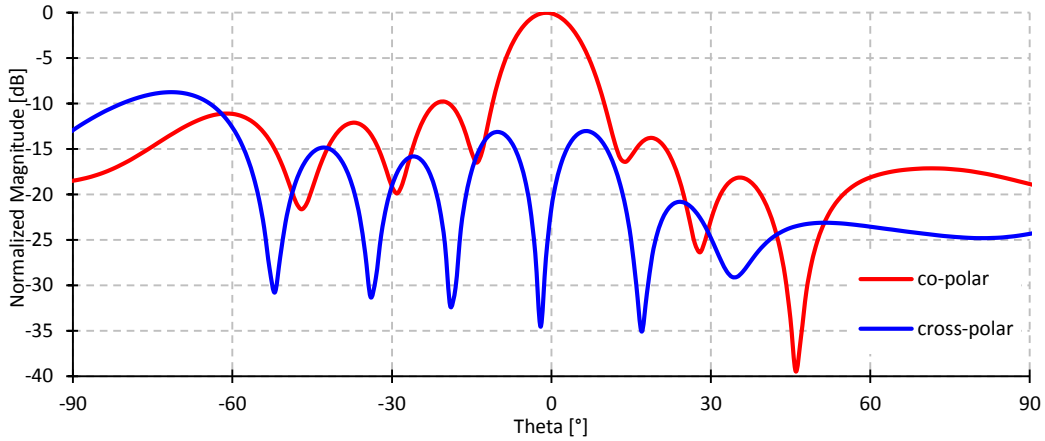

(a)

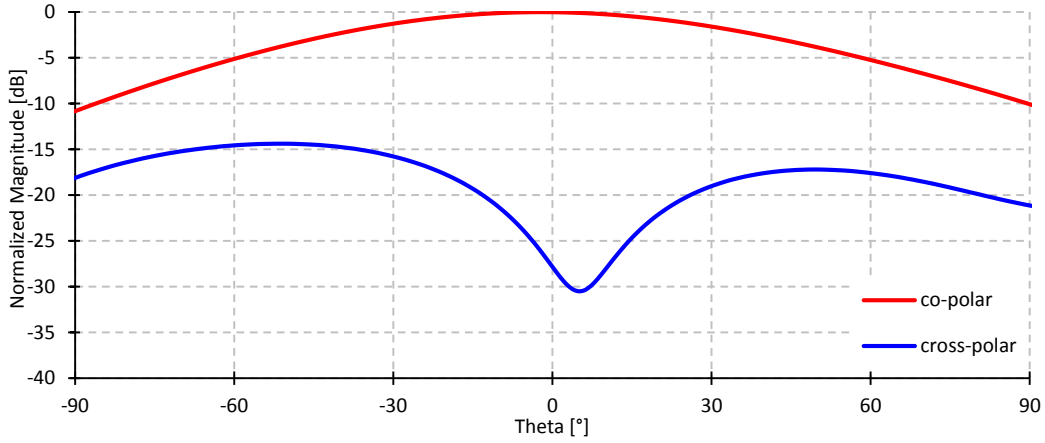

(b)

Fig. 92. Simulation of normalized magnitude of the antenna in (a) xz-plane and (b) yz-plane.

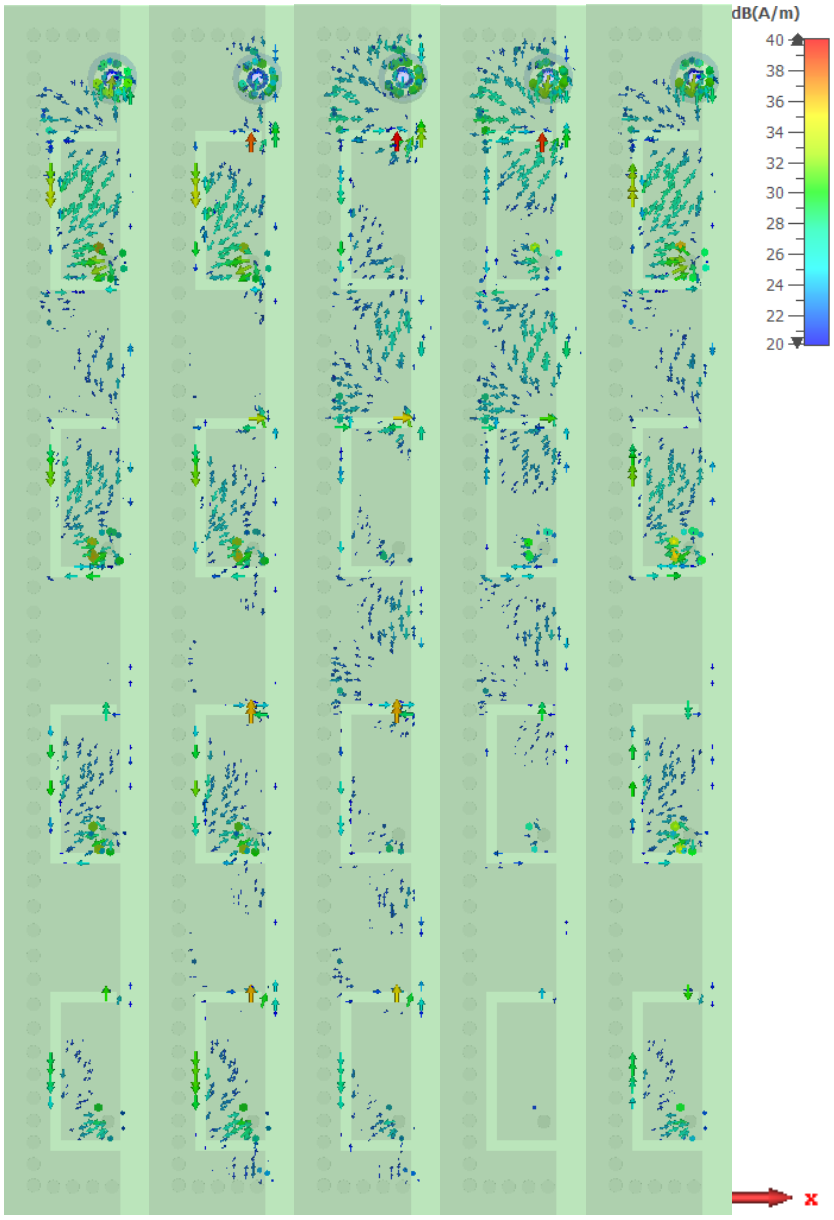

(a) (b) (c) (d) (e)

Fig. 93. Propagation of surface currents: (a) phase = 0° and (b) phase = 45°, (c) phase = 90°, (d) = phase 135° and (e) phase = 180°.

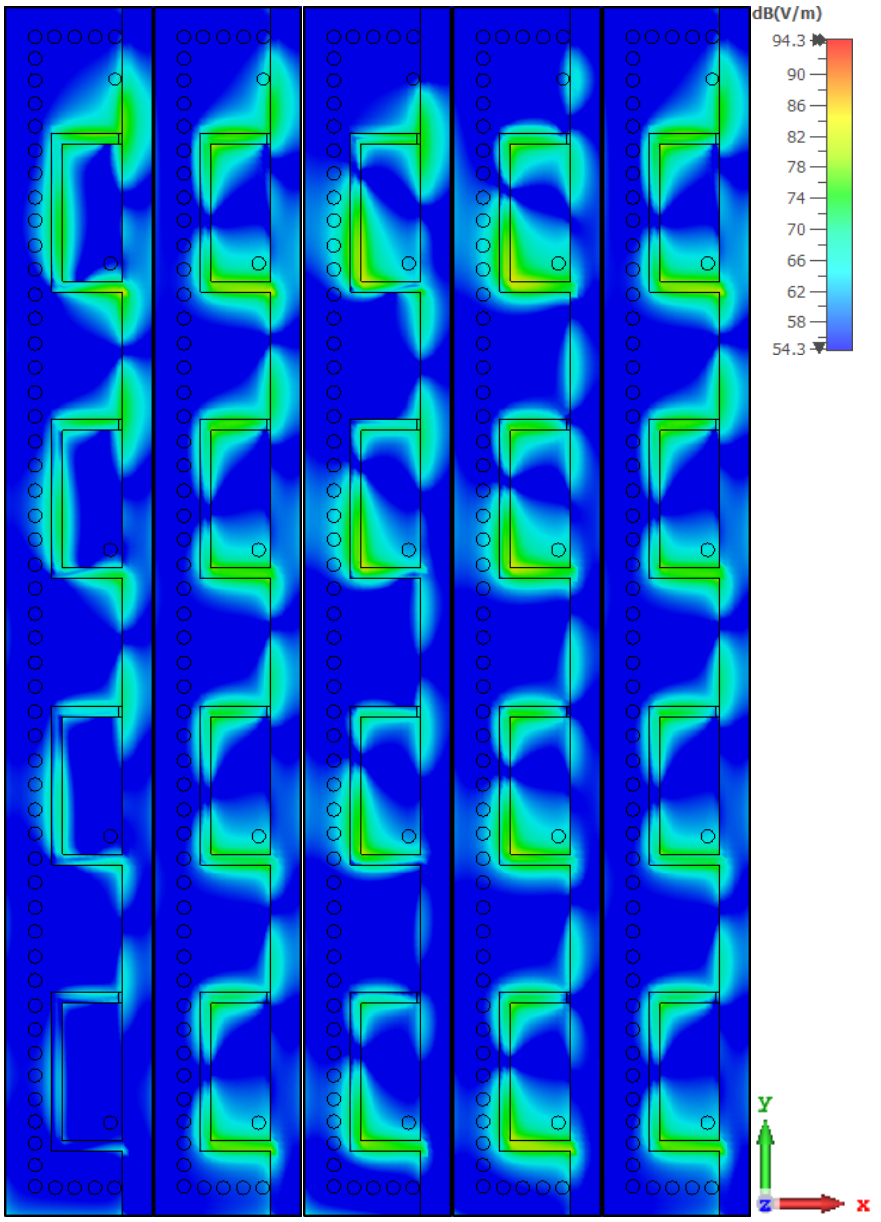

(a) (b) (c) (d) (e)

Fig. 94. Distribution of electric field intensity in substrate (magnitude): (a) phase = 0° and (b) phase = 45°, (c) phase = 90°, (d) = phase 135° and (e) phase = 180°.

5.1.3 Experimental Verification

The antenna was fabricated by a standard etching PCB process. The antenna is equipped with soldered SMA coaxial connector to carry out a conventional coaxial measurement. The manufactured sample of the antenna is depicted in Fig. 95.

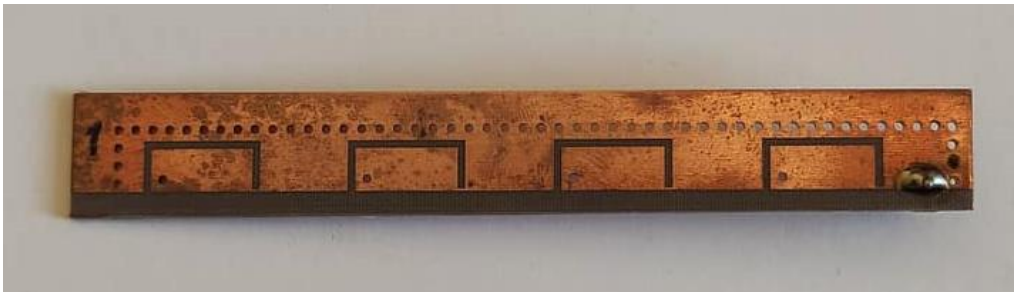

Fig. 95. Fabricated sample of the antenna array.

The reflection coefficient was measured in a laboratory environment and the radiation patterns for the Theta range from –90° to 90° were measured in an anechoic chamber. For the measurement, Rohde&Schwarz vector network analyzer ZVA67 was used. The measured reflection coefficient is shown in Fig. 96. The impedance bandwidth is 17.9 % for the reflection coefficient less than – 10 dB. The measured reflection coefficient is shifted about 350 MHz to lower frequencies. The difference is caused by the high sensitivity to the change of the physical dimensions of the proposed antenna to an inaccuracies during the manufacture process. On the other hand, the minimum of the axial ratio is shifted very slightly to the lower frequencies. The minimum of the axial ratio is 1.07 dB at 9.975 GHz meanwhile the axial ratio is 1.61 at 10 GHz. The measured axial ratio bandwidth 1.25 % is for AR < 3 dB (Fig. 97).

The measured radiation patterns in xz-plane and yz-plane are depicted in Figs. 98. The measured radiation patterns are in good agreement with the simulated ones except for the cross-polarization in the yz-plane. The measured peak gain of the antenna is 12.9 dBi.

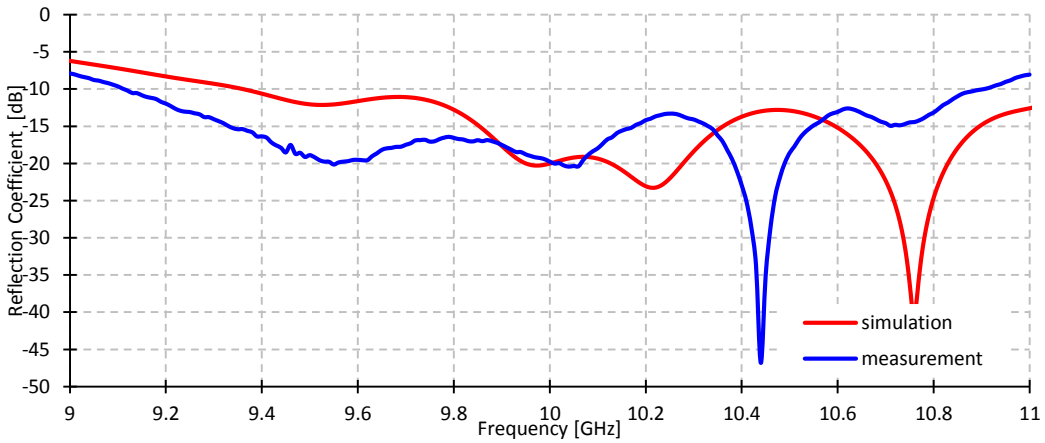

Fig. 96. Reflection coefficient of the proposed antenna array.

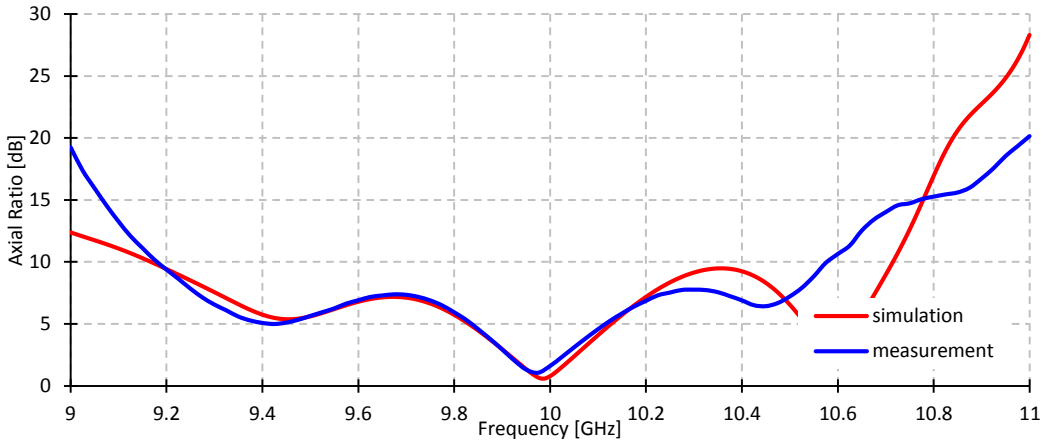

Fig. 97. Axial ratio of the proposed antenna array.

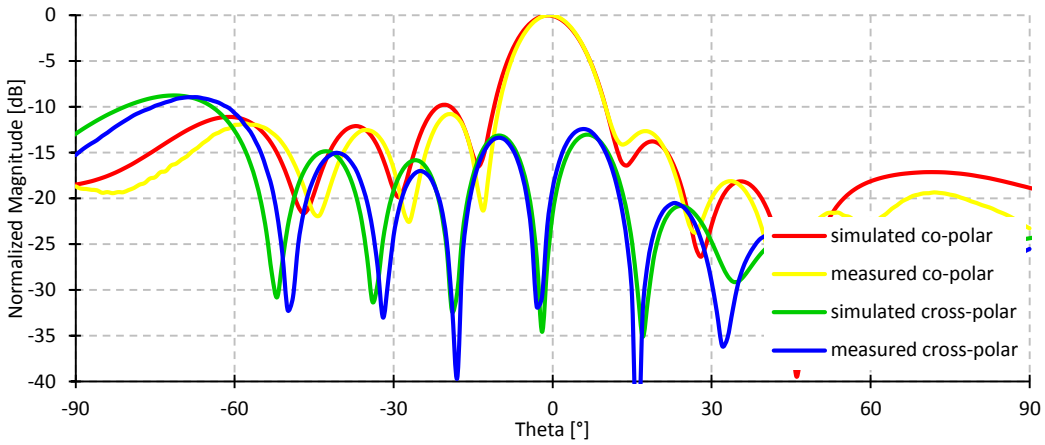

(a)

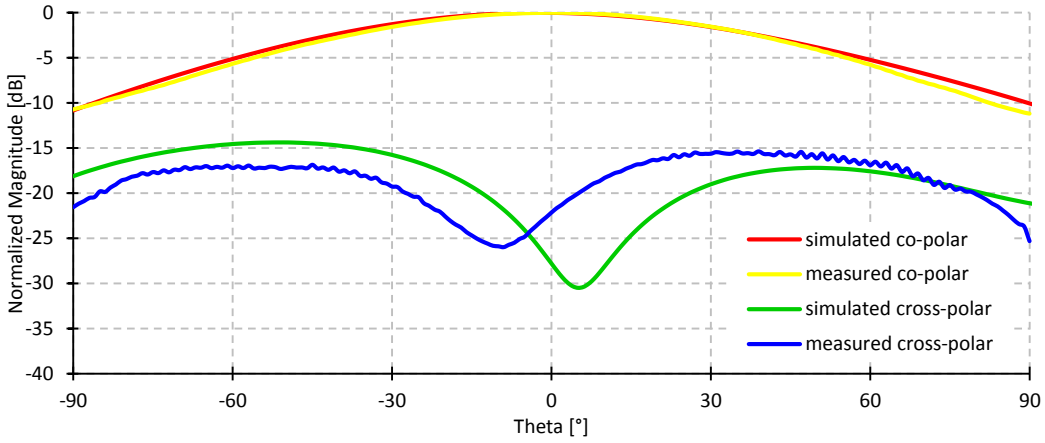

(b)

Fig. 98. Normalized radiation patterns of the proposed antenna in (a) xz-plane and (b) yz-plane.

5.1.4 Summary

The main purpose of this chapter was to demonstrate, that the circular polarized antenna mentioned in the chapter 4.2 is capable to be used as a basic resonator in an antenna array. For this reason, a simple antenna array in the linear organization of 1 × 4 basic radiators with a simple feeding network was designed. The simple feeding network caused a deterioration in the matching of the base radiators, which resulted in the degradation of the antenna performance. Nevertheless, the measured results proved that the antenna array achieved the satisfactory results in comparison to the similar HMSIW antenna array (Table 19).

For obtaining the linearly polarized antenna array, the basic radiator designed in the chapter 4.1 could be used.

Table 19. Proposed RHCP HMSIW antenna array in comparison to the other CP HMSIW antenna arrays (f_0 is operating frequency, SSL – side-lobe level; the axial ratio bandwidth was unable to extract from the literature).

	f_0 [GHz]	**s_{11} at f_0 [dB]**	**Impedance bandwidth [%] (s_{11}<-10 dB)**	**Peak gain [dBi]**	**Axial ratio at f_0, $\theta = 0°$ [dB]**	**SLL [dB]**	**length of antenna**
Proposed antenna	10	-19.5	17.9	12.9	1.6	-12.1	$5.83\lambda_0$
Fixed-frequency antenna [76]	6.5	-7.8	-	9.7	2.76	-12.5	$3.25\lambda_0$
CP LWA [77]	9	-11	59.2	8.7	2.6	-11.5	$5.25\lambda_0$
Frequency scanning antenna [80]	36	-15	16.1	14	1.6	-12.8	-

6. Conclusion

The doctoral thesis was focused on a research of novel HMSIW slot antenna concepts. By using HMSIW, the physical size of the antenna is reduced by approximately half while maintaining excellent antenna performance.

The thesis consists of five main chapters. The first on shortly introduced to the HMSIW technology. The second chapter described the state of the art of HMSIW antennas. The following third chapter defined the objectives of this thesis.

The first objective of the thesis was solved in the fourth chapter and it was related to detail description of a novel concept of HMSIW slot antenna to be able to radiate linearly and circularly polarized wave with focus on achieving better HMSIW slot antenna performance than the published ones. To tackle that objective, the HMSIW U-shaped antenna was introduced in different configurations to radiate the linearly [60] (chapter 4.1), [88] and circularly polarized [61] (chapter 4.2). The antennas were designed in the CST MWS, experimentally verified and deeply studied. Based on modal analysis and parametric studies, designed guides of those antennas were presented. The experimental results proved that the proposed linearly and circularly polarized HMSIW U-shape slot antennas reached better antenna performance in the most cases that published antennas based on HMSIW technology of the similar size.

The obtained results were exploited for the proposal of the HMSIW polarization reconfigurable U-shape slot antenna concept [62] (chapter 4.3). The proposed antenna was able to operate in a circularly and linearly polarized mode. Finally, the electronic control concept for this reconfigurable antenna was described and experimentally verified.

The second objective of the thesis was solved in the fifth chapter and it was related to exploitation of obtained knowledge from the first objective this thesis for the design of an antenna array. A simple RHCP antenna array was designed. It was demonstrated that the circular polarized antenna could be used as a basic resonator for an antenna array. The experimental results proved that the antenna array achieved the satisfactory results in comparison to the similar HMSIW antenna array.

Considering the objective of the thesis established in the chapter 3 and the obtained results shortly summarized above it can be concluded that the aims of the thesis were performed.

7. References

[1] UCHIMURA, H., TAKENOSHITA, T., FUJII, M. Development of a "laminated waveguide". *IEEE Transactions on Microwave Theory and Techniques*. 1998, vol. 46, no. 12, pp. 2438–2443.

[2] XU, F., WU, K. Guided-wave and Leakage Characteristics of Substrate Integrated Waveguide. *IEEE Transactions on Microwave Theory and Techniques*. 2005, vol.53, no.1, pp. 66–73.

[3] DING, Y., WU, K. A 4 × 4 Ridge Substrate Integrated Waveguide (RSIW) Slot Array Antenna. *IEEE Antennas and Wireless Propagation Letters*. 2008, vol. 8, pp. 561–564.

[4] IZQUIERDO, B.S., YOUNG, P.R., GRIGOROPOULOS, N., BATCHELOR, J.C., LANGLEY, R.J. Slot Antenna on C Type Compact Substrate Integrated Waveguide. *2005 European microwave Conference.* 2005, vol. 1, pp. 1–4.

[5] DING, Y., WU, K. T-Type Folded Substrate Integrated Waveguide (TFSIW) Slot Array Antenna. *IEEE Transactions on Antennas and Propagation*. 2010, vol. 58, no. 5, pp. 1792–1795.

[6] HONG, W., LIU, B., WANG, Y., LAI, Q., TANG, H., YIN, X.X., D. DONG, Y., ZHANG, Y., WU, K. Half Mode Substrate Integrated Waveguide: A New Guided Wave Structure for Microwave and Millimeter Wave Application. *Joint 31st International Conference on Infrared Millimeter Waves and 14th International Conference on Terahertz Electronics.* 2006, pp. 219.

[7] WU, L. Half Mode Substrate Integrated Waveguide Slot Antenna. *IEEE Antennas and Propagation Society International Symposium.* 2009, pp. 1–4.

[8] WEI, M., LIU, H., WAN, T., LIU, Y. A Compact Four-element MIMO Antenna Based on HMSIW Slot Antenna. *11th European Conference on Antennas and Propagation (EUCAP)*. 2017, pp. 2118–2120.

[9] RAZAVI, S.A., NESHATI, M.H. Development of a Linearly Polarized Cavity-Backed Antenna Using HMSIW Technique. *IEEE Antennas and Wireless Propagation Letters.* 2012, vol. 11, pp. 1307–1310.

[10] RAZAVI, S.A., NESHATI, M.H. Development of a Low-Profile Circularly Polarized Cavity-Backed Antenna Using HMSIW Technique. *IEEE Transactions on Antennas and Propagation.* 2013, vol. 61, no.3, pp. 1041–1047.

[11] KUMAR, A., RAGHAVAN, S., A Design of Miniaturized Half-Mode SIW Cavity Backed Antenna. *IEEE Indian Antenna Week (IAW 2016)*. 2016, pp. 4–7.

[12] ASTUTI, D.W., RAHARDJO, E.T. Size Reduction of Cavity Backed Slot Antenna using Half Mode Substrate Integrated Waveguide Structure. *4th International Conference on Nano Electronics Research and Education (ICNERE)*. 2018, pp. 1–4.

[13] DASHTI, H., NESHATI, M.H. Development of Low-Profile Patch and Semi-Circular SIW Cavity Hybrid Antennas. *IEEE Transactions on Antennas and Propagation.* 2014, vol. 62, no.9, pp. 4481–4488.

[14] BANERJEE, S., MOHANTY, T., DAS, S., RANA, B. HMSIW based Equilateral Triangular and Semi-Circular Antennas for WiMAX Applications. *International Conference on Communication and Signal Processing (ICCSP)*. 2016, pp. 741–744.

[15] BANERJEE, S., DEBNATH, M., BOSE, S., BHATTACHARYA, D., MONDAL, R. A., BASU, P. Compact HMSIW Semi-Hexagonal Antennas with Rectangular Slot. *International Conference on Opto-Electronics and Applied Optics (Optronix)*. 2019, pp. 1–6.

[16] BANERJEE, S., MOHANTY, T., DAS, S., RANA, B. Slot-loaded Compact HMSIW Triangular Antenna. *International Conference on Microelectronics, Computing and Communications (MicroCom)*. 2016, pp. 1–4.

[17] BANERJEE, S., MOHANTY, T., CHATTERJEE, S., MAZUMBAR, S. D. A Miniaturized Half-Mode SIW Based Semi-Circular Antenna with Arc-Shaped Slot. *2nd International Conference for Convergence in Technology (I2CT)*. 2017, pp. 128–131.

[18] BANERJEE, S., RANA, B., PARUI, S. K., CHATTERJEE, S., DEY, N. HMSIW-Based Miniaturized Sensing Antennas for S- and C-Band Applications. *IEEE Sensors Letters*. 2017, vol. 1, no. 1, pp. 1–5.

[19] LIU, S., XU, F., WU, K. A Compact E-Shaped Half-Mode Substrate Integrated Waveguide Semi-Circular Antenna. *IEEE MTT-S International Wireless Symposium (IWS)*. 2018, pp. 1–3.

[20] WU, Q., WANG, H., YU, CH., HONG, W. Low Profile Circularly PolarizedSIW-Like Cavity-Backed Slot Antennas. *10th European Conference on Antennas and Propagation (EuCAP).* 2016, pp. 1–4.

[21] RANA, B., PARUI, S.K. Half-Mode Substrate Integrated Waveguide Fed Compact Slot Antenna. *IEEE Applied Electromagnetics Conference (AEMC)*. 2013, pp. 1–2.

[22] KUMAR, K., DWARI, S., PRIYA, S. Dual band dual polarized cavity backed cross slot half mode substrate integrated waveguide antenna. *IEEE Applied Electromagnetics Conference (AEMC)*, 2017, pp. 1–2.

[23] LAI, Q.H., FUMEAUX, Ch., HONG, W., VAHLDIECK, R. 60 GHz Aperture-Coupled Dielectric Resonator Antennas Fed by a Half-Mode Substrate Integrated Waveguide. *IEEE Transactions on Antennas and Propagation.* 2010, vol. 58, no. 6, pp. 1856–1864.

[24] JIANG, S., WANG, Z., TANG, H. Design of Dual Band SIW and HMSIW Cavity Backed U-Shaped Slot Antennas. *10th International Conference on Communication Software and Networks (ICCSN)*, 2018, pp. 452–455.

[25] REDDY, G. V. K., MUKHERJEE, S., BISWAS, A. Design of HMSIW fed dual frequency microstrip patch antenna for X-band applications. *IEEE International Symposium on Antennas and Propagation (APSURSI)*, 2016, pp. 203–204.

[26] SAM, S., LIM, S. Compact Frequency-Reconfigurable Half-Mode Substrate-Integrated Waveguide Antenna. *IEEE Antennas and Wireless Propagation Letters*. 2013, vol. 12, pp. 951–954.

[27] DONG, Y., ITOH, T., Composite Right/Left-Handed Substrate Integrated Waveguide and Half Mode Substrate Integrated Waveguide Leaky-Wave Structures. *IEEE Transactions on Antennas and Propagation.* 2011, vol. 59, no. 3, pp. 767–775.

[28] TAN, L., WU, R., POO, Y. Magnetically Reconfigurable HMSIW Antenna With Broadband Frequency Tunability. *IEEE Antennas and Wireless Propagation Letters*. 2016, vol. 15, pp. 1373–1376.

[29] YE, M., LI, X., CHU, Q. Planar Circularly Polarized Endfire Antenna Based on Superposition of Complementary Dipoles. *IEEE International Symposium on Antennas and Propagation & USNC/URSI National Radio Science Meeting*. 2016, pp. 509–510.

[30] RAZAVI, S.A., NESHATI, M.H. Low profile H-plane Horn Antenna Based on Half Mode Substrate Integrated Waveguide Technique. *2012 20th Iranian Conference on Electrical Engineering (ICEE)*. 2012, pp. 1351–1354.

[31] QIN, P.Y., GUO, Y.J., DING, C. A Dual-band Polarization Reconfigurable Antenna for WLAN Systems. *IEEE Transactions on Antennas and Propagation*, 2013, vol. 61, no.11, pp. 5706–5713.

[32] HSU, S.H., CHANG, K. A Novel Reconfigurable Microstrip Antenna with Switchable Circular Polarization. *IEEE Antennas and Wireless Propagation Letters*, 2007, vol. 6, pp. 160–162.

[33] KIM, B., PAN B., NIKOLAOU, S., KIM, Y. S., PAPAPOLYMEROU, J., TENZERIS, M.M. A Novel Single-Feed Circular Microstrip Antenna with Reconfigurable Polarization Capability. *IEEE Transactions on Antennas and Propagation*, 2008 vol. 56, no. 3, 630–638.

[34] YOON, W.S., BAIK, J.W., LEE, H.S., PYO, S., HAM, S.M., KIM, Y.S. A Reconfigurable Circularly Polarized Microstrip Antenna with a Slotted Ground Plane. *IEEE Antennas and Wireless Propagation Letters*, 2010, vol. 9, pp. 1161–1164.

[35] FRIES, M.K., GRÄNI, M., VAHLDIECK R. A Reconfigurable Slot Antenna with Switchable Polarization. *IEEE Microwave and Wireless Components Letters*, 2003, vol. 13, no. 11, pp. 490–492.

[36] CAO, S.X., YANG, X.X., GONG, B., SHAO, B.C. A Reconfigurable Microstrip Antenna with Agile Polarization Using Diode Switches. *IEEE International Symposium on Antennas and Propagation (APSURSI)*, 2011, pp. 1566–1569.

[37] NISHAMOL, M.S., SARIN, V.P., TONY, D., AANANDAN, C.K., MOHANAN, P., VASUDEVAN, K. An Electronically Reconfigurable Microstrip Antenna with Switchable Slots for Polarization Diversity. *IEEE Transactions on Antennas and Propagation*, 2011, vol. 59, no. 9, pp. 3424–3427.

[38] OSMAN, M.N., RAHIM, M.K., HONG, P., GARDNER, Y, HAMID, M.R., MOHD, M.F., MAJID, H.A. An Electronically Reconfigurable Patch Antenna Design for Polarization Diversity with Fixed Resonant Frequency. *Radioengineering*, 2015, vol. 24, no. 1, pp. 45–53.

[39] KHIDRE, A., LEE, K.F., YANG, F., ELSHERBENI, A.Z. Circular Polarization Reconfigurable Wideband E-Shaped Patch Antenna for Wireless Applications." *IEEE Transactions on Antennas and Propagation*, 2013, vol. 61, no. 2, pp. 960–964.

[40] BOTI, M., DUSSOPT, L., LAHEURTE, J.M. Circularly Polarized Antenna with Switchable Polarization Sense. *Electronics Letters*, 2000, vol. 36, no. 18, pp. 1518–1519.

[41] SUNG, Y. Investigation into the Polarization of Asymmetrical-Feed Triangular Microstrip Antennas and its Application to Reconfigurable Antennas. *IEEE Transactions on Antennas and Propagation*, 2010, vol. 58, no. 4, pp. 1039–1046.

[42] TONG, K.F., HUANG, J. New Proximity Coupled Feeding Method for Reconfigurable Circularly Polarized Microstrip Ring Antennas. *IEEE Transactions on Antennas and Propagation*, 2008, vol. 56, no.7, pp. 1660–1866.

[43] QIN, P.Y., WEILY, A.R, GUO, Y.J., LIANG, C.H. Polarization Reconfigurable U-slot Patch Antenna. *IEEE Transactions on Antennas and Propagation*, 2010, vol. 58, no. 10, pp. 3383–3388.

[44] LI, Y., ZHANG, Z., CHEN, W., FENG, Z. Polarization Reconfigurable Slot Antenna with a Novel Compact CPW-to-Slotline Transition for WLAN Application. *IEEE Antennas and Wireless Propagation Letters*, 2010, vol. 9, pp. 252–255.

[45] KHALEGHI, A., KAMYAB M. Reconfigurable Single Port Antenna with Circular Polarization Diversity. I*EEE Transactions on Antennas and Propagation*, 2009 vol. 57, no. 2, pp. 555–559.

[46] YANG, F., SAMII, Y.R. A Reconfigurable Patch Antenna Using Switchable Slots for Circular Polarization Diversity. *IEEE Microwave and Wireless Components Letters*, 2002, vol. 12, no. 3, pp. 96–98.

[47] WU, Y.F., WU, C.H., LAI, D.Y., CHEN, F.C. A Reconfigurable Quadri-Polarization Diversity Aperture-Coupled Patch Antenna. *IEEE Transactions on Antennas and Propagation*, 2007, vol. 55, no. 3, pp. 1009–1012.

[48] CHEN, R.H., ROW, J.S. Single-Fed Microstrip Patch Antenna with Switchable Polarization. *IEEE Transactions on Antennas and Propagation*, 2008, vol. 56, no. 4, pp. 922–926.

[49] JUENEMANN, R. Patch Antenna Fed by a 3 Line System for Dual Orthogonal Linear and Circular Polarization. *2012 42nd European Microwave Conference (EuMC)*, 2012, pp. 305–308.

[50] DORSEY, W.M., ZAGHLOUL, A.I., PARENT M.G. Perturbed Square-Ring Slot Antenna with Reconfigurable Polarization. *IEEE Antennas and Wireless Propagation Letters*, 2009, vol. 8, pp. 603–606.

[51] HSU, S.H, CHANG, K. A Novel Reconfigurable Microstrip Antenna with Switchable Circular Polarization. *IEEE Antennas and Wireless Propagation Letters*, 2007 vol. 6, pp. 160–162.

[52] AGNEESSENS, S., ROGIER, H. Compact Half Diamond Dual-Band Textile HMSIW On-Body Antenna. *IEEE Transactions on Antennas and Propagation.* 2014, vol. 62, no. 5, pp. 2374–2381.

[53] SALONEN, P., HUMRE, L. A novel fabric WLAN antenna for wearable applications. *In Proceedings of the IEEE Antennas and Propagation Society International Symposium*, 2003, vol. 2, pp. 700–703.

[54] KAHN, I., YU, L., NECHAYEV, Y.I., HALL, P.S. Space and pattern diversity for on-body communication channels in an indoor environment at 2.45GHz. *In Proceedings of the Second European Conference on Antenna and Propagation (EUCAP 2007)*, 2007, pp. 1–6.

[55] PANZIN, L., LEVIATAN, Y. A compact 60-GHz tapered slot antenna printed on LCP substrate for WPAN applications. *IEEE Antennas and Wireless Propagation Letters*, 2010, vol. 9, pp. 272–275.

[56] KAHN, I., HALL, P.S. Multiple Antenna Reception at 5.8 and 10 GHz for Body-Centric Wireless Communication Channels. *IEEE Transactions on Antennas and Propagation*. 2009, vol. 57, no. 1.

[57] BAI, Q., LANGLEY, R. Crumpled textile antennas," *Electronics Letters*, 2009, vol. 45, pp. 436–438.

[58] HUBKA, P., LÁČÍK, J. Linearly Polarized HMSIW U-Slot Antenna. *Proceedings of Microwave and Radio Electronics Week MAREW 2015, 14th Conference on Microwave Techniques COMITE*

2015.2015. pp. 23–26.

[59] HUBKA, P., LACIK, J. X-Band Circularly Polarized HMSIW U-Slot Antenna. *Radioengineering*. 2016, vol. 25, no. 4, pp. 687–692.

[60] HUBKA, P., LACIK, J. Polarization Reconfigurable HMSIW U-Slot Antenna. *21st International Conference on Microwave, Radar and Wireless Communications (MIKON)*. 2016, pp. 1–4.

[61] LAI, Q., FUMEAUX, CH., HONG, W., VAHLDIECK, R. Characterization of the Propagation Properties of the Half-Mode Substrate Integrated Waveguide. *IEEE Transactions on Microwave Theory and Techniques*. 2009, vol. 57, pp. 1996–2004.

[62] RAINES, B.D., ELGHANNAI, E.A., ROJAS, R.G. Computer-Aided Antenna Feed Design Using Characteristic Modes. *European Microwave Conference (EuMC)*. 2015, pp. 13–16.

[63] LACIK. J., MIKULASEK, T. Substrate Integrated Waveguide Rectangular Ring Slot Antenna. *Microwave and optical technology letters*. 2011, pp. 1164–1167.

[64] LACIK. J. Circularly Polarized SIW Squatering-Slot Antenna for X-Band Applications. *Microwave and optical technology letters*. 2012, vol. 54, issue 11, pp. 2590-2594.

[65] MA4GP907, GaAs Flip Chip PIN datasheet, Aug. 2021 [REV V10]

[66] LQP03TQ2N0B02D, Chip Coil chip inductors datasheet, AUG. 2021 [REV 1]

[67] RANA, B., PARUI, S.K., ROY, A., GHOSH, CH. K. Half-Mode Substrate Integrated Waveguide Fed T-Shaped Slot Array Antenna. *5th International Conference on Computers and Devices for Communication (CODEC)*. 2012, pp. 1–3.

[68] LAI, Q. H., Hong, W., KUAI, Z. Q., ZHANG, Y. S., WU, K. Half-Mode Substrate Integrated Waveguide Transverse Slot Array Antennas. *IEEE Transactions on Antennas and Propagation*. 2009, vol. 57, no. 4, pp. 1064–1072.

[69] ZOU, X., TONG, CH. M, LI, X.M., YU, D.W. Half-Mode Substrate Integrated Waveguide Omnidirectional Slot Antenna. *IEEE Transactions on Antennas and Propagation*. 2015, vol. 51, no. 12, pp. 886–888.

[70] ANJU, P.M., LINDO, A.O., AANANDAN, C.K., KRISHNA D.D., YOUNG, P.R. Novel Millimeter-Wave Antenna Array Using Half Mode Substrate Integrated Waveguide (HMSIW). *International Conference on Advances in Computing and Communications*. 2012, pp. 274–277.

[71] AMMAR ALI, S.M., AHMED, Z., IHSAN, M.B. Beam Steering in HMSIW LWA at Fixed Millimeter Wave Frequency. *12th International Conference on High-capacity Optical Networks and Enabling/Emerging Technologies (HONET)*. 2015, pp. 1–2.

[72] HONG, W., XU, J., LAI, Q., CHEN P. Design and Implementation of Low Side-lobe Slot Array Antennas with Full and Half Mode Substrate Integrated Waveguide Technology. *European Microwave Conference*. 2007, pp. 428–429.

[73] HENRY, R., OKONIEWSKI, M. Half Mode Substrate Integrated Waveguide Periodic Leaky Wave Antenna with Antipodal Tapered Slots. *IEEE Antennas and Propagation Society International Symposium (APSURSI)*. 2014, pp. 1284–1285.

[74] HENRY, R., OKONIEWSKI, M. A New Half Mode Substrate Integrated Waveguide Leaky Wave Antenna. *The 8th European Conference on Antennas and Propagation (EuCAP 2014)*. 2014, pp. 586–589.

[75] SUNTIVES, A., HUM S.V. An Electronically Tunable Half-Mode Substrate Integrated Waveguide Leaky-Wave Antenna. *Proceedings of the 5th European Conference on Antennas and Propagation (EUCAP)*. 2011, pp. 3670–3674.

[76] SUNTIVES, A., HUM S.V. A Fixed-Frequency Beam-Steerable Half-Mode Substrate Integrated Waveguide Leaky-Wave Antenna. *IEEE Transactions on Antennas and Propagation*. 2012, vol. 60, no. 5, pp. 2540 – 2544.

[77] SAGHATI, A.P., MIRSALEHI, M.M., NESHATI, M.H. A HMSIW Circularly Polarized Leaky-Wave Antenna With Backward, Broadside, and Forward Radiation. *IEEE Antennas and Wireless Propagation Letters*. 2014, vol. 13, pp. 451 – 454.

[78] MUJUMDAR, M., ALPHONES A, NASIMUDDIN. Compact Leaky Wave Antenna with Periodical Slots on Half Mode Substrate Integrated Waveguide. *IEEE International Symposium on Antennas and Propagation & USNC/URSI National Radio Science Meeting*. 2015, pp. 1740–741.

[79] DONG , Y., ITOH, T. Composite Right/Left-Handed Substrate Integrated Waveguide and Half Mode Substrate Integrated Waveguide Leaky-Wave Structures. *IEEE Transactions on Antennas and Propagation*. 2011, vol. 59, no. 3, pp. 767–775.

[80] CHENG, Y. J., HONG, W., WU K. Millimeter-Wave Half Mode Substrate Integrated Waveguide Frequency Scanning Antenna With Quadri-Polarization. *IEEE Transactions on Antennas and Propagation*. 2010, vol. 58, no. 6, pp. 1848–1855.

[81] XU, J., HONG, W., TANG, H., KUAI, Z., WU, K. Half-Mode Substrate Integrated Waveguide (HMSIW) Leaky-Wave Antenna for Millimeter-Wave Applications. *IEEE Antennas and Wireless Propagation Letters*. 2008, vol. 7, pp. 85–88.

[82] LAI, Q., FUMEAUX, CH., HONG, W. Periodic Leaky-Wave Antennas Fed by a Modified Half-Mode Substrate Integrated Waveguide. *IET Microwaves Antennas & Propagation*. 2012, vol. 6, pp. 594–601

[83] HUBKA, P., LACIK, J. Design of a Linearly Polarized HMSIW U-Slot Antenna. *Radioengineering*. 2021, vol. 30, no. 3, pp. 1–10.

[84] ELLIOTT, R.S. *Antenna Theory and Design*. Rev ed. Hoboken (US-NJ), 2003. Chapter VIII.

[85] MIKULÁŠEK, T. *Microstrip patch antennas fed by substrate integrated waveguide*. Doctoral thesis. Brno: FEKT VUT v Brně, 2013. pp. 1–87.

List of Abbreviations

AR	axial ratio
CFSIW	C-type folded SIW
CMA	characteristic modal analysis
co-polar	co-polarization
cross-polar	cross-polarization
CP	circular polarization
DRA	dielectric resonator antenna
GCPW	grounded coplanar waveguide
HMSIW	half mode substrate integrated waveguide
LHCP	left-handed circular polarization
LP	linear polarization
LTCC	low-temperature co-fired ceramic
LWA	leaky wave antenna
MIMO	multiple input multiple output
MMIC	monolithic microwave integrated circuit
MWS	CST Microwave Studio
PCB	printed circuit process
PEC	perfect electric conductor
RHCP	right-handed circular polarization
RSIW	ridge SIW
SIW	substrate integrated waveguide
SLL	side-lobe level
TFSIW	T-type folded SIW

List of Figures

Fig. 1. Structure of HMSIW. 2

Fig. 2. Geometry of the first HMSIW slot antenna (the bottom side of the antenna is fully coated by metal). 3

Fig. 3. Geometry of the simple HMSIW slot antenna (the bottom side of the antenna is fully coated by metal). 3

Fig. 4. Geometry of the HMSIW cavity-backed (a) linearly polarized antenna (the bottom side of the antenna is fully coated by metal.), (b) RHCP antenna (the bottom side of the antenna is fully coated by metal.) and (c) LHCP antenna and its (d) bottom view. 4

Fig. 5. Geometry of the HMSIW cavity-backed antenna (the bottom side of the antenna is fully coated by metal). 4

Fig. 6. Geometry of the HMSIW cavity-backed antenna with the slot: (a) top view and (b) bottom view. . 5

Fig. 7. Geometry of patch HMSIW cavity hybrid antennas: (a) linearly polarize version and (b) circularly polarized version. 5

Fig. 8. Geometry of the HMSIW (a) equilateral triangular, (b) semi-circular antennas, (c) semi-hexagonal #1 and (d) semi-hexagonal #2. The bottom sides of all antenna are fully coated by metal. 6

Fig. 9. Geometry of the HMSIW (a) equilateral triangular with the slot, (b) semi-circular antennas with the arc shaped slot, (c) semi-circular antennas with the slot, (d) semi-circular antennas with the two slot, (e) semi-hexagonal #1 with the slot and (f) semi-hexagonal #2 with the slot. The bottom sides of all antennas are fully coated by metal. 7

Fig. 10. Geometry of the E-shaped HMSIW semi-circular antenna (the bottom side of the antenna is fully coated by metal). 8

Fig. 11. Geometry of the HMSIW semi-circular slot antenna (the bottom side of the antenna is fully coated by metal). 8

Fig. 12. Geometry of the HMSIW compact slot antenna (the bottom side of the antenna is fully coated by metal). 9

Fig. 13. Geometry of the HMSIW dual band cavity-backed antenna: (a) top view and (b) bottom view. ... 9

Fig. 14. Geometry of the HMSIW slot antenna loaded by the dielectric resonator with: (a) LP and (b) CP and (c) common top plane. 10

Fig. 15. Geometry of the duel band HMSIW cavity-backed U-slot antenna (the bottom side of the antenna is fully coated by metal). 10

Fig. 16. Geometry of the frequency reconfigurable HMSIW antenna (a) top view and (b) bottom view. . 11

Fig. 17. Geometry of the frequency reconfigurable HMSIW antenna with ferrite slab: (a) topview, (b) bottom view and (c) measurement setup. 11

Fig. 18. Top (a) and side (b) view of the linearly polarized antenna (the bottom side of the antenna is fully coated by metal). 16

Fig. 19. Simulated reflection coefficient of the linearly polarized antenna. 18

Fig. 20. Simulation of normalized magnitude of the antenna in (a) E-plane and (b) H-plane. 18

Fig. 21. Propagation of Surface currents: (a) phase = 0° and (b) phase = 45°, (c) phase = 90°, (d) = phase 135° and (e) phase = 180°. 19

Fig. 22. Distribution of electric field intensity in substrate (magnitude): (a) phase = 0° and (b) phase = 45°, (c) phase = 90°, (d) = phase 135° and (e) phase = 180°. 19

Fig. 23. Fabricated sample of the proposed HMSIW U-slot antenna. 19

Fig. 24. Reflection coefficient of the proposed antenna. 20

Fig. 25. Normalized radiation patterns of the proposed antenna in (a) E-plane and (b) H-plane. 21

Fig. 26. CMA – Modal significance. 21

Fig. 27. CMA – Modal surface currents. 22

Fig. 28. CMA – Radiation patterns. 23

Fig. 29. Variation of the length L_{slot_x}. 24

Fig. 30. Variation of the length L_{slot_y}. 25

Fig. 31. Variation of the length W_{slot}. 26

Fig. 32. Variation of the shift of the short S1. 27

Fig. 33. The selected parameters for the design guide. 28

Fig. 34. Physical dimension of (a) L_{SLOT-X}, (b) L_{SLOT-Y}, (c) L_{viaX}, (d) W_{SLOT}, (e) W_{HMSIW}. 31

Fig. 35. Fabricated sample of the antennas: (a) FoamClad, (b) CuClad 217, (c) Arlon 25N, (d) Arlon 600. 32

Fig. 36. Reflection coefficient (a) FoamClad, (b) CuClad 217, (c) Arlon25N, (d) Arlon 600. 33

Fig. 37. Normalized magnitude measured at 10 GHz, substrate FoamClad: (a) E-plane, (b) H-plane. 34

Fig. 38. Normalized magnitude measured at 12 GHz, substrate CuClad 217: (a) E-plane, (b) H-plane. ... 34

Fig. 39. Normalized magnitude measured at 8 GHz, substrate Arlon25N: (a) E-plane, (b) H-plane. 34

Fig. 40. Normalized magnitude measured at 7 GHz, substrate Arlon600: (a) E-plane, (b) H-plane. 34

Fig. 41. Top (a) and side (b) view of the circularly polarized antenna (the bottom side of the antenna is fully coated by metal). 36

Fig. 42. Simulated reflection coefficient of the circularly polarized antenna. 37

Fig. 43. Simulated axial ratio of the circularly polarized antenna. 38

Fig. 44. Simulation of normalized magnitude of the antenna in (a) xz-plane and (b) yz-plane. 38

Fig. 45. Propagation of surface currents: (a) phase = 0° and (b) phase = 45°, (c) phase = 90°, (d) = phase 135° and (e) phase = 180°. 39

Fig. 46. Distribution of electric field intensity in substrate (magnitude): (a) phase = 0°, (b) phase = 45°, (c) phase = 90°, (d) phase = 135° and (e) = 180°. 39

Fig. 47. Fabricated sample of the proposed HMSIW U-slot antenna. 39

Fig. 48. Reflection coefficient of the proposed antenna. 40

Fig. 49. Axial ratio of the proposed antenna. 40

Fig. 50. Normalized radiation patterns of the proposed antenna in (a) xz-plane and (b) yz-plane. 41

Fig. 51. CMA – Modal significance. 42

Fig. 52. CMA – Modal surface currents. 43

Fig. 53. CMA – Radiations patterns: polarization of the wave in the x-direction. 43

Fig. 54. CMA – Radiations patterns: polarization of the wave in the y-direction. 43

Fig. 55. Parametric study of the shorting via I_1. Physical dimensions for position **0** (original) are X_{via} = 3.21 mm and Y_{via} = 2.65 mm, for position **1** are X_{via} = 3.46 mm and Y_{via} = 2.40 mm, for position **2** are = X_{via} = 2.40 mm and Y_{via} = 2.71 mm, for position **3** are X_{via} = 2.90 mm and Y_{via} = 3.46 mm and for position **4** are X_{via} = 2.90 mm and Y_{via} = 2.96 mm. 44

Fig. 56. Variation of the length L_{SLOT-X}: (a) reflection coefficient, (b) axial ratio, (c) co-polar in xz-plane, (d) cross-polar in xz-plane, (e) co-polar in yz-plane and (f) cross-polar in yz-plane. 45

Fig. 57. Variation of the length L_{SLOT-Y}: (a) reflection coefficient, (b) axial ratio, (c) co-polar in xz-plane, (d) cross-polar in xz-plane, (e) co-polar in yz-plane and (f) cross-polar in yz-plane. 46

Fig. 58. Variation of the length W_{SLOT}: (a) reflection coefficient, (b) axial ratio, (c) co-polar in xz-plane, (d) cross-polar in xz-plane, (e) co-polar in yz-plane and (f) cross-polar in yz-plane. 47

Fig. 59. Variation of via I_1 position in x-direction X_{via}: (a) reflection coefficient, (b) axial ratio, (c) co-polar in xz-plane, (d) cross-polar in xz-plane, (e) co-polar in yz-plane and (f) cross-polar in yz-plane. 48

Fig. 60. Variation of via I_1 position in y-direction Y_{via}: (a) reflection coefficient, (b) axial ratio, (c) co-polar in xz-plane, (d) cross-polar in xz-plane, (e) co-polar in yz-plane and (f) cross-polar in yz-plane..... 49

Fig. 61. Variation of via I_1 position 1 – 4: (a) reflection coefficient, (b) axial ratio, (c) co-polar in xz-plane, (d) cross-polar in xz-plane, (e) co-polar in yz-plane and (f) cross-polar in yz-plane. 50

Fig. 62. Top (a) and side (b) view of the reconfigurable HMSIW antenna (the bottom side of the antenna is fully coated by metal). 53

Fig. 63. Simulated reflection coefficient. 54

Fig. 64. Simulated axial ratio of LHCP mode. 54

Fig. 65. Simulated radiation pattern for LHPC and LP mode in (a) xz-plane and (b) yz-plane. 55

Fig. 66. Propagation of surface currents of antenna operating in LP mode: (a) phase = 0° and (b) phase = 45°, (c) phase = 90°, (d) = phase 135° and (e) phase = 180°. 55

Fig. 67. Distribution of electric field intensity in substrate (magnitude) of antenna operating in LP mode: (a) phase = 0° and (b) phase = 45°, (c) phase = 90°, (d) = phase 135° and (e) phase = 180°. 56

Fig. 68. Propagation of surface currents of antenna operating in LHCP mode: (a) phase = 0° and (b) phase = 45°, (c) phase = 90°, (d) = phase 135° and (e) phase = 180°. 56

Fig. 69. Distribution of electric field intensity in substrate (magnitude) of antenna operating in LHCP mode: (a) phase = 0° and (b) phase = 45°, (c) phase = 90°, (d) = phase 135° and (e) phase = 180°. 56

Fig. 70. Fabricated sample of the antenna concept operating in (a) LHCP and (b) LP mode. 57

Fig. 71. Reflection coefficient. 58

Fig. 72. Axial ratio of LHCP mode. 58

Fig. 73. Normalized radiation pattern of antenna operating in LP mode: (a) xz-plane (E-plane) and (b) yz-plane (H-plane). 59

Fig. 74. Normalized radiation pattern of antenna operating in LHCP mode: (a) xz-plane and (b) yz-plane. 59

Fig. 75. Implementation of the electronic switching control between LHCP and LP mode: (a) circuit diagram and (b) realization on the boar. 60

Fig. 76. Reflection coefficient. 61

Fig. 77. Axial ratio of LHCP mode. 62

Fig. 78. Simulated radiation pattern for LHPC and LP mode in (a) xz-plane and (b) yz-plane. 62

Fig. 79. Propagation of surface currents of antenna operating in LP mode (electronic components are set to “hidden”): (a) phase = 0° and (b) phase = 45°, (c) phase = 90°, (d) = phase 135° and (e) phase = 180°. 63

Fig. 80. Distribution of electric field intensity in substrate of antenna operating in LP mode (magnitude) (electronic components are set to “hidden”): (a) phase = 0° and (b) phase = 45°, (c) phase = 90°, (d) = phase 135° and (e) phase = 180°. 63

Fig. 81. Propagation of surface currents of antenna operating in LHCP mode (electronic components are set to “hidden”): (a) phase = 0° and (b) phase = 45°, (c) phase = 90°, (d) = phase 135° and (e) phase = 180°. 63

Fig. 82. Distribution of electric field intensity in substrate of antenna operating in LHCP mode (magnitude) (electronic components are set to “hidden”): (a) phase = 0° and (b) phase = 45°, (c) phase = 90°, (d) = phase 135° and (e) phase = 180°. 64

Fig. 83. Fabricated sample of the antenna with the electronic control of the polarization mode. 64

Fig. 84. Measured reflection coefficient of the antenna in LHCP mode. 65

Fig. 85. Measured reflection coefficient of the antenna in LP mode. 65

Fig. 86. Measured axial ratio of antenna in LHCP mode. 65

Fig. 87. Normalized radiation pattern for LHCP mode in: (a) xz-plane and (b) yz-plane. 66

Fig. 88. Normalized radiation pattern for LP mode in: (a) xz-plane (E-plane) and (b) yz-plane (H-plane). 67

Fig. 89. Top (a) and side (b) view of the RHCP antenna array (the bottom side of the antenna is fully coated by metal). 69

Fig. 90. Simulated reflection coefficient of the circularly polarized antenna array. 70

Fig. 91. Simulated axial ratio of the circularly polarized antenna array. 71

Fig. 92. Simulation of normalized magnitude of the antenna in (a) xz-plane and (b) yz-plane. 71

Fig. 93. Propagation of surface currents: (a) phase = 0° and (b) phase = 45°, (c) phase = 90°, (d) = phase 135° and (e) phase = 180°. 72

Fig. 94. Distribution of electric field intensity in substrate (magnitude): (a) phase = 0° and (b) phase = 45°, (c) phase = 90°, (d) = phase 135° and (e) phase = 180°. 73

Fig. 95. Fabricated sample of the antenna array. 73

Fig. 96. Reflection coefficient of the proposed antenna array. 74

Fig. 97. Axial ratio of the proposed antenna array. 74

Fig. 98. Normalized radiation patterns of the proposed antenna in (a) xz-plane and (b) yz-plane. 75

List of Tables

Table 1. Measured results of the HMSIW cavity-backed antennas. 4

Table 2. Measured results of the HMSIW triangular, semi-circular and two semi-hexagonal antennas. 6

Table 3. Measured shift of reflection coefficient minimum. 7

Table 4. Dimensions of the antenna. 17

Table 5. Resonant frequency of the modes. 22

Table 6. Dielectric substrates used for design guide. 28

Table 7. Correction factors $k_x(f)$, $k_y(f)$ and $k_f(f)$ and width W_{HMSIW}. 29

Table 8. Operating frequency of the antennas. 31

Table 9. Measured and simulated gain in E-plane. 32

Table 10. The proposed antenna in comparison to other HMSIW antennas (λ_0 is wavelength in vacuum). 35

Table 11. Physical dimensions of the circularly polarized antenna. 37

Table 12. Resonant frequency of the modes. 42

Table 13. Proposed CP U-shape slot antenna in comparison to the other CP HMSIW antennas (λ_0 is wavelength in vacuum). 52

Table 14. Physical dimensions of the reconfigurable antenna concept. 54

Table 15. Specification of the components used for the implementation of the electronic switching control between LHCP and LP. 60

Table 16. Physical dimensions of antenna with electronic switching between LHCP and LP operating mode. 61

Table 17. Proposed polarization reconfigurable slot antenna in comparison to the other polarization reconfigurable antennas (f_o is operating frequency and λ_0 is wavelength in vacuum). 67

Table 18. Dimensions of the antenna array. 70

Table 19. Proposed RHCP HMSIW antenna array in comparison to the other CP HMSIW antenna arrays (f_o is operating frequency, SSL – side-lobe level; the axial ratio bandwidth was unable to extract from the literature). 76

A Curriculum Vitae

Personal

Name	Patrik Hubka
Born	August 5th 1987 in Čeladná
Contact	Patrik.hubka@seznam.cz

Education

2013 – 2021 Brno University of Technology (Department of Radio Electronics)

Doctoral's degree, Electronics and Communications

Thesis: Half Mode Substrate Integrated Waveguide Slot Antennas

2011 – 2013 Brno University of Technology (Department of Radio Electronics)

Master's degree, Electronics and Communications

Thesis: Rectangular Patch Antenna for the Frequency Band 60 GHz

2008 - 2011 Brno University of Technology (Department of Radio Electronics)

Bachelor's degree, Electronics and Communications

Thesis: Digitally Controlled Multifunctional Filter

Languages

Czech, English

Specialization

analysis and design of antennas, modeling and simulation of microwave and RF structures, antenna measurement

Projects

2013 Versatile, Integrated, and Signal-aware Technologies for Antennas (VISTA)